THE UNIVERSITY OF MICHIGAN
COLLEGE OF ENGINEERING
Department of Engineering Mechanics

Special Technical Report

AN INVESTIGATION OF INITIAL YIELDING AND STRAIN HARDENING IN A CAST ZINC ALLOY

David R. Jenkins

ORA Project 02797

under contract with:

AERONAUTICAL SYSTEMS DIVISION
CONTRACT NO. AF 33(616)-6041
WRIGHT-PATTERSON AIR FORCE BASE
OHIO

administered through:

OFFICE OF RESEARCH ADMINISTRATION ANN ARBOR

April 1962

PREFACE

This study was undertaken as a part of a broader program which deals with the effect of state of stress on the failure of metals at various temperatures under the sponsorship of the United States Air Force, Contract No. AF 33(616)-6041. The work discussed here deals specifically with the behavior of a single material in the plastic range. Fracture is not considered.

The author expresses his thanks to the United States Air Force, in particular Dr. J. A. Herzog, who made possible the extensive experimental program. Especial thanks are due to Professor R. M. Haythornthwaite for his guidance during the research and for his encouragement to pursue this particular problem. Many persons should be thanked for their assistance during the experimental phases of the work but the author wishes to single out Mr. Milo Kaufman, Senior Laboratory Machinist, for his expert aid when it was most needed.

TABLE OF CONTENTS

		Page
PREFACE		ii
LIST OF TABLES		v
LIST OF ILLUSTRATIONS		vi
ABSTRACT		viii
CHAPTER		
I.	INTRODUCTION	1
II.	EXPERIMENTAL APPARATUS AND TECHNIQUE	9
	Material	9
	Combined Load Testing Machine	10
	Load Measurement	16
	Strain Measurement	16
	Temperature Control	17
III.	THEORETICAL PREDICTIONS OF STRAIN HARDENING BEHAVIOR IN THE OCTAHEDRAL PLANE	18
	The Material Model and the Octahedral Plane	18
	Initial Yielding	20
	Isotropic Hardening	23
	Kinematic Hardening	27
	Piecewise Linear Hardening	36
	Anisotropy	45
IV.	PREDICTION OF THE KINEMATIC THEORY OF STRAIN HARDENING IN SUBSPACES	49
	Subspaces for Axial Tension-Torsion	50
	Subspaces for Axial Tension-Internal Pressure	59
V.	REVIEW OF PREVIOUS EXPERIMENTAL INVESTIGATIONS	70
	Initial Yielding	70
	Strain-Hardening by the Isotropic Theory	73
	Strain-Hardening by the Slip Theory	79
	The Form of Subsequent Yield Surfaces	81

TABLE OF CONTENTS (Concluded)

		Page
VI.	COMPARISON OF EXPERIMENTAL RESULTS AND THEORETICAL PREDICTIONS	84
	Isotropy	84
	Material Response to Simple States of Stress	90
	Initial Yielding under Complex States of Stress	92
	Strain Hardening under Complex States of Stress	105
'II.	CONCLUSIONS OF THE RESEARCH	117
EFERENCES		118

LIST OF TABLES

Table		Page
1.	Test Designations	97
2.	Yield Values at 78°F	99
3.	Yield Values at 32°F	102

LIST OF ILLUSTRATIONS

Figure		Page
1.	Sketch of tubular specimen.	4
2.	Coordinate system and stresses in tube.	6
3.	Photomicrograph of Zamak-3.	11
4.	Combined load testing machine.	12
5.	Load proportioning system.	14
6.	Hydraulic diagram for the combined load testing machine.	15
7.	Various initial yield criteria in the octahedral plane.	22
8.	Isotropic hardening for stress path 01.	28
9.	Kinematic hardening for stress path 01.	33
10.	Sanders' hardening for a Tresca yield surface.	38
11.	Piecewise linear hardening for a stress state point in a corner.	42
12.	Piecewise linear hardening for a stress state point on AF.	44
13.	Kinematic hardening for the von Mises yield condition. Combined tension-torsion loading.	55
14.	Kinematic hardening for the Tresca yield condition. Combined tension-torsion loading.	56
15.	Kinematic hardening for plane stress, maximum reduced stress yield condition.	60
16.	Kinematic hardening for the von Mises yield condition. Tension-internal pressure loading.	65
17.	Kinematic hardening for the Tresca yield condition. Tension-internal pressure loading.	66

LIST OF ILLUSTRATIONS (Concluded)

Figure		Page
18.	Kinematic hardening for the maximum reduced stress yield condition. Tension-internal pressure loading.	68
19.	Axial and circumferential plastic strains in pure tension.	86
20.	Specimen adapted for measurement of internal volume change.	87
21.	Volume change in internal cavity of tube.	89
22.	Tensile stress-strain curves, 78°F, 32°F.	91
23.	Compressive stress-strain curve, 32°F.	93
24.	Torsion stress-strain curves, 78°F, 32°F.	94
25.	Stress-strain diagrams for test PP-4, combined axial tension and internal pressure.	96
26.	Initial yield data at 78°F.	98
27.	Initial yield data at 32°F.	101
28.	Representative stress vs. I_1 for data at 32°F.	103
29.	Strain-hardening behavior, test X-1, 78°F.	106
30.	Strain-hardening behavior, test X-3, 78°F.	108
31.	Strain-hardening behavior, test X-4, 78°F.	109
32.	Strain-hardening behavior, test X-9, 78°F.	111
33.	Strain-hardening behavior, test X-5, 32°F.	112
34.	Strain-hardening behavior, test X-6, 32°F.	113
35.	Strain-hardening behavior, test X-7, 32°F.	114
36.	Strain-hardening behavior, test X-8, 32°F.	115

ABSTRACT

The twofold objectives of this research are first to determine whether initial yielding in a material which ruptures in a brittle manner can be predicted by a yield condition which assumes independence of mean stress and isotropy, and second to determine whether contemporary theories of strain hardening can be used to predict the effect of plastic strain on the yield condition for this material. If applicable, these contemporary theories of strain hardening offer a better description of the behavior of technically significant materials than do theories assuming ideal plasticity and yet are mathematically tractable in the solution of boundary value problems.

A thorough exploration is presented of various theories of initial yielding and of strain hardening including the isotropic hardening theory after R. Hill, the kinematic hardening theory of W. Prager, and the piecewise linear hardening theory of P. G. Hodge, Jr. The predictions of these theories are then described as motions of the several yield surfaces in the octahedral plane of principal stress space. In addition, predictions are made of yield surface motions in appropriate subspaces.

The specific material considered in the experimental portion of the research is cast Zamak-3, a zinc-base material containing about four percent aluminum. Thin tubular specimens of this material were subjected to various combinations of axial force and torque or axial force and internal pressure in a combined load testing machine. In this device, the applied loads can be held in a fixed ratio. Two testing temperatures,

namely 32°F and 78°F, were employed. In all cases the ultimate rupture is brittle with no evidence of localized plastic deformation.

One set of results concerns the isotropy of the material. For tubes subjected to axial tension, axial and circumferential plastic strains were compared. Also the plastic volume change in the internal cavity of the tube was noted. Both of these types of experiments show that Zamak-3 responds to plastic straining as if isotropic.

Initial yielding at each testing temperature was investigated by applying various ratios of axial force and torque or axial force and internal pressure to the tubular specimens. Initial yielding is defined in the sense of the "proportional limit" stress. The degree of scatter in the initial yielding data obviates the selection of a particular initial yielding criterion. However, yield criteria such as Tresca or maximum reduced stress fit the data as well as the Mises criterion. Thus these criteria are used in the analysis of strain hardening since they give plastic strain increments which are partially independent of the stress path. Initial yielding at 78°F appears to be independent of mean stress but there is some evidence to indicate that there may be an effect of mean stress at 32°F.

Behavior in the strain hardening range was investigated in a series of multiple loading path tests. The procedure was to load first along a given radial loading path (i.e., constant stress ratios) to a point well beyond the initial yield surface, then to completely unload the specimen and to reload along a second radial loading path until yielding had

occurred. Here combinations of axial force and internal pressure were used so that rotation of the principal axes of stress would not occur. The results indicate that the kinematic hardening theory in conjunction with either Tresca or maximum reduced stress yield criteria gives good predictions of the state of stress at yielding on second loading. This appears to be true even for fairly large translations of the yield surface.

CHAPTER I

INTRODUCTION

The research described in this dissertation has two major objectives:

1. To determine whether a material whose rupture behavior is brittle, i.e., exhibits a relatively small total plastic strain before rupture occurs, would yield initially in accordance with a yield condition which assumes independence of mean or average normal stress and isotropy of material.

2. To investigate the effect of plastic strain on the yield condition under combined stress and in particular to assess the validity of contemporary theories of strain-hardening for predicting this strain-hardening behavior in the material mentioned above. All of the strain hardening theories that are considered fall within the concept of the plastic potential.

In large measure, investigations of initial yielding and of strain-hardening have related to ductile materials (i.e., materials which undergo a large plastic strain before rupture). Initial yielding for ductile materials of technical significance has been shown to be insensitive to mean stress to a good approximation. Further if isotropy of the material can be established, it would be expected that a yield criterion in terms of the deviatoric stress components, such as the von Mises or the

Tresca, might apply. As will be seen in the literature review of Chapter V, relatively few investigators have been concerned with the predictions of recently conceived strain hardening theories even for ductile materials. Thus it appears that the present research might furnish some unique results.

Rather remarkable success has been attained in solving boundary value problems by means of the theory of plasticity in conjunction with a rigid-ideally plastic material model. Ideally plastic defines a mode of behavior in which the yield condition is invariable with increasing plastic strain. In short, plastic flow initiates and continues at an unchanging state of stress if that state of stress satisfies the yield condition. With the exception of mild steel, technically significant materials do not exhibit this ideally plastic behavior. Thus for most materials a rigid-strain hardening model must be assumed so that the effect of plastic strain on the yield condition can be properly taken into account. This is of particular importance when multiple loading paths for a given body or structure are to be investigated. It is not implied, however, that the yield conditions or stress-strain laws postulated in the theory of plasticity are intended to describe, in detail, the material behavior. Their purpose is, on the contrary, to predict correct general trends in the framework of a theory which is simple enough to be mathematically tractable in the solution of boundary value problems.

The specific material considered in this research is a cast zinc-

alloy designated Zamak-3. This is primarily a zinc-aluminum alloy which has the following composition:

Element	Percent of Total
Aluminum	3.99
Iron	Trace
Magnesium	0.040
Copper	0.084
Lead	0.0016
Tin	0.0013
Cadmium	0.001
Zinc	Balance

The rupture behavior of this material is brittle in the sense already defined although it does undergo a "ductile to brittle" transition in that the principal strain at fracture changes from about 0.030 for the "ductile" state to about 0.004 or less for the "brittle" state. These variations in behavior can be produced by changing the state of stress or the temperature. Two testing temperatures, namely 32°F and 78°F, were employed so that the range of states of stress for which brittle fracture occurred could be varied. However, the ultimate rupture appears to be transgranular and is not accompanied by localized plastic deformation processes, such as necking, in the separated region. Such behavior is advantageous in the sense of computing stresses from the observed loads in the plastic range since gross changes in the geometry of a tubular specimen do not occur. Further details of casting procedure and material properties are discussed in Chapter II.

The data reported herein were obtained by subjecting tubular specimens, of the type shown in Figure 1, to various combinations of axial force and torque or axial force and internal pressure in a com-

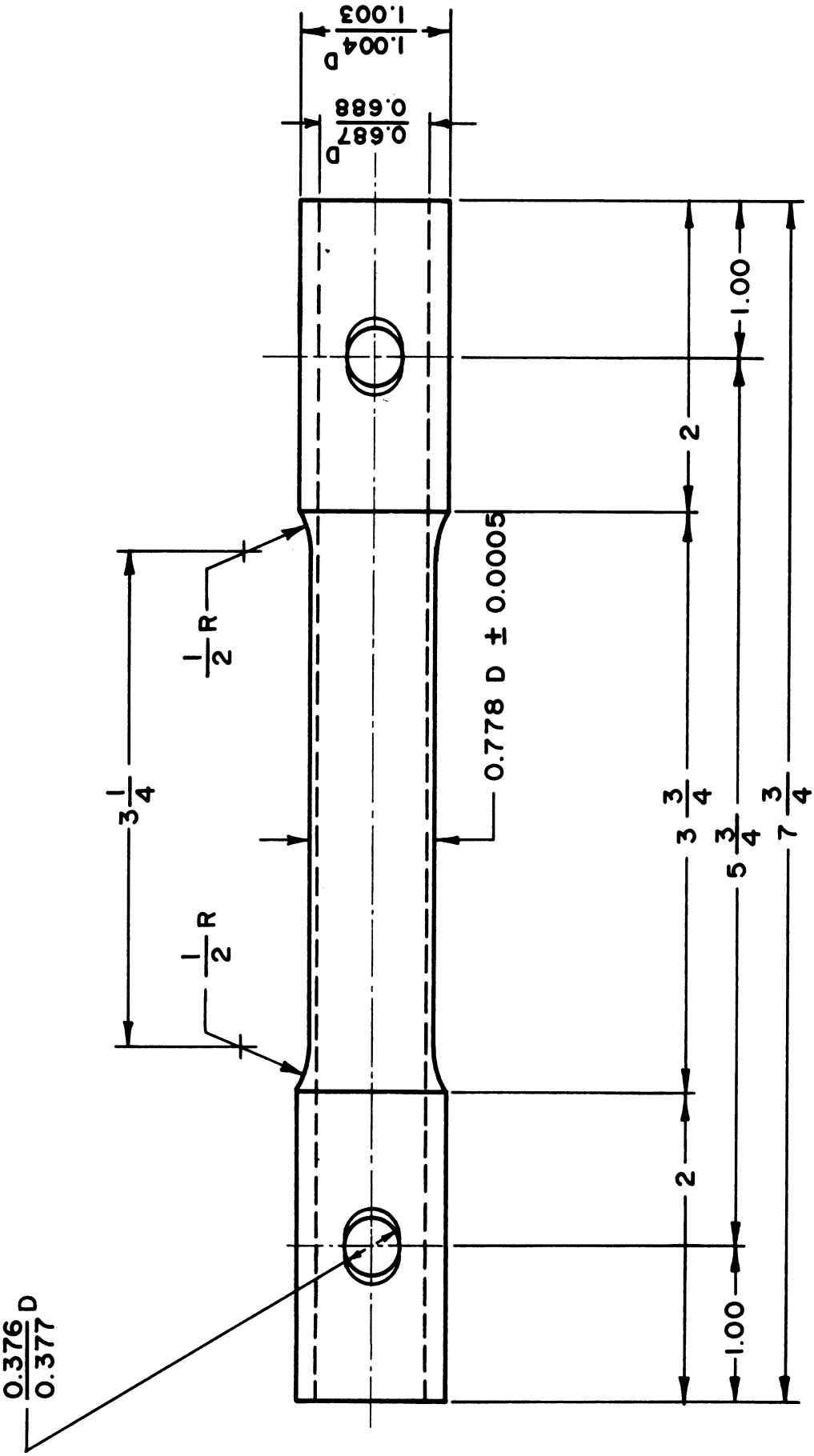

Figure 1. Sketch of tubular specimen.

bined load testing machine. A complete description of the machine is presented in Chapter II but it is noted in particular here that the ratio of axial force to torque or axial force to internal pressure can be held constant throughout a test run by a unique mechanico-hydraulic system. Thus for the most part loading paths are what are so-called radial loading paths.

The thin-walled tubular specimen has been used by many investigators. This sort of test specimen is advantageous since stresses are statically determinate to a good approximation for axial loading, torque, and internal pressure. In a material evaluation, it is of course essential that one be able to determine the state of stress directly from the applied loads without reference to the material properties.

For reference purposes, a sketch of the cylindrical coordinate system appropriate to the tubular specimen is presented in Figure 2. The stresses which are uniform throughout the reduced section, are computed in accordance with the usual assumptions for the membrane stresses in a thin-walled tube, i.e., plane stress is assumed. For a test in which axial force and torque are applied, the stresses in the reduced section of the specimen are

$$\sigma_z = \frac{P}{2\pi r t}$$

$$\tau_{\theta z} = \frac{T}{2\pi r^2 t}$$

$$\sigma_r = \sigma_\theta = \tau_{\theta r} = \tau_{rz} = 0$$

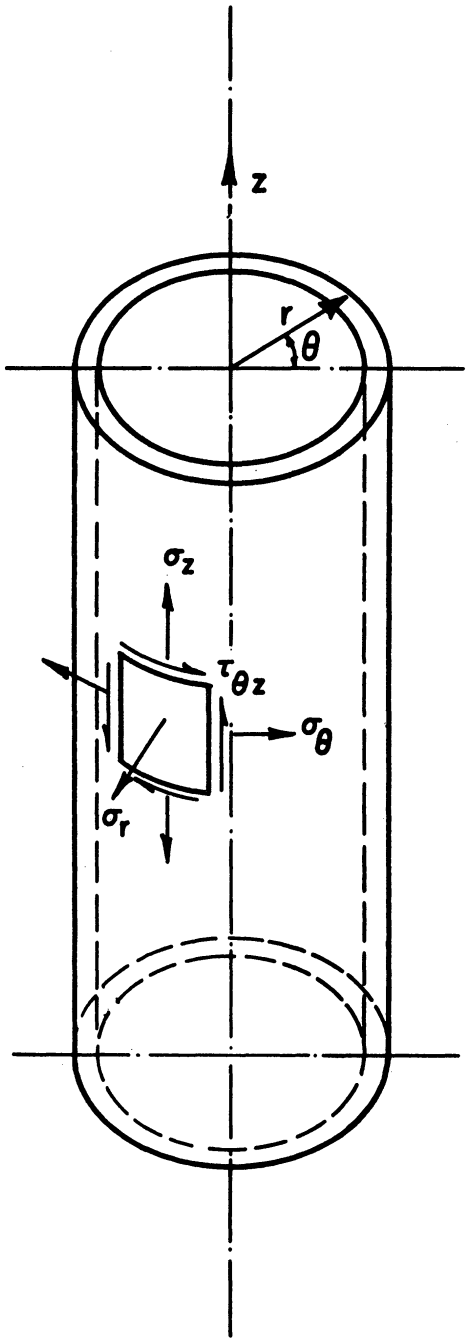

Figure 2. Coordinate system and stresses in tube.

where:

r = mean radius of the reduced section

t = wall thickness

P = axial force along z-axis

T = torque about z-axis.

Alternatively for a test combining axial force and internal pressure, the stresses are

$$\sigma_z = \frac{P}{2\pi r t} + \frac{pr}{2t}$$

$$\sigma_\theta = \frac{pr}{t}$$

$$\sigma_r = \tau_{r\theta} = \tau_{\theta z} = \tau_{rz} = 0$$

where p = internal pressure. When internal pressure is present, $\sigma_r \approx 1/8\ \sigma_\theta$ at the inner surface of the tube. This suggests that stress combinations where σ_z is much less than σ_θ be avoided since the membrane assumption of $\sigma_r = 0$ relative to the other stresses would not be acceptable in that case. Consequently the smallest ratio used was $\sigma_z = 1/2\ \sigma_\theta$ which occurs for internal pressure without axial force.

In combined axial force and torque, σ_r is a principal stress since $\tau_{r\theta} = \tau_{rz} = 0$ and the principal directions lying in the θ-z plane depend on the ratio of σ_z to $\tau_{\theta z}$. The combined load testing machine should hold this ratio fixed in a given test and the principal directions of stress would then remain fixed relative to an element of the material.

For combined axial force and internal pressure, the stresses σ_r,

σ_θ, and σ_z are the principal stresses for all combinations of these loads since $\tau_{r\theta} = \tau_{\theta z} = \tau_{rz} = 0$ in all of them.

CHAPTER II

EXPERIMENTAL APPARATUS AND TECHNIQUE

This chapter contains a discussion of the specimen material, the loading apparatus and the strain measuring technique which were employed. It will be useful to discuss some of these items before the more theoretical aspects of the research are considered. Thus those aspects of experimental procedure which can logically be separated from the data analysis are presented here.

MATERIAL

All of the tubular specimens used in this research were machined from solid cylinders, about 1-1/8-inch in diameter, of cast Zamak-3 zinc alloy. The solid cylinders were cast in two equal batches, totaling 154 altogether. The casting procedure was to heat the melt of commercially available Zamak-3 pigs to 1100°F in an induction furnace and to pour in graphite split-molds. Molds were machined from solid blocks of graphite and were sufficient in number that five cylinders could be cast in each pour. No effort was made to preheat the molds. A relatively large proportion of sound castings was obtained and those castings containing blow-holes were rejected by visual inspection either before or during machining.

The microstructure of this material appears to be stable since no changes in a small sample from a cast cylinder have been observed in

the period since July, 1960. A photomicrograph of an area of a cast cylinder in the region of a specimen cross-section is shown in Figure 3.

COMBINED LOAD TESTING MACHINE

This apparatus was developed as a part of the research program at The University of Michigan under the sponsorship of the United States Air Force of which this dissertation is also a part. The author does not take credit for developing the testing machine.

Figure 4 shows the main features of this unique machine which is essentially a "loading" device rather than a "straining" device, i.e., loads are achieved by hydraulic rather than mechanical means. Axial forces are obtained on a specimen inserted in the grips by introducing a controlled pressure to the tension-compression cylinder. The load in the cylinder is transmitted along the vertical center shaft through the thrust bearing to the specimen. The thrust bearing is actually a set of roller thrust bearings which prevent transmission of torsional loads to the tension-compression cylinder above. Torque is applied to the vertical center shaft and in turn the specimen by introducing a controlled pressure to the torsion cylinder. The force in the cylinder is transmitted through a cable to a wheel fastened to the central shaft, thus producing a torque. This torque is a true couple since a cable also runs from the opposite side of the central wheel to the "floating" frame. Both cables are attached to the "floating" frame, one through the torsion cylinder and the other directly, so that the resultant

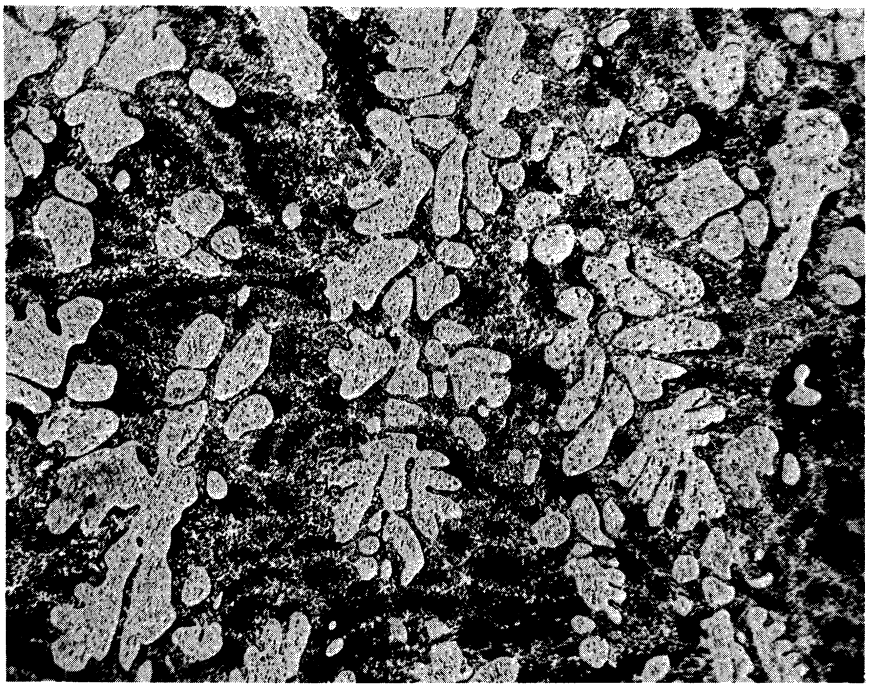

250X

Figure 3. Photomicrograph of Zamak-3.

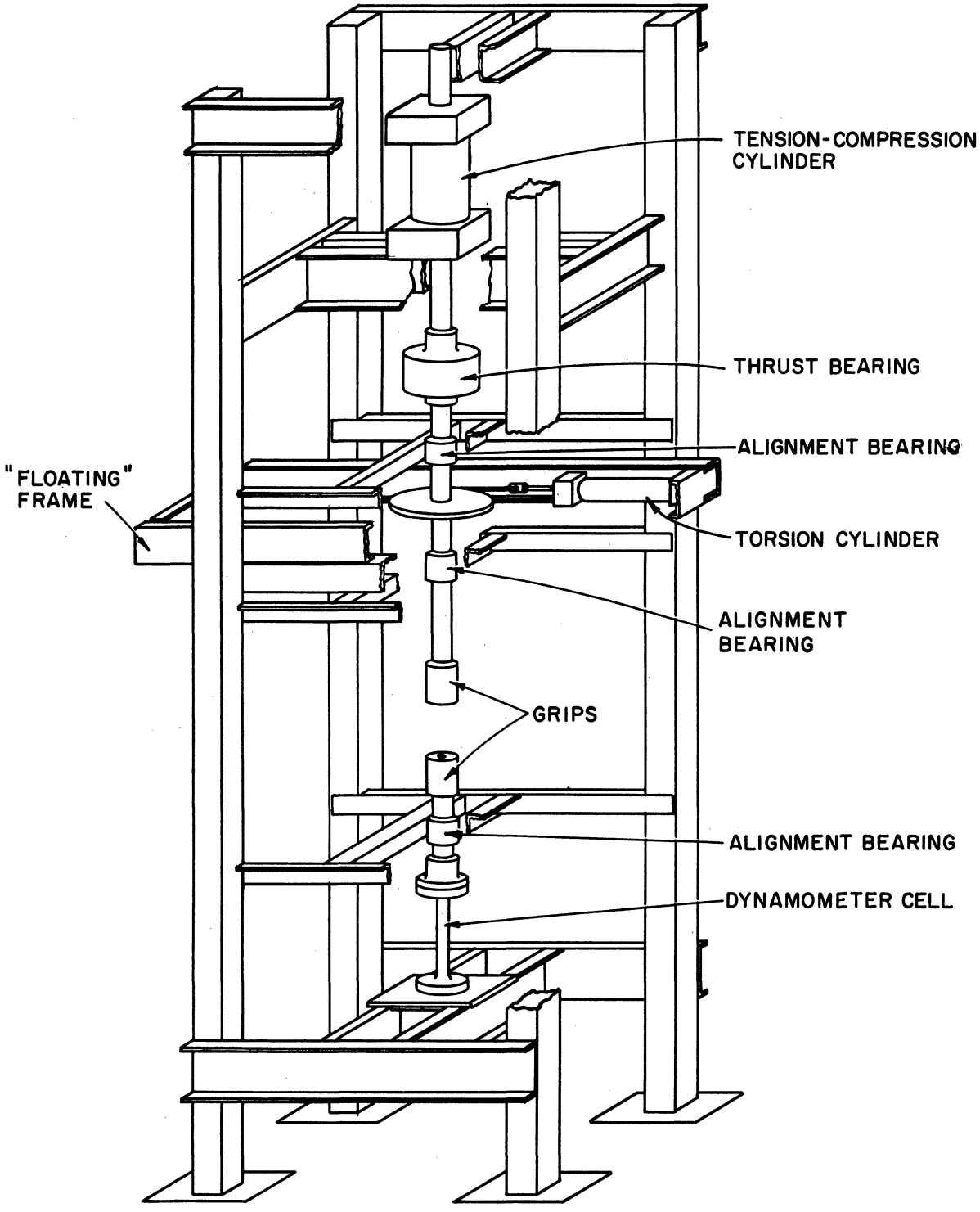

Figure 4. Combined load testing machine.

lateral force on the central shaft is zero. External lateral reactions on the "floating" frame are carried by the structural frame of the machine. The specimen grips are designed so as to allow a path for hydraulic fluid which furnishes the internal pressure to reach the specimen. Tensions or compressions up to 10,000 pounds, torques as high as 5,000 inch-pounds, and internal pressures as high as 4,000 psi are possible.

The supply pressure to the hydraulic cylinders and for internal pressure in the specimen is controlled by specially designed valves. The controlled pressure from these valves is proportional to the force acting on the top of a shaft penetrating the top of the valve body.

The load proportioning system, shown in Figure 5, consists of a system of levers which apply forces to the shafts on the various control valves. A single force at the end of lever A actuates the entire system and this force is obtained by filling a tank with water at a desired rate. By moving lever C relative to lever B, various ratios of axial force to torsion or of axial force to internal pressure can be obtained.

Two entirely separate hydraulic systems are provided, as shown in Figure 6. The low-pressure system operates at about 1,000 psi and actuates the tension-compression cylinder and the torsion cylinder. The high-pressure system can reach pressures of 5,000 psi and supplies the pressure in the internal cavity of the specimen.

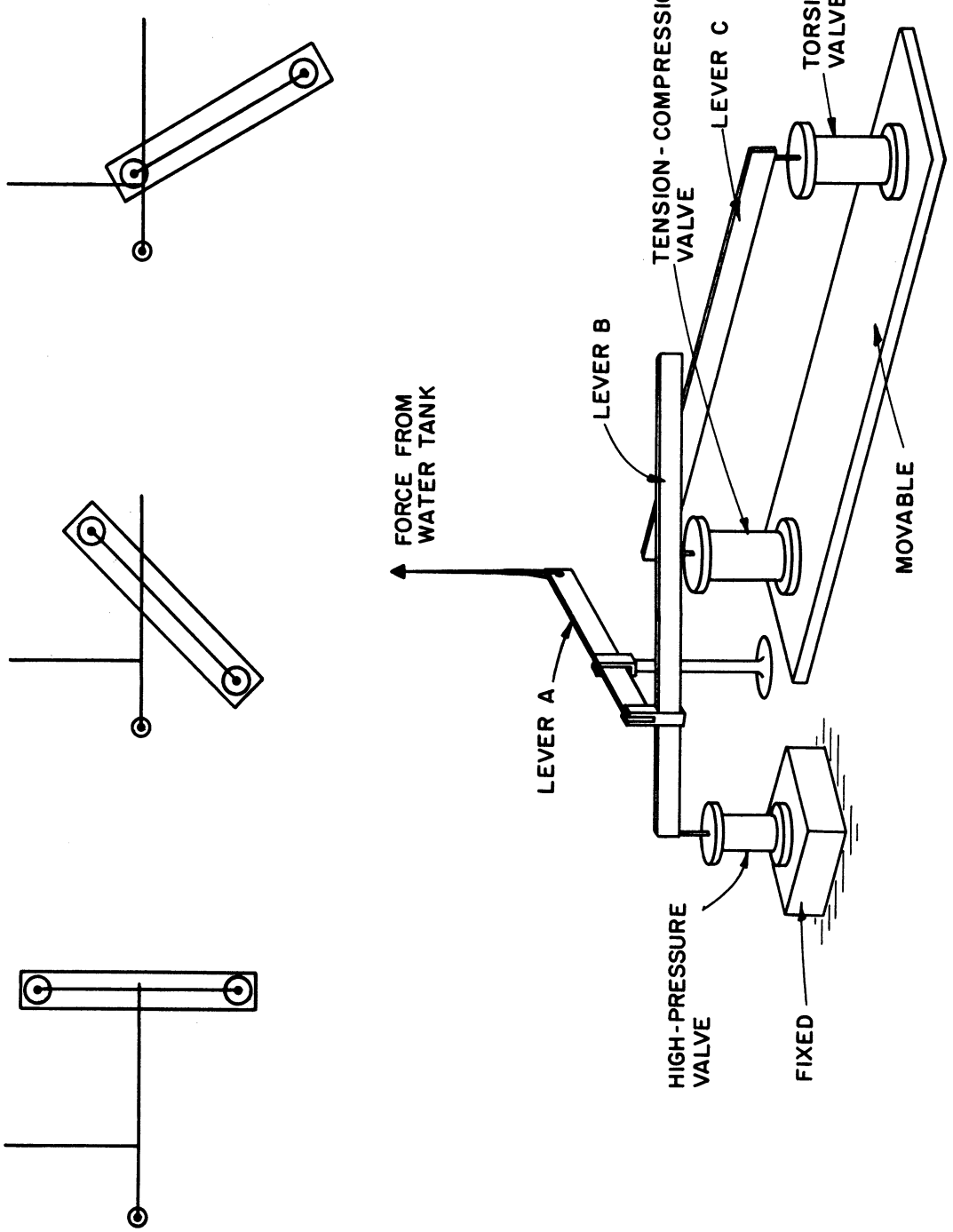

Figure 5. Load proportioning system.

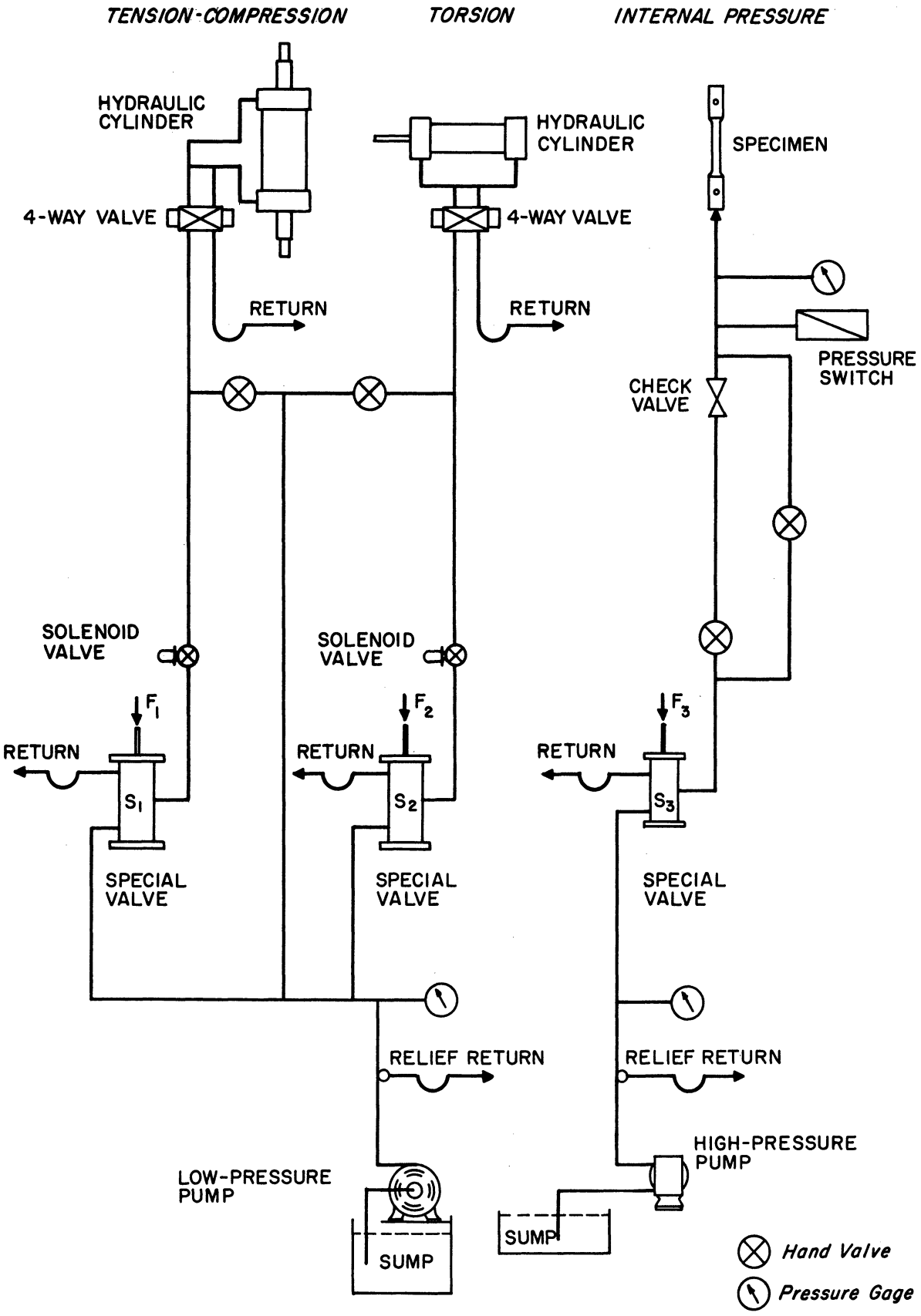

Figure 6. Hydraulic diagram for the combined load testing machine.

LOAD MEASUREMENT

Axial force and torque were measured by means of a strain-gage dynamometer, specially designed for this apparatus. In essence it is a tubular member with flanged ends. Two Wheatstone bridge arrangements of four electrical resistance strain-gages each are affixed to the tube. The torque measuring bridge consists of two elements at 45° to the tube axis and two elements at 135° to the tube axis while the axial load measuring bridge consists of two axial elements and two circumferential elements. These elements are introduced into the bridge hook-up so as to provide temperature compensation and to avoid interaction between axial loading and torque measurement and vice versa. The outputs of the strain-gage bridges can be read on a strain indicator or can be recorded. In addition to the dynamometer just described, a standard Baldwin SR-4 Load Cell, Type U-1, of 5,000 pounds capacity was used axial force measurement in many of the tests in combined tension and internal pressure.

Internal pressure in the specimen was read on a 5,000 psi, Bourdon tube type test gage manufactured by United States Gage Company. This gage has a 16-inch dial with 10 psi divisions and a tolerance of ± 5 percent of the current reading.

STRAIN-MEASUREMENT

Measurements of strain on the test specimen were made by means of Tatnall C15-141-B, foil-type strain gages which were attached to the specimen with Eastman 910 cement. This combination of gage and cement

was selected since it permits measurement of strains as large as 0.04. Thus for specimens made of Zamak-3, strains could be measured throughout the entire plastic range; in most tests the strains at the instant of fracture were observed. Temperature compensation was provided by similar strain gages attached to a piece of Zamak-3 placed adjacent to the specimen.

Strains from the test specimen, and in many cases the output from one of the dynamometer bridges were recorded on a Heiland Model 712-B recording oscillograph equipped with Heiland No. 40-1000 galvanometers and a Heiland Model 119B-1 bridge balance unit. This combination provided adequate sensitivity for determining the measurable quantities during the tests.

TEMPERATURE CONTROL

This research program involved tests at both 78°F and 32°F. The higher temperature is essentially the room temperature of the laboratory and measured specimen temperatures were within + 3°F of this value. Tests at 32°F were made by immersing the specimen and grips in a tank or jacket containing an ice-water bath. By this technique uniform specimen temperatures could be maintained for fairly long periods of time (1-2 hours) and the conditions could be reproduced from test to test without difficulty.

CHAPTER III

THEORETICAL PREDICTIONS OF STRAIN-HARDENING BEHAVIOR IN THE OCTAHEDRAL PLANE

In this chapter, the implications of three contemporary theories of strain-hardening and appropriate collateral work are reviewed. These theories are then used to predict the motion of the yield surface in principal stress space as strain-hardening occurs. To aid in the experimental evaluation to follow some consideration is given to development of a plausible type of anisotropy and its expected effects.

THE MATERIAL MODEL AND THE OCTAHEDRAL PLANE

For a rigid-strain hardening material, no strain (i.e. no plastic strain) occurs for states of stress which do not satisfy the initial yield condition or which lie inside the initial yield surface. If a stress path reaches the initial yield surface but then moves tangentially to the surface, the yield surface does not move or in other words strain-hardening does not occur and the material remains rigid. However when a stress state point reaches the initial yield surface and the ensuing stress increment tends to cross the yield surface, the yield surface moves in some prescribed manner corresponding to strain hardening and (plastic) strains are produced as long as the state point remains in contact with the yield surface. Now if the stress is removed and another stress path is considered, strain hardening or motion of the yield sur-

face and further (plastic) strain will occur only when this new stress path tends to cross the previous final position of the yield surface.

Assuming that the material to be considered is isotropic initially, the reference directions may be chosen at random and the principal directions of the stress tensor may be chosen for convenience. Thus yield conditions may be stated in terms of the principal stresses and the yield surface presented in a principal stress space in a perfectly general manner. In addition, assume that yielding is independent of mean stress or the hydrostatic component of the state of stress defined by

$$\sigma = \frac{\sigma_1 + \sigma_2 + \sigma_3}{3} \tag{3.1}$$

where σ_1, σ_2, and σ_3 are the principal stresses. The result of the latter assumption is that the yield surface in principal stress space is a cylinder with generators parallel to the octahedral ($\sigma_1 = \sigma_2 = \sigma_3$) axis. The latter assumption follows from the observation that a hydrostatic state of stress, in which all principal stresses are equal, does not produce yielding.

In view of these two assumptions, a typical octahedral plane, for which

$$\sigma_1 + \sigma_2 + \sigma_3 = \text{Constant} \tag{3.2}$$

and the normal is in the direction of the octahedral axis, would intersect the yield surface at right angles. Each intersection of octahedral plane and yield surface would be identical so any octahedral plane

may be used. Presentation of results on an octahedral plane, then, is not only a convenience but also a means of confirming or denying that yield is independent of mean stress.

INITIAL YIELDING

The general characteristics of an initial yield condition will now be considered.

Since yielding has been assumed independent of mean stress, it follows that the yield condition can be expressed as a function of the invariants of the stress deviator tensor or

$$F(J_2, J_3) = k^2 \tag{3.3}$$

where

$$J_2 = \frac{1}{2} s_{ij} s_{ij}$$
$$J_3 = \frac{1}{3} s_{ij} s_{jk} s_{ki}$$
$$s_{ij} = \sigma_{ij} - \delta_{ij} \sigma.$$

The general character of a yield condition, entirely apart from the preceding assumptions, can be derived the "fundamental postulate" for a stable plastic material enunciated by Drucker.[1,2] From this postulate one deduces that the yield surface must be convex. For convex yield surfaces it can be shown that the plastic strain increment vector must be normal to the yield surface at the state point or

$$d\varepsilon_{ij} = \lambda \frac{\partial F}{\partial \sigma_{ij}} \tag{3.4}$$

where $d\epsilon_{ij}$ is the plastic strain increment and $F(\sigma_{ij})$ is the yield function. Equation (3.4) is, of course, the well-known flow rule which was postulated earlier by von Mises[3] without proof.

The flow rule will give the result that

$$d\varepsilon_1 + d\varepsilon_2 + d\varepsilon_3 = 0 \tag{3.5}$$

for any yield condition which is independent of mean stress. Since the strain increment is normal to the yield surface it would be expected to lie in an octahedral plane.

In accord with the observed behavior of most wrought metals, it is assumed that the yield stresses in simple tension and simple compression are the same or that the yield process is sensitive to the magnitude of the stress and not its sign.

Initial yield criteria which are consistent with the preceding restrictions will now be enumerated. These are shown plotted in the octahedral plane in Figure 7. The von Mises[4] criterion for initial yielding, in terms of the principal stresses, is

$$(\sigma_1 - \sigma_2)^2 + (\sigma_2 - \sigma_3)^2 + (\sigma_1 - \sigma_3)^2 = 2\sigma_0^2 \tag{3.6}$$

where σ_0 is the initial yield stress in simple tension. In essence this condition states that $J_2 = k^2$. It plots as a circle of radius $\sqrt{2/3}\ \sigma_0$ in the octahedral plane.

A criterion based on a limiting value of the maximum shearing stress was first proposed by Tresca[5] and in terms of the principal stress is

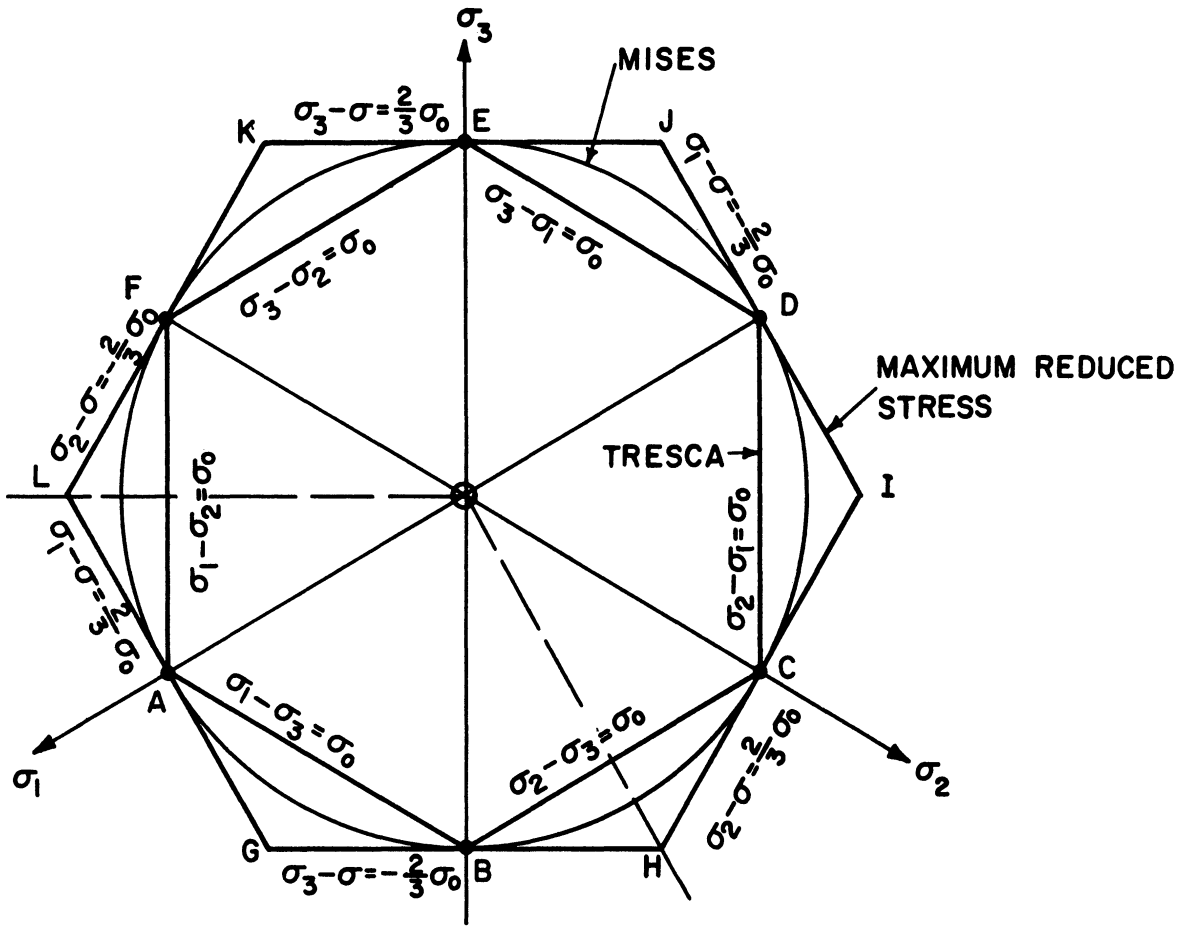

Figure 7. Various initial yield criteria in the octahedral plane.

$$\text{Max}\left\{|\sigma_1-\sigma_2|, |\sigma_2-\sigma_3|, |\sigma_1-\sigma_3|\right\} = \sigma_o \quad . \tag{3.7}$$

The hexagon ABCDEFA corresponds to the Tresca criterion.

Recently, Haythornthwaite[6] has proposed a maximum "reduced" stress criterion primarily for use as a bounding yield criterion when relatively few data on yielding are available. However, this feature will prove useful later. In terms of the principal stresses, the criterion is stated

$$\text{Max}\left\{|\sigma_1-\sigma|, |\sigma_2-\sigma|, |\sigma_3-\sigma|\right\} = \frac{2}{3}\sigma_o \tag{3.8}$$

where σ is defined by Equation (3.1). This criterion states that yielding occurs when the absolute value of the largest principal stress deviator reaches a limiting value. It is represented by the external hexagon GHIJKLG.

The choice of pure tension as a point of agreement between the various theories was arbitrary. By so doing however, the bounding properties of the Tresca criterion and the maximum reduced stress criterion are shown. If only tensile yield data were available the criteria would have to coincide at the points shown and Tresca would represent the minimum curve through the points while the maximum reduced stress would represent the maximum curve through the points.

ISOTROPIC HARDENING

Following a discussion by Hill,[7] the isotropic hardening theory

assumes that the yield surface, say in principal stress space, merely enlarges as the plastic strain increases. The enlargement occurs in such a manner that the yield surface, which was initially symmetric with respect to the origin, remains symmetric. It follows from this description that isotropic hardening theory would predict no Bauschinger effect. The final position of the yield surface after hardening is assumed to depend only on the final state of plastic strain and not on the path.

For this theory, then, the initial yield surface might be expressed in a 9-space of the components of the stress tensor as

$$F(\sigma_{ij}) = k^2 \tag{3.9}$$

and subsequent yield surfaces after hardening has occurred as

$$F(\sigma_{ij}) = c^2 \geq k^2 \quad . \tag{3.10}$$

To obtain a stress increment-strain increment relationship, note that when the stress state point moves on the yield surface,

$$dF = 0 = \frac{\partial F}{\partial \sigma_{ij}} d\sigma_{ij} \quad . \tag{3.11}$$

For a strain-hardening material, the plastic strain would be zero for such a "neutral" change in stress suggesting for dF > 0 the form

$$d\varepsilon_{ij} = G_{ij}\, dF \tag{3.12}$$

G_{ij} is a tensor having the same basic properties that $d\varepsilon_{ij}$ has. Now by use of the flow rule (3.4), and Equations (3.11) and (3.12) we obtain

$$d\varepsilon_{ij} = Q \frac{\partial F}{\partial \sigma_{ij}} \cdot \frac{\partial F}{\partial \sigma_{kl}} d\sigma_{kl} \tag{3.13}$$

where Q is a scalar function which may depend on the stress, the strain, and their histories. Drucker[2] demonstrates from stability in the small that Q is not a function of $d\sigma_{ij}$.

Interpreting the preceding geometrically, Equation (3.11) gives a quantity proportional to the magnitude of motion of the yield surface for given stress increment $d\sigma_{ij}$. By Equation (3.12) this motion of the yield surface proceeds in the direction of the plastic strain increment vector or in the direction of the outward normal to the yield surface at the current stress state point. To predict the motion of the yield surface during strain hardening one need know only the stress increment and the direction of the normal. The stress increment, in terms of the principal stresses, has the components $d\sigma_1$, $d\sigma_2$, and $d\sigma_3$ which represent the incremental changes as the stress state point proceeds beyond the initial yield surface.

To obtain the values of the components of the plastic strain increment, flow laws are needed which can be found by the use of Equation (3.13) and the various yield criteria.

For the Mises criterion, Equation (3.6) the following flow laws are obtained:

$$d\varepsilon_1 = Q\left[2(2\sigma_1-\sigma_2-\sigma_3)\right]\left[2(2\sigma_1-\sigma_2-\sigma_3)d\sigma_1 + 2(2\sigma_2-\sigma_1-\sigma_3)d\sigma_2 + 2(2\sigma_3-\sigma_1-\sigma_2)\,d\sigma_3\right]$$

$$d\varepsilon_2 = Q[2(2\sigma_2-\sigma_1-\sigma_3)][2(2\sigma_1-\sigma_2-\sigma_3)d\sigma_1 + 2(2\sigma_2-\sigma_1-\sigma_3)d\sigma_2 + 2(2\sigma_3-\sigma_1-\sigma_2)d\sigma_3] \quad (3.14)$$

$$d\varepsilon_3 = Q[2(2\sigma_3-\sigma_1-\sigma_2)][2(2\sigma_1-\sigma_2-\sigma_3)d\sigma_1 + 2(2\sigma_2-\sigma_1-\sigma_3)d\sigma_2 + 2(2\sigma_3-\sigma_1-\sigma_2)d\sigma_3] .$$

The second bracketed term in each equation relates to the motion of the yield surface (a radial expansion) during the incremental stress changes $d\sigma_1$, $d\sigma_2$, and $d\sigma_3$. It is apparent that computation of plastic strain increments from Equation (3.14) might be somewhat inconvenient. For this reason, yield criteria having plane sides, such as Tresca and maximum reduced stress, may be found more tractable.

Consider the flow laws for the Tresca criterion, Equation (3.7). For a stress state point which contacts and remains in contact with side AB, for example, see Figure 7, the flow laws are

$$\begin{aligned} d\varepsilon_1 &= Q(d\sigma_1 - d\sigma_3) \\ -d\varepsilon_3 &= Q(d\sigma_1 - d\sigma_3) \\ d\varepsilon_2 &= 0 \end{aligned} \quad (3.15)$$

since on that side $F = \sigma_1 - \sigma_3 = \sigma_0$. Thus it can be seen that the strain increments would be given by Equation (3.15) as long as the stress point remained in contact with side AB. The values are independent of an exact stress path but with the latter restriction. According to the isotropic hardening theory, side AB moves in the direction of the outward normal a distance proportional to $dF = d\sigma_1 - d\sigma_3$ and the other

sides will move the same distance along their outward normals.

Considering now the maximum reduced stress criterion, Equation (3.8), the flow laws for a stress state point on side LG are

$$\begin{aligned} d\varepsilon_1 &= Q\left(\frac{2}{9}\right)(2d\sigma_1 - d\sigma_2 - d\sigma_3) \\ d\varepsilon_2 &= Q\left(-\frac{1}{9}\right)(2d\sigma_1 - d\sigma_2 - d\sigma_3) \\ d\varepsilon_3 &= Q\left(-\frac{1}{9}\right)(2d\sigma_1 - d\sigma_2 - d\sigma_3) \,. \end{aligned} \tag{3.16}$$

As with the Tresca criterion, the plastic strain increments are partially independent of the stress path. Motion of the side LG during hardening would be along the outward normal in an amount proportional to $(2d\sigma_1 - d\sigma_2 - d\sigma_3)$ and by the isotropic hardening hypothesis the other sides move along their outward normals like amounts.

Figure 8 presents geometrically a typical prediction of isotropic hardening theory for the stress path 01. The solid circle and hexagons represent the final positions of the various yield surfaces or loading surfaces presuming loading is stopped at point 1. Relating this to the tube test, if σ_3 is treated as σ_r and $\sigma_1 = \sigma_z$ and $\sigma_2 = \sigma_\theta$, then the path 01 could be produced by a combination of axial tensile force and internal pressure.

KINEMATIC HARDENING

The kinematic theory of hardening, originally proposed by Prager[8] and discussed extensively by Shield and Ziegler[9] states that, in a 9-space, the initial yield surface

$$F(\sigma_{ij}) = k^2 \tag{3.9}$$

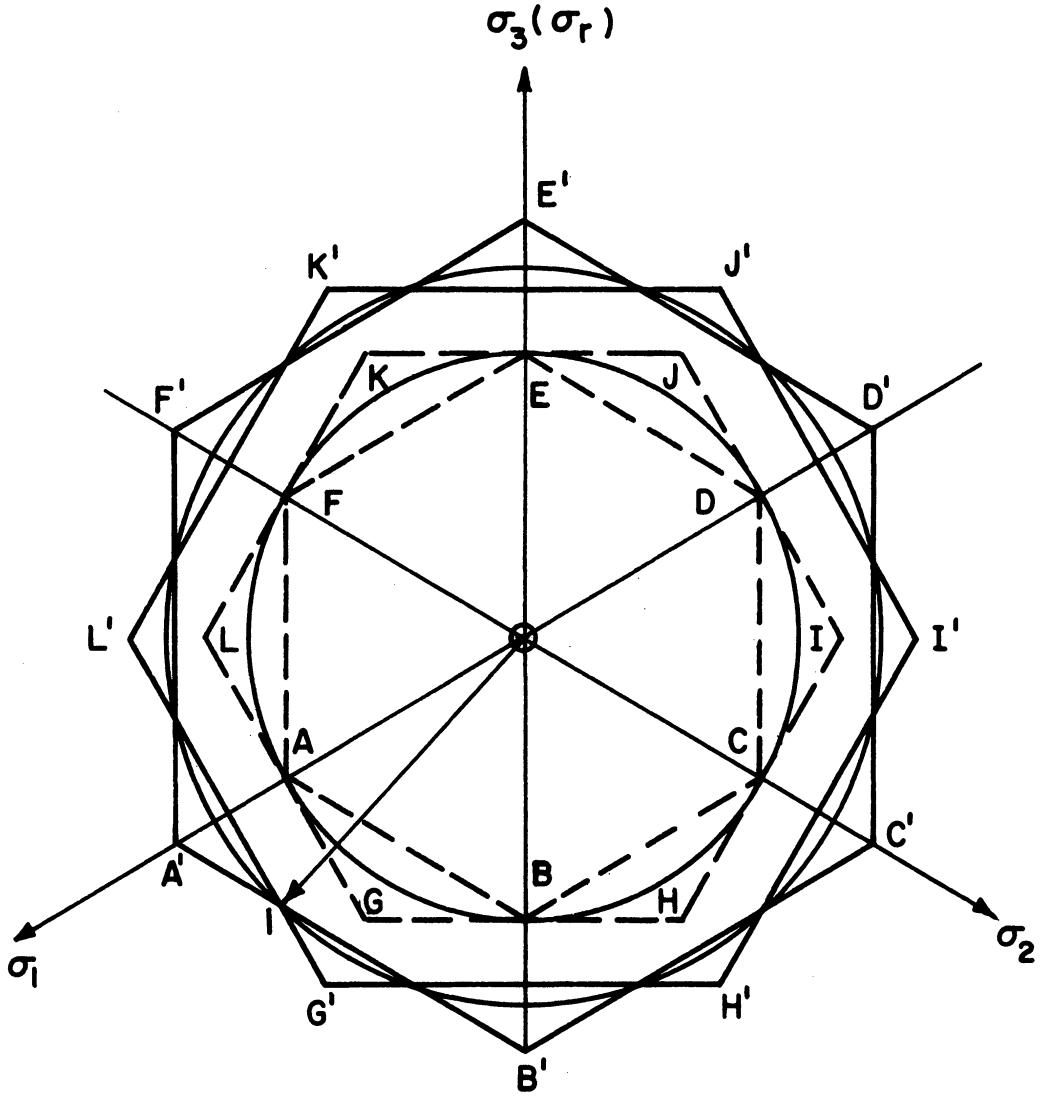

Figure 8. Isotropic hardening for stress path Ol.

becomes after plastic flow

$$F(\sigma_{ij} - \alpha_{ij}) = k^2 \quad . \tag{3.17}$$

The flow rule (3.4) is assumed to apply and the yield surface is assumed to translate without changing the form of $F(\sigma_{ij})$. The tensor α_{ij} represents the rigid body translation of the yield surface which occurs in the direction of $d\epsilon_{ij}$ (i.e., the outward drawn normal to the yield surface). Thus

$$d\alpha_{ij} = c\, d\epsilon_{ij} \quad . \tag{3.18}$$

This strain hardening theory gives predictions of material behavior which include the Bauschinger effect.

Using the condition that the state point remains on the translating yield surface, one is led to the requirement that

$$(d\sigma_{ij} - d\alpha_{ij}) \frac{\partial F}{\partial \sigma_{ij}} = 0 \quad . \tag{3.19}$$

Another way of stating the foregoing requirement is that $d\alpha_{ij}$ is equal to the projection of $d\sigma_{ij}$ on the normal to the yield surface at the initial stress state point. Combining Equation (3.19) with the flow rule, Equation (3.4), and with the condition expressed by Equation (3.18) gives

$$d\epsilon_{ij} = \frac{1}{c} \frac{1}{\frac{\partial F}{\partial \sigma_{mn}} \cdot \frac{\partial F}{\partial \sigma_{mn}}} \cdot \frac{\partial F}{\partial \sigma_{ij}} \frac{\partial F}{\partial \sigma_{kl}} d\sigma_{kl} \quad . \tag{3.20}$$

This equation, like Equation (3.13) in isotropic hardening, indicates

that plastic strain increments and stress increments are linearly related.

Since α_{ij} is not necessarily an isotropic tensor (i.e., components invariant with rotation), it is possible that an initially isotropic material may become anisotropic with strain hardening in view of Equation (3.17). However, as suggested by Shield and Ziegler let us restrict the loading so that the principal axes of the stress tensor are fixed in an element of the material during plastic straining. These principal axes can then be treated as the reference axes. For an initially isotropic material, Equation (3.9) holds and $\alpha_{ij} = 0$. The flow rule then gives the information that

$$d\varepsilon_{ij} = 0 \quad (i \neq j) \quad , \tag{3.21}$$

Since the principal axes of the stress tensor and plastic strain increment tensors coincide. Equation (3.21) would not be correct if the reference axes were not the principal axes of stress during the initial strain increment. From Equation (3.18) it follows that

$$d\alpha_{ij} = 0 \quad (i \neq j) \tag{3.22}$$

under these conditions and principal axes of stress remain principal axes during hardening.

It has already been noted that the principal axes of stress in the tubular specimen are fixed in an element of the material for all combinations of axial force and internal pressure. When axial force is

combined with torque, the principal axes of stress are also fixed as long as the control system maintains a constant ratio of axial force to torque.

For convenience, let us restate the kinematic hardening theory in terms of the principal stresses as follows:

$$F(\sigma_1, \sigma_2, \sigma_3) = k^2 \tag{3.23}$$

before hardening becomes

$$F(\sigma_1 - c\varepsilon_1, \sigma_2 - c\varepsilon_2, \sigma_3 - c\varepsilon_3) = k^2 \tag{3.24}$$

after hardening. The quantities $c\epsilon_1$, $c\epsilon_2$, and $c\epsilon_3$ represent the translation of the yield surface as a rigid body in principal stress space, the translation occurring in the direction of the outward normal to the yield surface at the stress state point.

As would be expected from the observed similarity between Equations (3.13) and (3.20), the flow laws for kinematic hardening are quite similar to those for isotropic hardening. For the von Mises criterion of yielding we obtain

$$d\varepsilon_1 = \frac{1}{c} \cdot \frac{1}{24\sigma_0^2} [2(2\sigma_1 - \sigma_2 - \sigma_3)][2(2\sigma_1 - \sigma_2 - \sigma_3)d\sigma_1 + 2(2\sigma_2 - \sigma_1 - \sigma_3)d\sigma_2 + 2(2\sigma_3 - \sigma_1 - \sigma_2)d\sigma_3] . \tag{3.25}$$

$d\epsilon_2$ and $d\epsilon_3$ have similar form, the only differences arising in the first bracketed term. Comparing this result with Equations (3.14) for isotropic hardening, it is apparent that the flow laws for the two theories

differ in the nature of the initial constants and are identical in other respects. This renders it unnecessary to state again all of the flow laws as done in Equation (3.14) for isotropic hardening. It should be noted, however, that the components $cd\epsilon_1$, $cd\epsilon_2$, and $cd\epsilon_3$ of rigid body motion of the yield surface also represent the motion of the center of the circle which represents the von Mises criterion in the octahedral plane.

Figure 9 shows the motions of various yield surfaces as predicted by kinematic hardening theory for the stress path 01. The dashed circle represents the initial position of the Mises circle and the solid circle represents the Mises condition after hardening as caused by stress-path 01. Vector 03 represents the total amount of this motion, $d\alpha_{ij}$, which in view of Equation (3.18) and (3.20) has in general the components

$$d\alpha_{ij} = \frac{1}{\frac{\partial F}{\partial \sigma_{mn}} \frac{\partial F}{\partial \sigma_{mn}}} \cdot \frac{\partial F}{\partial \sigma_{ij}} \cdot \frac{\partial F}{\partial \sigma_{kl}} d\sigma_{kl} \quad . \tag{3.26}$$

If one wishes to obtain the total distance the yield surface moves rather than the components, consider the problem in the vector sense in principal stress space. $d\sigma_{ij}$ is then a vector and its magnitude in the direction normal to the yield surface is obtained by performing the dot product between $d\sigma_{ij}$ and a unit vector in the direction of the normal, i.e., a "unitized" gradient vector $\frac{\partial F}{\partial \sigma_{ij}} \frac{1}{\left(\frac{\partial F}{\partial \sigma_{mn}} \cdot \frac{\partial F}{\partial \sigma_{mn}}\right)}$. With this in mind one obtains for the distance moved

$$\overline{d\alpha_{ij}} = \frac{1}{\left(\frac{\partial F}{\partial \sigma_{mn}} \frac{\partial F}{\partial \sigma_{mn}}\right)^{1/2}} \cdot \frac{\partial F}{\partial \sigma_{kl}} d\sigma_{kl} \tag{3.27}$$

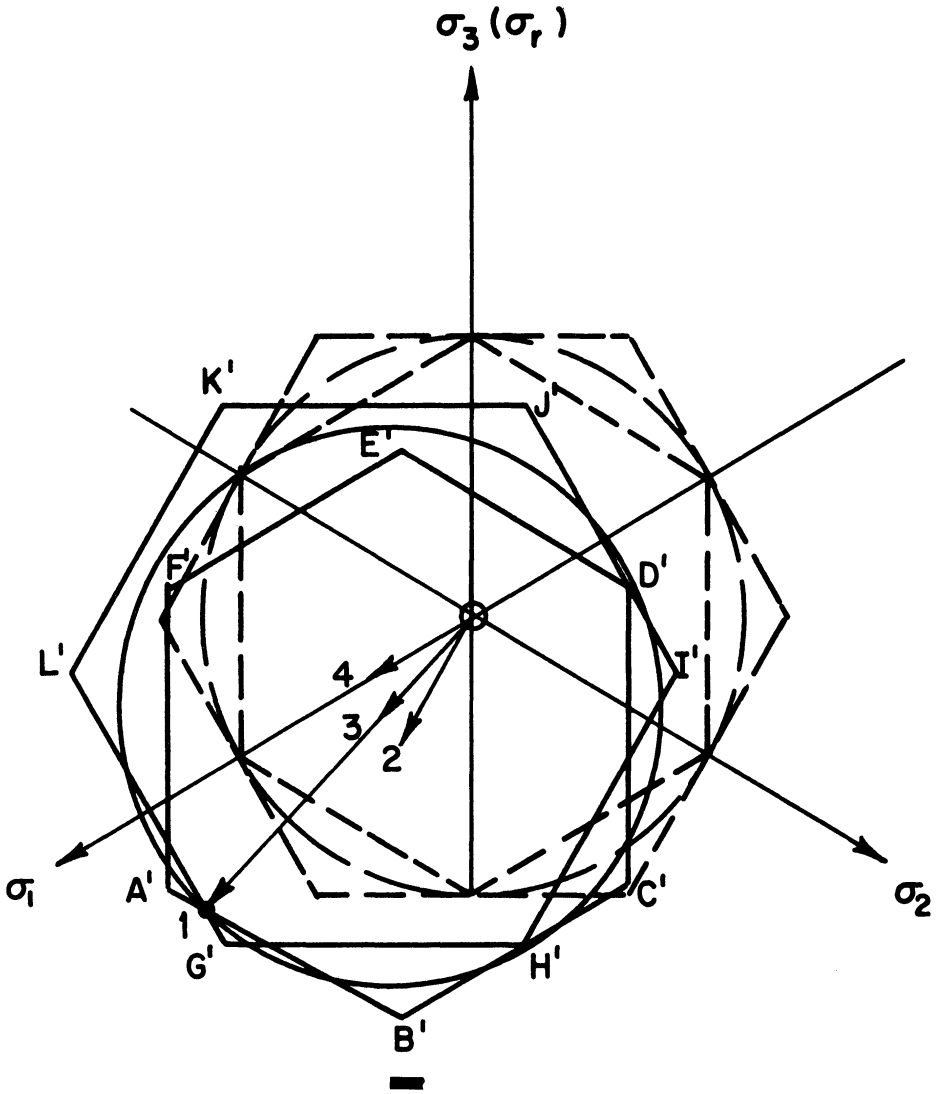

Figure 9. Kinematic hardening for stress path 01.

Thus for the von Mises criterion the distance $\overline{03}$ in the octahedral plane is given by

$$\overline{03} = d\alpha_{ij} = \frac{1}{\sqrt{6}\,\sigma_0}\left[(2\sigma_1-\sigma_2-\sigma_3)d\sigma_1+(2\sigma_2-\sigma_1-\sigma_3)d\sigma_2 + (2\sigma_3-\sigma_1-\sigma_2)d\sigma_3\right] \tag{3.28}$$

for the motion beyond the initial yield surface. The preceding analysis for the von Mises yield criterion is valid only for incremental motions of the yield surface or for incremental changes in the state of stress beyond the initial yield surface.

Now consider the situation where the Tresca yield criterion applies and the stress state point remains on side AB, see Figure 9. The flow laws or stress-strain laws from Equations (3.7) and (3.20) are

$$\begin{aligned} d\varepsilon_1 &= \frac{1}{c}\cdot\frac{1}{2}(d\sigma_1 - d\sigma_3) \\ -d\varepsilon_3 &= \frac{1}{c}\cdot\frac{1}{2}(d\sigma_1 - d\sigma_3) \\ d\varepsilon_2 &= 0 \end{aligned} \tag{3.29}$$

since on side AB, $F(\sigma_{ij}) = \sigma_1 - \sigma_3 = \sigma_0$. During hardening the components of motion of the yield surface would be $cd\epsilon_1$ and $-cd\epsilon_3$. The total distance moved, from Equation (3.27) would be $\frac{1}{\sqrt{2}}(d\sigma_1 - d\sigma_3)$ and in Figure 9 this would be the length of the vector 02. The solid hexagon A'B'C'D'E'F'A' in Figure 9 represents the final position of the Tresca yield surface for a stress path 01. When $\sigma_3 = \sigma_r$, $\sigma_1 = \sigma_z$, and $\sigma_2 = \sigma_\theta$, the stress path 01 would result from a combination of axial tensile force and internal pressure.

For yield surfaces like the Tresca or the maximum reduced stress, the corners formed by intersection of plane sides give rise to singularities which require special treatment. Should the stress state point enter a corner, such as corner A for Tresca, the yield surface will move in the direction of the stress increment vector. This requires that

$$d\sigma_{ij} = d\alpha_{ij} = c\, d\varepsilon_{ij} \tag{3.30}$$

if the state point remains in a corner. To determine whether a state point remains in a corner, the possible directions of the strain increment vector in view of Equation (3.30) must be considered. Koiter[10] has shown that at a singular point in the yield surface, the strain increment vector must lie between the outward normals to the bounding sides. Thus for a state point at a corner, the state point remains in the corner if $d\sigma_{ij}$ lies between the outward normals to the bounding sides. Otherwise the yield surface moves as if the state point were on a side.

Consider now the case when the maximum reduced stress criterion applies and the side LG is contacted by the stress state point. From Equations (3.8) and (3.20) the following flow laws are obtained:

$$\begin{aligned} d\varepsilon_1 &= \frac{1}{c}\left(\frac{1}{3}\right)(2d\sigma_1 - d\sigma_2 - d\sigma_3) \\ d\varepsilon_2 &= \frac{1}{c}\left(-\frac{1}{6}\right)(2d\sigma_1 - d\sigma_2 - d\sigma_3) \\ d\varepsilon_3 &= \frac{1}{c}\left(-\frac{1}{6}\right)(2d\sigma_1 - d\sigma_2 - d\sigma_3)\ . \end{aligned} \tag{3.31}$$

Note that on side LG, $F(\sigma_{ij}) = 2/3\sigma_1 - 1/3\sigma_2 - 1/3\sigma_3 = 2/3\sigma_o$. The vector $\overline{04}$ in Figure 9 represents the motion of the maximum reduced stress yield surface to the final position G'H'I'J'K'L'G' for the stress path 01. Components of this motion are given by $cd\epsilon_1$, $cd\epsilon_2$, and $cd\epsilon_3$ from Equation (3.31). By Equation (3.27) the length of $\overline{04}$ or the magnitude of the motion of the yield surface is found to be

$$\overline{04} = \frac{1}{\sqrt{6}} (2\,d\sigma_1 - d\sigma_2 - d\sigma_3) . \qquad (3.32)$$

The comments relative to motion of the yield surface for a stress state point in a corner presented in the preceding discussion for the Tresca yield criterion also apply in this case.

The forms for the various criteria of yielding after kinematic strain hardening has occurred are as follows:

Mises

$$\left[(\sigma_1-\sigma_3) - c(\epsilon_1-\epsilon_3)\right]^2 + \left[(\sigma_1-\sigma_2) - c(\epsilon_1-\epsilon_2)\right]^2 + \left[(\sigma_2-\sigma_3) - c(\epsilon_2-\epsilon_3)\right]^2 = 2\sigma_o^2$$

Tresca

$$\text{Max}\left\{ \left|(\sigma_1-\sigma_2) - c(\epsilon_1-\epsilon_2)\right|, \left|(\sigma_2-\sigma_3) - c(\epsilon_1-\epsilon_3)\right|, \left|(\sigma_1-\sigma_3) - c(\epsilon_1-\epsilon_3)\right| \right\} = \sigma_o$$

Maximum Reduced Stress (3.33)

$$\text{Max}\left\{ \left|\sigma_1-\sigma-c\epsilon_1\right|, \left|\sigma_2-\sigma-c\epsilon_2\right|, \left|\sigma_3-\sigma-c\epsilon_3\right| \right\} = \frac{2}{3}\sigma_o .$$

PIECEWISE LINEAR HARDENING

A third strain hardening theory has been developed by Hodge[11,12] and the name used here is that selected by Hodge. Hodge's work is based solely on the Tresca yield criterion and takes advantage of the limited stress path independence of such a criterion. It will be obvious as the

theory is developed that the maximum reduced stress criterion could serve equally well as the basis for development of a parallel theory.

The general concept of piecewise linear hardening differs from the isotropic or kinematic hardening theories in that relative motions between the sides of the yield surface during plastic straining are permitted. As noted, the yield surface moves as a rigid body in kinematic hardening and merely enlarges symmetrically for isotropic hardening.

Sanders[13] suggested earlier the idea of using a yield surface having a finite number of plane sides as a tractable means of describing strain hardening. Sanders discusses in particular, the case of a finite number of plane yield or loading surfaces which act independently. A plane loading surface is postulated to move only when "pushed" by the stress increment vector. The sketch of Figure 10 shows this behavior applied to the Tresca criterion in the octahedral plane for a typical stress path. When the state point reaches P, yielding (or plastic straining) begins and the surface AB is activated and moves in the direction of its normal. All other sides remain stationary. If loading continues, eventually point P' is reached and surface AF is also activated. Now the state point lies in a corner and the type and degree of hardening depends on the direction of the ensuing stress increment. If $d\sigma_{ij}$ lies between the normals to AF and AB, "total loading" occurs and the stress increment moves both AB and AF. Sanders did not fully develop these ideas however.

In Hodge's theory, rotation of sides of the yield surface, for-

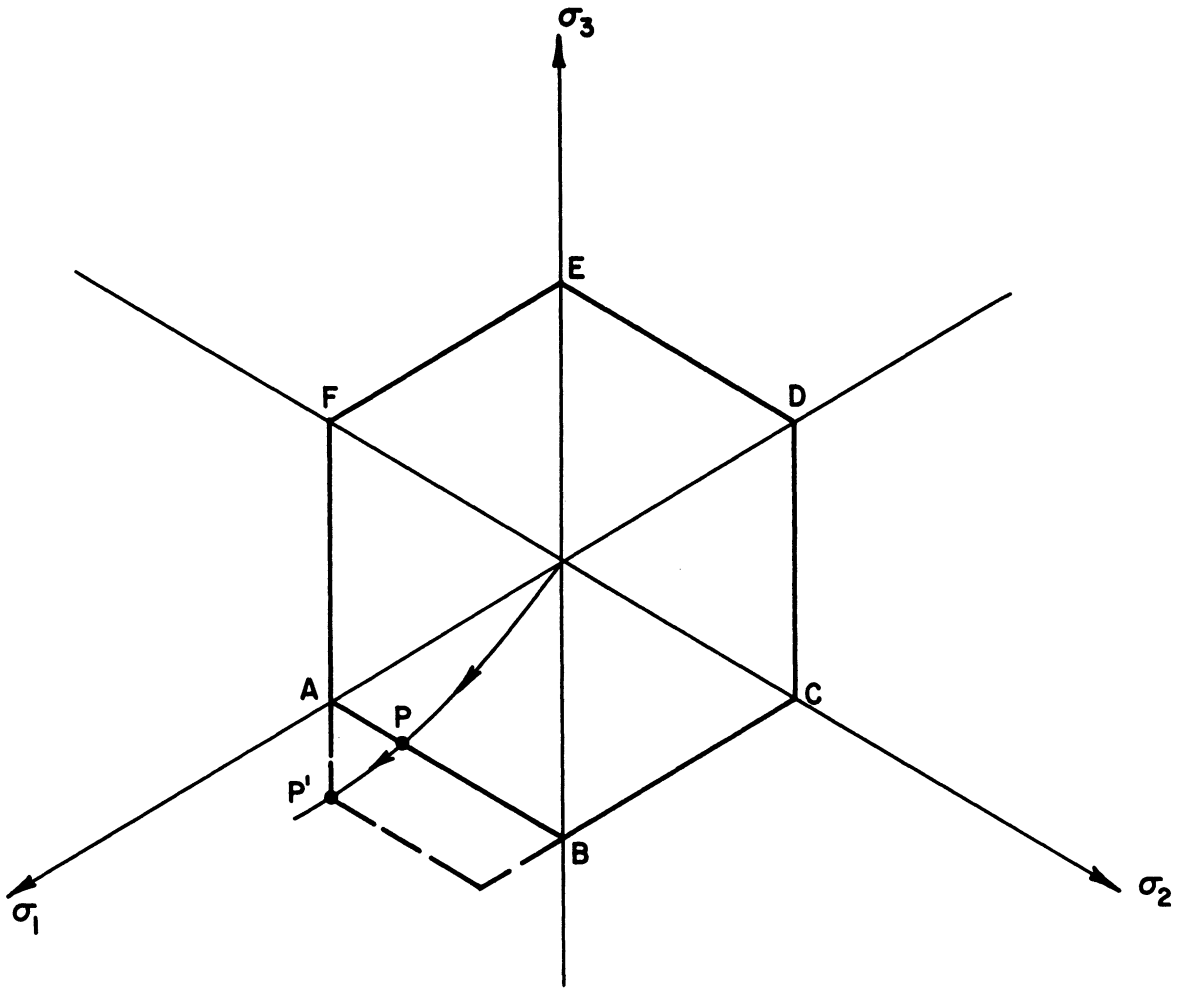

Figure 10. Sanders' hardening for a Tresca yield surface.

mation of sides, or disappearance of sides is not permitted. In short, the sides may move independently but the individual motions are each pure translations.

As with kinematic hardening, principal axes of stress and strain must coincide initially and remain fixed in an element of the material throughout the plastic straining process.

Using a somewhat different technique from that of Hodge, the theory is developed by establishing flow laws for each side of the yield surface. This is done first for a stress state point in contact with a selected side and then for a stress state point in a corner of the yield surface. Again refer to Figure 7, noting that only the Tresca criterion of yielding is being considered.

Suppose first that the stress state point remains on side AF where $F = \sigma_1 - \sigma_2 = \sigma_o$. Equation (3.20) is valid in this development so that the flow laws for AF are

$$\begin{aligned} d\varepsilon_1 &= \frac{1}{C} \cdot \frac{1}{2}(d\sigma_1 - d\sigma_2) \\ -d\varepsilon_2 &= \frac{1}{C} \cdot \frac{1}{2}(d\sigma_1 - d\sigma_2) \\ d\varepsilon_3 &= 0. \end{aligned} \tag{3.34}$$

As for the Tresca criterion in kinematic hardening the total movement of side AF along its outward normal is $\frac{1}{\sqrt{2}}(d\sigma_1 - d\sigma_2)$ by Equation (3.27). For convenience the motion of side AF can be stated in terms of $d\epsilon_1$ as follows:

$$K d\varepsilon_1 = \frac{1}{\sqrt{2}}(d\sigma_1 - d\sigma_2) \tag{3.35}$$

where $K = \sqrt{2}C$. Now consider the motions of the other sides while the stress state point remains on AF. Side AB may move a distance proportional to the motion of AF so that its movement along its normal is given by

$$\alpha K d\varepsilon_1 = \frac{1}{\sqrt{2}} (d\sigma_1 - d\sigma_3) \tag{3.36}$$

where α is the constant of proportionality. The side EF by symmetry would move a distance equal to that of AB along its own normal so that for EF

$$\alpha K d\varepsilon_1 = \frac{1}{\sqrt{2}} (d\sigma_3 - d\sigma_2). \tag{3.37}$$

Side BC may also move independently but still an amount proportional to that of AF resulting in

$$\beta K d\varepsilon_1 = \frac{1}{\sqrt{2}} (d\sigma_2 - d\sigma_3) \tag{3.38}$$

where β is a second constant of proportionality. Side DE moves a like amount to BC so that for DE

$$\beta K d\varepsilon_1 = \frac{1}{\sqrt{2}} (d\sigma_3 - d\sigma_1). \tag{3.39}$$

Finally side CD may be independent of the others but have a motion proportional to that of AF so its motion is

$$\gamma K d\varepsilon_1 = \frac{1}{\sqrt{2}} (d\sigma_2 - d\sigma_1) \tag{3.40}$$

where γ is still another constant of proportionality. To prevent disappearance of sides, Hodge[11] shows that

$$-2\beta \leq -\gamma \leq \alpha - \beta \leq 1 \leq 2\alpha \tag{3.41}$$

The preceding development will coincide with the predictions of kinematic hardening theory if $\alpha = 1/2$, $\beta = -1/2$, and $\gamma = -1$ and will coincide with the isotropic theory if $\alpha = \beta = \gamma = 1$.

The behavior of the yield surface for a stress state point entering a corner is exposed by considering the state point to be in contact with two sides simultaneously. This however, requires consideration of the motions for the state point on another side, say AB. Then with the motion of the yield surface known for state points in contact with two adjacent sides, the behavior for a state point in corner A can be treated.

On side AB, $\sigma_1 - \sigma_3 = \sigma_0$, and when the state point contacts this side we have Equation (3.29) for the flow laws. The side AB moves a distance given by

$$K d\varepsilon_1 = \frac{1}{\sqrt{2}} (d\sigma_1 - d\sigma_3) \tag{3.42}$$

where $K = \sqrt{2}C$ as before. In this case adjacent side AF moves along its outward normal the distance

$$\alpha K d\varepsilon_1 = \frac{1}{\sqrt{2}} (d\sigma_1 - d\sigma_2). \tag{3.43}$$

Now let the stress state point enter corner A as shown in Figure 11. In this instance, sides AB and AF are both moved directly by the state point. Note that for a state point on AF that $d\epsilon_1 = -d\epsilon_2$ while

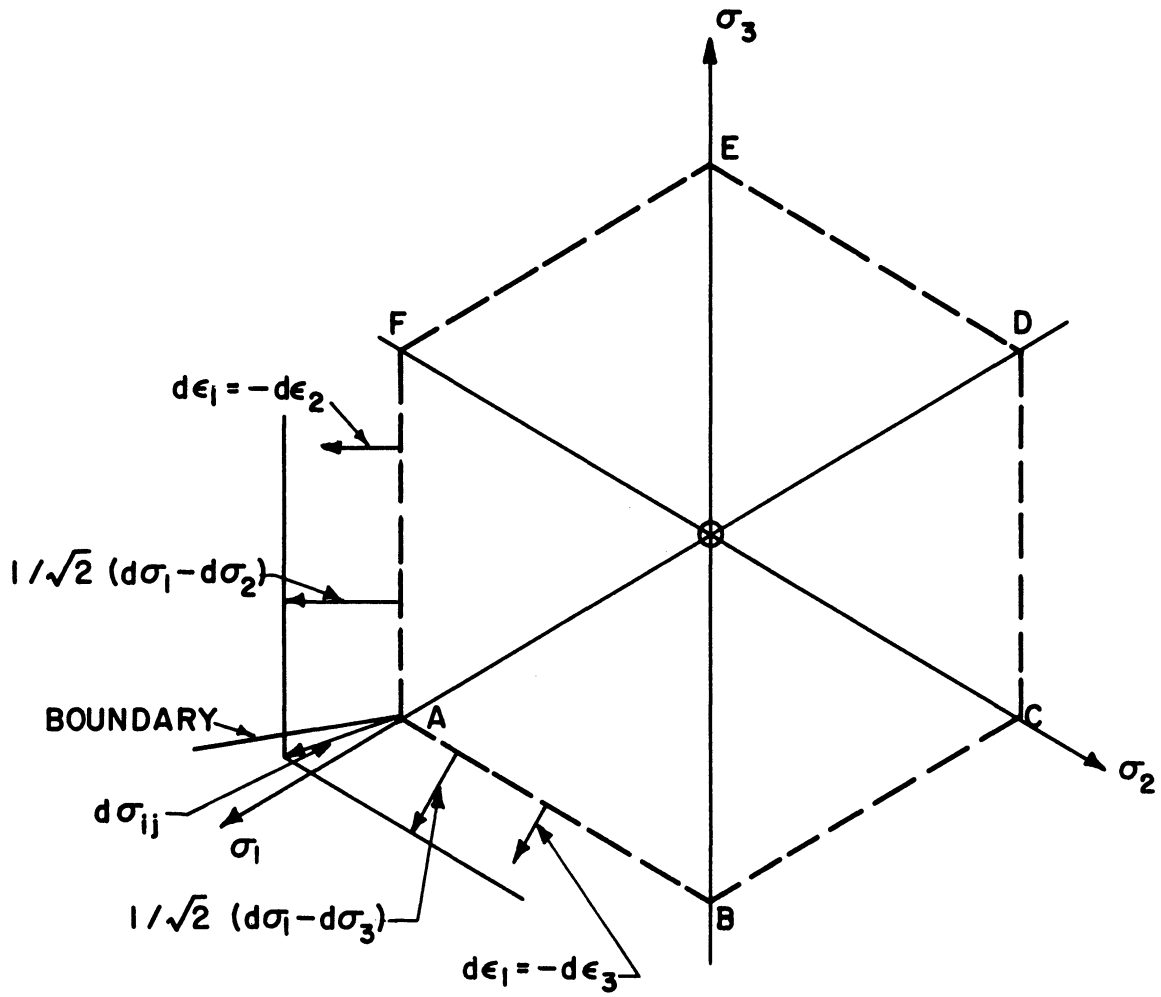

Figure 11. Piecewise linear hardening for a stress state point in a corner.

for a state point on AB that $d\epsilon_1 = -d\epsilon_3$. Then superpose the two simultaneous motions and obtain the flow law for AB

$$\frac{1}{\sqrt{2}}(d\sigma_3 - d\sigma_1) = K d\varepsilon_3 + \alpha K d\varepsilon_2 \tag{3.44}$$

and for AF

$$\frac{1}{\sqrt{2}}(d\sigma_2 - d\sigma_1) = K d\varepsilon_2 + \alpha K d\varepsilon_3. \tag{3.45}$$

The boundary line between side AF and corner A is defined by considering the flow laws when a state point is on the boundary. In this situation, $d\epsilon_3 = 0$ since conditions on side AF must be satisfied. Using this information in Equations (3.44) and (3.45), since the state point is also in the corner, we obtain.

$$\frac{1}{\sqrt{2}}(d\sigma_3 - d\sigma_1) = \alpha K d\varepsilon_2 = \alpha \frac{1}{\sqrt{2}}(d\sigma_2 - d\sigma_1)$$

$$d\sigma_1 - d\sigma_3 = \alpha (d\sigma_1 - d\sigma_2). \tag{3.46}$$

Thus α is the ratio of adjacent side motions when the stress state point is on the boundary. When α is known, a stress state point can be established as being on side AF if $d\sigma_1 - d\sigma_3 < \alpha (d\sigma_1 - d\sigma_2)$ and as being in corner A if $d\sigma_1 - d\sigma_3 > \alpha (d\sigma_1 - d\sigma_2)$.

Figure 12 presents the motions of the sides of the yield surface for a stress state point which remains on side AF and for $\alpha = 0.6$, $\beta = 0$, and $\gamma = -0.3$. The indicated stress path 01 is a radial one

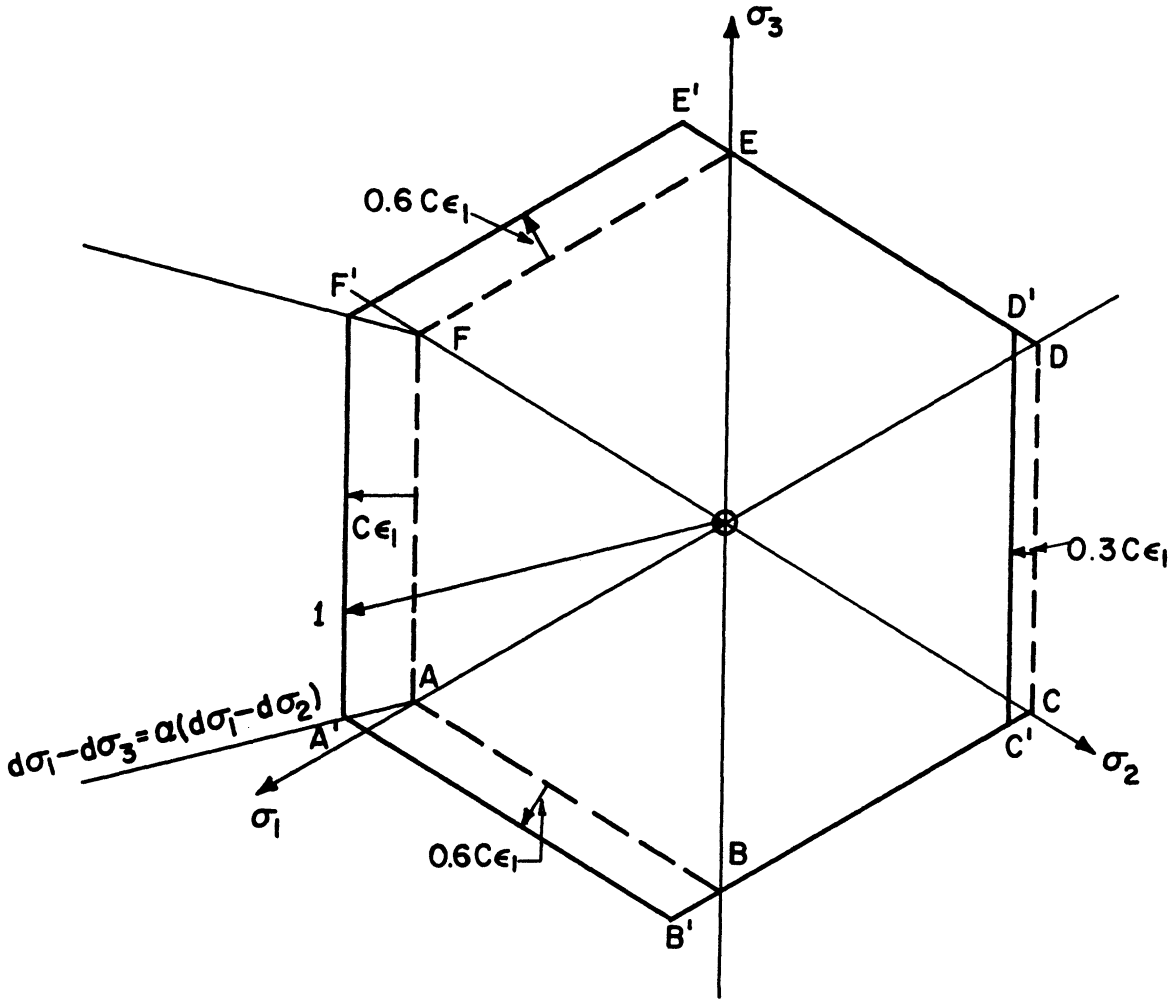

Figure 12. Piecewise linear hardening for a stress state point on AF.

although it is not necessary to these motions of the yield surface that it be radial as long as the state point remains on AF.

ANISOTROPY

Since one of the functions of the experimental program is to establish the isotropy or lack of it of the Zamak-3 tubes, the nature of the anisotropy that might be present will be considered.

Hill[14] has suggested an analysis for a particularly simple type of anisotropy and the following is adapted from it.

First assume that the principal axes of anisotropy in cast Zamak-3 tubes are the radial, circumferential, and axial directions. Further assume that yielding in the material remains insensitive to mean stress and that the general form of the von Mises yield criterion is applicable. A yield function in accord with these assumptions is

$$F(\sigma_\theta - \sigma_z)^2 + G(\sigma_z - \sigma_r)^2 + H(\sigma_r - \sigma_\theta)^2 + 2L\tau_{\theta z}^2 + 2M\tau_{rz}^2 + 2N\tau_{r\theta}^2 = 1. \qquad (3.47)$$

The constants F, G, and H are related to the yield stresses σ_r^*, σ_θ^*, and σ_z^* in the r-, θ-, and z-directions as follows:

$$\frac{1}{(\sigma_r^*)^2} = G+H \;;\; \frac{1}{(\sigma_\theta^*)^2} = H+F \;;\; \frac{1}{(\sigma_z^*)^2} = F+G \,. \qquad (3.48)$$

Similarly the yield stresses in shear relative to the principal axes are related to the constant L, M, and N by

$$\frac{1}{(\tau_{\theta z}^*)^2} = 2L \;;\; \frac{1}{(\tau_{rz}^*)^2} = 2M \;;\; \frac{1}{(\tau_{r\theta}^*)^2} = 2N \,. \qquad (3.49)$$

It would appear that a particular type of anisotropy which might occur in a cast cylindrical bar would be characterized by rotational symmetry of anisotropy about the r-axes. This means that the yield stresses in the θ- and z-directions would be equal. Since the Zamak-3 specimens were cast as solid cylindrical bars, it is possible that slight radial variations in grain structure might occur as a result of a varying rate of cooling in the radial direction. Such a situation could lead to the type of anisotropy described.

Now if one restricts the values of the constants in Equation (3.47) so that isotropy is present for a rotation of the coordinate system about the r-axis, the following relationships result:

$$\begin{aligned} H &= G \\ 2F + H &= L \\ M &= N . \end{aligned} \tag{3.50}$$

The yield function, Equation (3.47) then becomes

$$F(\sigma_\theta - \sigma_z)^2 + H(\sigma_z - \sigma_r)^2 + H(\sigma_r - \sigma_\theta)^2 + 2(2F+H)\tau_{\theta z}^2 + 2M\tau_{rz}^2 + 2M\tau_{r\theta}^2 = 1. \tag{3.51}$$

Applying the flow rule, the following plastic strain increments are obtained:

$$\begin{aligned} d\varepsilon_z &= \lambda\left[2F(\sigma_z - \sigma_\theta) + 2H(\sigma_z - \sigma_r)\right] \\ d\varepsilon_\theta &= \lambda\left[2F(\sigma_\theta - \sigma_z) + 2H(\sigma_\theta - \sigma_r)\right] \\ d\varepsilon_r &= \lambda\left[2H(\sigma_r - \sigma_z) + 2H(\sigma_r - \sigma_\theta)\right] \\ d\gamma_{\theta z} &= \lambda \cdot 4(2F+H)\tau_{\theta z} \end{aligned} \tag{3.52}$$

$$d\gamma_{rz} = \lambda \cdot 4M\tau_{rz}$$
$$d\gamma_{r\theta} = \lambda \cdot 4M\tau_{r\theta} \ .$$

As would be expected, it follows from the above that $d\epsilon_r + d\epsilon_\theta + d\epsilon_z = 0$. For a pure tension test where σ_z is the only non-zero stress, the ratio of the circumferential plastic strain increment to axial plastic strain increment is

$$-\frac{d\varepsilon_\theta}{d\varepsilon_z} = \frac{F}{F+H} \ . \tag{3.53}$$

In totally isotropic material, tho von Mises criterion is given by Equation (3.6) and, if we let $\sigma_1 = \sigma_z$, $\sigma_2 = \sigma_\theta$, and $\sigma_3 = \sigma_r$, the flow rule gives

$$-\frac{d\varepsilon_\theta}{d\varepsilon_z} = \frac{1}{2} \ . \tag{3.54}$$

It can be shown that Equation (3.54) is true for any yield criterion which is independent of the mean stress when σ_z is the only non-zero stress. Thus a comparison of axial and circumferential plastic strain increments might detect the presence of a radially symmetric anisotropy.

The comparison of strain increments suggested above is equivalent to the measurement of internal volume change performed by Taylor and Quinney.[15] This plastic change in the volume of the internal cavity of a tube is given by

$$\Delta V = \pi r^2 l \, (d\varepsilon_z + 2\, d\varepsilon_\theta) \tag{3.55}$$

where r is the tube radius and ℓ the length. Equation (3.55) is obtained from

$$\Delta V = V_{final} - V_{original} = \pi(r + u)^2 (\ell + w) - \pi r^2 \ell$$

where

u = radial displacement = $r d\epsilon_\theta$

w = axial displacement = $\ell d\epsilon_z$.

It must also be considered that products of strain increments are small and can be disregarded. Obviously Equation (3.54) must hold if the volume of the internal cavity is to remain unchanged. It follows that the type of anisotropy described in this section would cause a plastic or permanent change in volume of the internal cavity.

Pugh[16] notes that measurement of internal volume change cannot detect the presence of another type of anisotropy which is rotationally symmetric about the z-axes. While such anisotropy could be present in, say, cold-drawn tubes, it is not considered to be a likely occurrence in cast bars.

CHAPTER IV

PREDICTION OF THE KINEMATIC THEORY OF STRAIN HARDENING IN SUBSPACES

As a convenience in analysis or for interpreting test data, it may be useful to work in a space composed of the non-zero components of the state of stress. In short the yield function

$$F(\sigma_{ij}', \sigma_{ij}'') = k^2 \tag{4.1}$$

where σ_{ij}' are the non-zero stress components and σ_{ij}'' are the vanishing components is reduced in a subspace to

$$g(\sigma_{ij}') = k^2. \tag{4.2}$$

The flow rule, Equation (3.4) remains valid in a subspace although in general the engineering components of strain rather than the tensor components of strain must be used. However, in the subspace where Equation (4.2) applies, no information would be obtained regarding the plastic strain increments which correspond to the zero components of stress.

Further Shield and Ziegler[9] show that the kinematic hardening theory of Prager may not hold in a subspace except under special circumstances. To use the kinematic hardening theory in a subspace it must be possible to eliminate the α_{ij} corresponding to the zero components of stress or else the yield surface would move out of the subspace. In addition the remaining α_{ij} must be adjusted so that the yield surface moves in the

direction of the normal to the yield surface at the current stress state point. To some extent success in solving these problems depends on the yield condition chosen.

SUBSPACES FOR AXIAL TENSION—TORSION

As discussed in the Introduction, the non-zero stresses in the tubular specimen for this load combination are σ_z and $\tau_{\theta z}$. Thus the initial yield condition, following Equation (4.2), would be stated in general as

$$q(\sigma_z, \tau_{\theta z}) = k^2. \tag{4.3}$$

As discussed in Chapter III, the yield condition for an isotropic material whose yield process is independent of mean stress is

$$q(J_2, J_3) = k^2 \tag{4.4}$$

where J_2 is the second invariant and J_3 is the third invariant of the stress deviator tensor [see Equation (3.3)]. Consequently the flow rule might become

$$d\varepsilon_{ij} = d\lambda\left(\frac{\partial q}{\partial J_2}\cdot\frac{\partial J_2}{\partial \sigma_{ij}} + \frac{\partial q}{\partial J_3}\cdot\frac{\partial J_3}{\partial \sigma_{ij}}\right). \tag{4.5}$$

For the case at hand, it is shown by Shield and Ziegler that

$$d\gamma_{r\theta} = d\gamma_{rz} = 0 \tag{4.6}$$

as long as $\tau_{r\theta} = \tau_{rz} = 0$ by Equation (4.5) regardless of the yield condition. It follows by Equation (3.18) that $\alpha_{r\theta} = \alpha_{rz} = 0$.

Before proceeding further with the strain hardening analysis for the axial force-torque load combination acting on the tube, it must be recalled that kinematic theory predicts the development of anisotropy unless the principal axes of stress are fixed in an element of the material. There is the requirement then that the ratio of σ_z to $\tau_{\theta z}$ remain constant.

First consider that the von Mises criterion of yielding applies, i.e., the yield function depends on J_2 only. It follows, in this case that

$$d\varepsilon_r = d\varepsilon_\theta \,, \tag{4.7}$$

since by Equation (4.5)

$$d\varepsilon_r = \left\{ \frac{\partial q}{\partial J_2}\left(-\frac{1}{3}\right)\sigma_z + \frac{\partial q}{\partial J_3}\left[\left(-\frac{1}{9}\right)\sigma_z^2 - \frac{2}{3}(\tau_{\theta z})^2\right]\right\} d\lambda$$

and (4.8)

$$d\varepsilon_\theta = \left\{ \frac{\partial q}{\partial J_2}\left(-\frac{1}{3}\right)\sigma_z + \frac{\partial q}{\partial J_3}\left[\left(-\frac{1}{9}\right)\sigma_z^2 + \frac{1}{3}(\tau_{\theta z})^2\right]\right\} d\lambda$$

and the Mises yield criterion does not involve J_3.

After plastic straining or strain hardening occurs, Equation (4.3), noting Equation (3.18) for $d\alpha_{ij}$, becomes

$$q\left(\sigma_z - c\varepsilon_z, -c\varepsilon_r, -c\varepsilon_\theta, \tau_{\theta z} - \tfrac{1}{2}c\gamma_{\theta z}\right) = k^2 \tag{4.9}$$

where $\gamma_{\theta z} = 2\epsilon_{\theta z}$ ($\gamma_{\theta z}$ is the engineering shearing strain). Since yielding is independent of mean stress, a hydrostatic component can be added to each of the normal stresses without effect. Thus add $c\epsilon_r$ to each

stress. However we know that Equation (4.7) is valid and that the volume remains constant or

$$\varepsilon_r + \varepsilon_\theta + \varepsilon_z = 0. \tag{4.10}$$

Use of these converts Equation (4.9) to

$$q\left(\sigma_z - \tfrac{3}{2} c\varepsilon_z,\ \tau_{\theta z} - \tfrac{1}{2} c\gamma_{\theta z}\right) = k^2 \tag{4.11}$$

which lies in the same subspace as Equation (4.3) but normality of motion of the yield surface is not maintained. However, using the transformation

$$t_{\theta z} = \sqrt{3}\,\tau_{\theta z}\ ;\ q_{\theta z} = \frac{1}{\sqrt{3}}\gamma_{\theta z} \tag{4.12}$$

Equations (4.3) and (4.11) become

$$h(\sigma_z, t_{\theta z}) = k^2 \tag{4.13}$$

and

$$h\left(\sigma_z - \tfrac{3}{2} c\varepsilon_z,\ t_{\theta z} - \tfrac{3}{2} c q_{\theta z}\right) = k^2. \tag{4.14}$$

For the tension-torsion test, the Mises yield condition in the subspace defined by Equation (4.12) is initially

$$\sigma_z^2 + t_{\theta z}^2 = \sigma_0^2 \tag{4.13a}$$

and after plastic flow this becomes

$$\left(\sigma_z - \tfrac{3}{2} c\varepsilon_z\right)^2 + \left(t_{\theta z} - \tfrac{3}{2} c q_{\theta z}\right)^2 = \sigma_0^2 \tag{4.14a}$$

as given by Shield and Ziegler. In this subspace the Mises yield con-

dition is represented by a circle of radius σ_o whose center moves to the point $(\frac{3}{2} c\epsilon_z, \frac{3}{2} cg_{\theta z})$ during hardening.

For the Tresca yield condition, Equation (4.7) is not available to aid in reducing Equation (4.9) to a form in which the yield surface is not deformed since the Tresca condition involves J_3 as well as J_2. However, it has already been observed, in the Introduction, that σ_r is a principal stress because $\tau_{r\theta} = \tau_{rz} = 0$ for combined tension and torsion. Let us consider, further, that σ_1 and σ_2 in Figure 7 are the principal stresses which lie in the θ-z plane of the tube. In this case, state points will lie on side AF of the Tresca yield surface, and the flow rule requires that $d\epsilon_r = 0$. The volume constancy condition, Equation (4.10) then gives the information that

$$d\epsilon_z = -d\epsilon_\theta \ . \tag{4.15}$$

The preceding permits of reduction of Equation (4.9) to

$$q(\sigma_z - 2c\epsilon_z, \tau_{\theta z} - \tfrac{1}{2} c\gamma_{\theta z}) = k^2 \tag{4.16}$$

after $c\epsilon_z$ is subtracted from all of the normal stress terms. As noted the latter is valid since the yield condition is independent of the mean stress.

Considering Equation (4.3) and (4.16) it is apparent that we have the same subspace both before and after strain hardening. However, normality of motion is not maintained.

Use here of the transformation

$$s_{\theta z} = 2\tau_{\theta z} \ ; \ e_{\theta z} = \tfrac{1}{2}\gamma_{\theta z} \tag{4.17}$$

converts Equation (4.3) and (4.16) to

$$h(\sigma_z, s_{\theta z}) = k^2 \tag{4.18}$$

and

$$h(\sigma_z - 2c\varepsilon_z, s_{\theta z} - 2ce_{\theta z}) = k^2 \tag{4.19}$$

respectively. The form $h = k^2$ for the Tresca yield condition is

$$\sigma_z^2 + s_{\theta z}^2 = \sigma_0^2 \tag{4.18a}$$

initially, and after strain hardening is

$$(\sigma_z - 2c\varepsilon_z)^2 + (s_{\theta z} - 2ce_{\theta z})^2 = \sigma_0^2 . \tag{4.19a}$$

The Tresca yield surface is a circle in the subspace defined by Equation (4.17).

The preceding analysis for the Tresca yield criterion in terms of σ_z and $\tau_{\theta z}$ is not presented by Shield and Ziegler and is believed by the author to be original.

Results of the analyses for the Mises and Tresca yield conditions are depicted graphically in Figures 13 and 14. These kinematic models, as suggested by Prager,[8] represent the yield surface as a rigid ring which moves when a pin (i.e., the stress state point) contacts it. Note that in both figures, PP' represents the stress increment $d\sigma_{ij}$ while OP' represents the total stress at the final state. The corresponding plastic strain increments are shown as well as the translation of the origin OO'. Obviously the figures are geometrically similar but

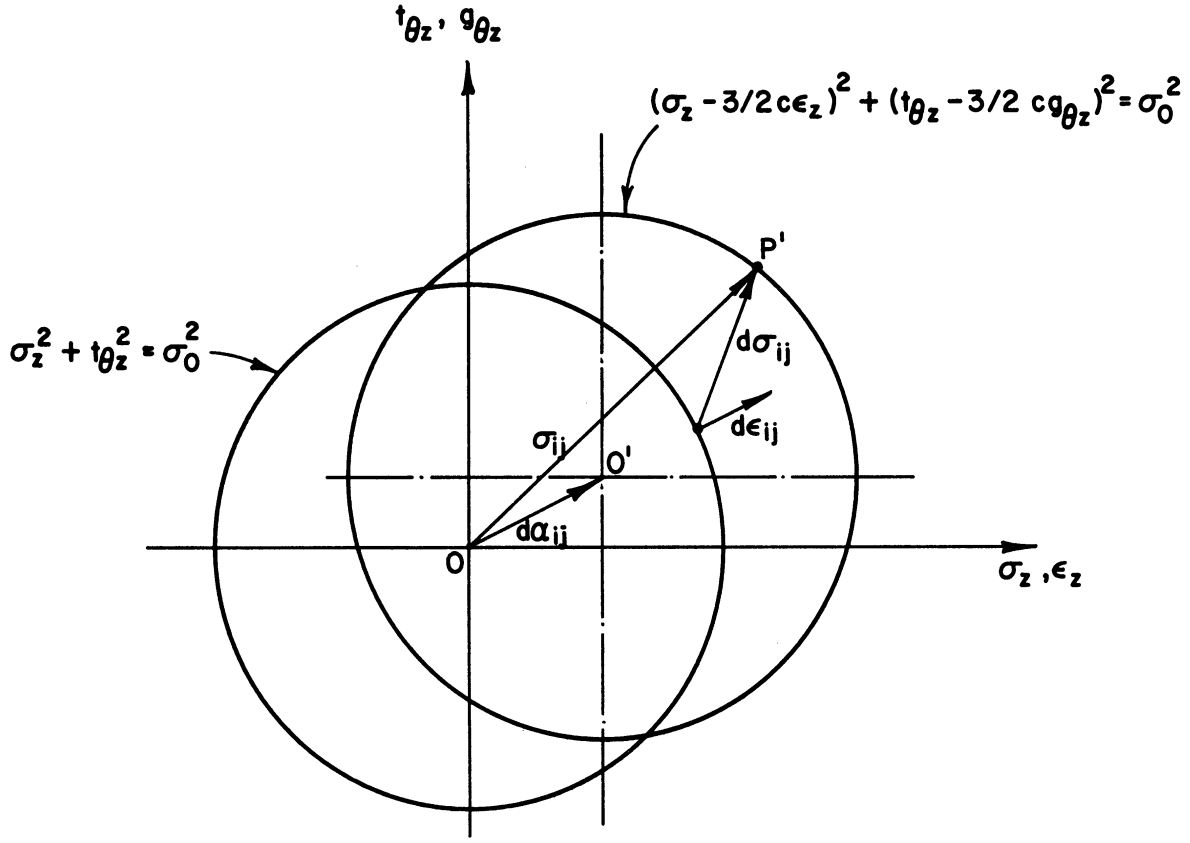

Figure 13. Kinematic hardening for the von Mises yield condition. Combined tension-torsion loading.

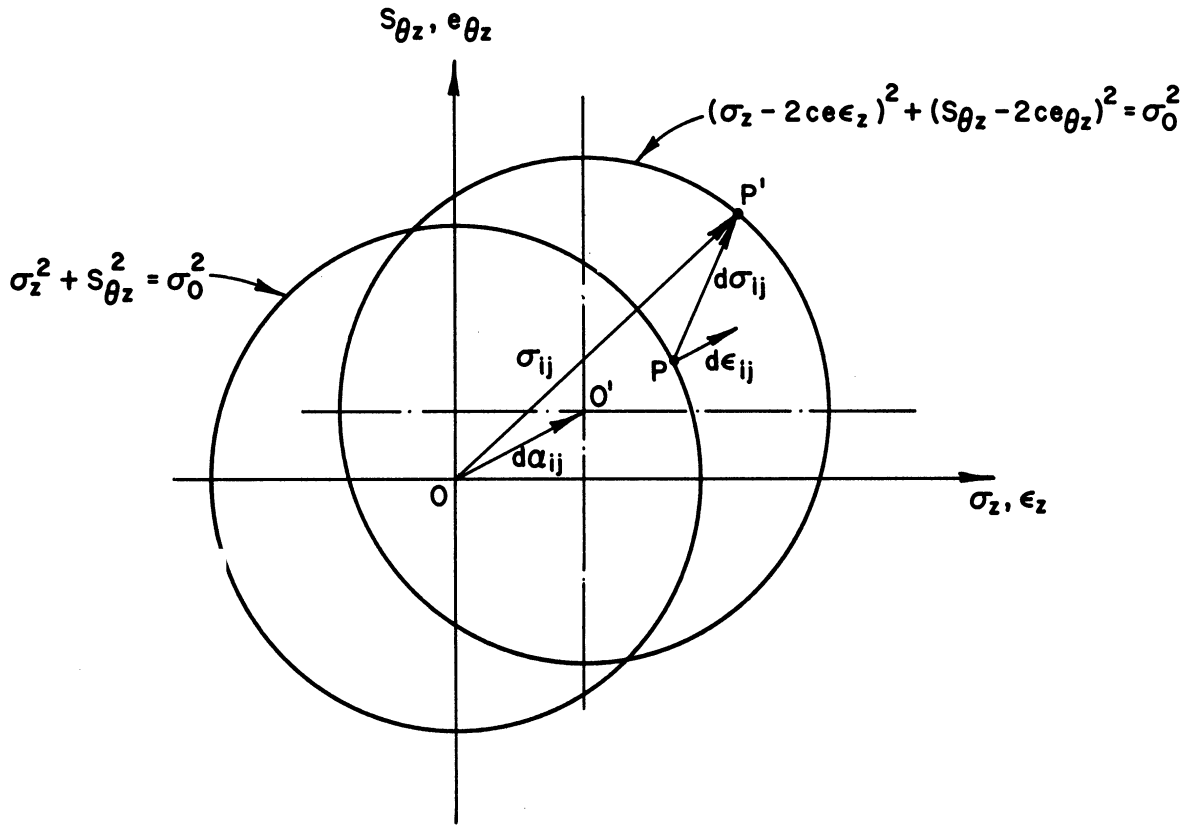

Figure 14. Kinematic hardening for the Tresca yield condition. Combined tension-torsion loading.

only because the vertical coordinate is suitably defined.

A suitable subspace of the non-zero stresses for the maximum reduced stress yield criterion will now be considered. In line with the discussion for Tresca, if σ_1 and σ_2 are the principal stresses which lie in the θ-z plane of the tube, then the tension-torsion stress state points will lie on side GL. See Figure 7.

If attention is confined to a σ_z - $\tau_{\theta z}$, or equivalent, subspace, the author's analysis indicates that hardening always causes motion out of the subspace. In short, it has not been possible to eliminate both $c\epsilon_r$ and $c\epsilon_\theta$ in Equation (4.9) for this case.

However a three dimensional subspace composed of σ_z, σ_θ, and $\tau_{\theta z}$ (plane stress) does lead to useful results. The inclusion of σ_θ, in essence, expands the analysis to include stress combinations obtained from both combined axial tension-torsion and combined axial tension-internal pressure. The results for axial tension-torsion, where $\sigma_\theta = 0$, will be on a specific plane in the larger subspace.

Now on side GL of the maximum reduced stress criterion,

$$2\sigma_1 - \sigma_2 - \sigma_3 = 0 . \tag{4.20}$$

However these principal stresses are

$$\begin{aligned} \sigma_1 &= \frac{\sigma_z + \sigma_\theta}{2} + \sqrt{\left(\frac{\sigma_z - \sigma_\theta}{2}\right)^2 + \tau_{\theta z}^2} \\ \sigma_2 &= \frac{\sigma_z + \sigma_\theta}{2} - \sqrt{\left(\frac{\sigma_z - \sigma_\theta}{2}\right)^2 + \tau_{\theta z}^2} \\ \sigma_3 &= \sigma_r = 0 \end{aligned} \tag{4.21}$$

so that Equation (4.20) becomes

$$\frac{\sigma_z+\sigma_\theta}{2} + 3\sqrt{\left(\frac{\sigma_z-\sigma_\theta}{2}\right)^2+\tau_{\theta z}^2} = 2\sigma_o. \tag{4.22}$$

Before strain hardening occurs, the yield condition is, in general,

$$q(\sigma_z, \sigma_\theta, \tau_{\theta z}) = k^2 \tag{4.23}$$

which, after strain hardening becomes

$$q(\sigma_z - c\varepsilon_z, \sigma_\theta - c\varepsilon_\theta, -c\varepsilon_r, \tau_{\theta z} - \tfrac{1}{2}c\gamma_{\theta z}) = k^2 \tag{4.24}$$

according to the kinematic theory. The yield is independent of mean stress so that $c\epsilon_r$ may be added to each of the normal stresses. Further $\epsilon_r = -(\epsilon_\theta + \epsilon_z)$ by Equation (4.10) and Equation (4.24) reduces to

$$q\left\{[\sigma_z - c(2\varepsilon_z+\varepsilon_\theta)], [\sigma_\theta - c(2\varepsilon_\theta+\varepsilon_z)], (\tau_{\theta z} - \tfrac{1}{2}c\gamma_{\theta z})\right\} = k^2. \tag{4.25}$$

Apparently Equations (4.23) and (4.25) represent the same subspace but normality of motion of the yield surface is not maintained. However, if one makes use of the following transformation

$$\begin{aligned} s_\xi &= \tfrac{1}{2}(\sigma_\theta+\sigma_z) & s_\eta &= \tfrac{\sqrt{3}}{2}(\sigma_\theta-\sigma_z) & t_{\theta z} &= \sqrt{3}\,\tau_{\theta z} \\ e_\xi &= \varepsilon_\theta+\varepsilon_z & e_\eta &= \tfrac{1}{\sqrt{3}}(\varepsilon_\theta-\varepsilon_z) & g_{\theta z} &= \tfrac{1}{\sqrt{3}}\gamma_{\theta z} \end{aligned} \tag{4.26}$$

this objection is removed. This transformation also has been suggested by Shield and Ziegler.[9] Applying the transformation, Equations (4.26) to Equations (4.23) and (4.25) gives

$$h(s_\xi, s_\eta, t_{\theta z}) = k^2 \tag{4.27}$$

and

$$h(S_\xi - \tfrac{3}{2}c e_\xi, S_\eta - \tfrac{3}{2}c e_\eta, t_{\theta z} - \tfrac{3}{2}c q_{\theta z}) = k^2 \quad (4.28)$$

respectively.

The side GL of the maximum reduced stress criterion in this subspace is explicitly

$$3 S_\eta^2 + 3 t_{\theta z}^2 - (S_\xi - 2\sigma_o)^2 = 0 \quad (4.27a)$$

initially, and after strain hardening is

$$3(S_\eta - \tfrac{3}{2}c e_\eta)^2 + 3(t_{\theta z} - \tfrac{3}{2}c q_{\theta z})^2 - (S_\xi - \tfrac{3}{2}c e_\xi - 2\sigma_o)^2 = 0. \quad (4.28a)$$

Equation (4.27a) represents a cone of revolution with its axes on the S_ξ-axis and its vertex at $S_\xi = 2\sigma_o$. A sketch of the surface is presented in Figure 15. From Equation (4.26) one observes that, when $\sigma_\theta = 0$, we have $S_\xi = \frac{1}{2}\sigma_z$ and $S_\eta = -\frac{\sqrt{3}}{2}\sigma_z$. This condition defines a plane in the subspace of Figure 15 and the trace of the intersection of this plane and the cone is shown in the sketch. It is apparent that the noted intersection does not form another subspace since normality of motion would not be maintained. This treatment of the maximum reduced stress criterion in the S_ξ, S_η, $\tau_{\theta z}$ subspace is unique.

SUBSPACES FOR AXIAL TENSION—INTERNAL PRESSURE

Again recalling the discussion in the Introduction, the non-zero stresses in the tube under this combination of loads are σ_z and σ_θ. In a subspace of the non-zero stresses, the initial yield function is

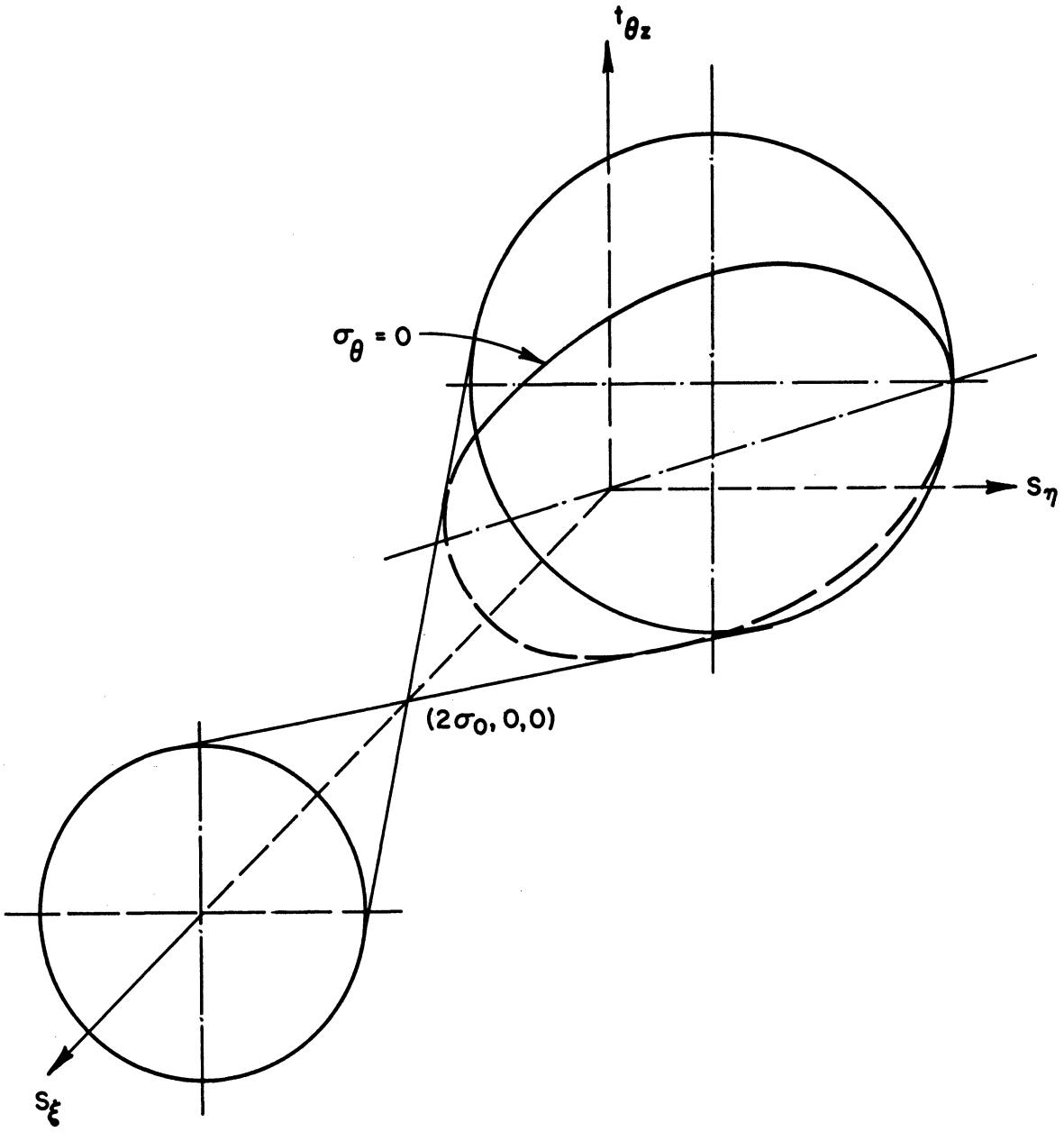

Figure 15. Kinematic hardening for plane stress, maximum reduced stress yield condition.

$$g(\sigma_\theta, \sigma_z) = k^2. \tag{4.29}$$

After plastic strain has occurred, the yield function becomes

$$g(\sigma_\theta - c\varepsilon_\theta, \sigma_z - c\varepsilon_z, -c\varepsilon_r) = k^2. \tag{4.30}$$

Equation (4.30) applies to an initially isotropic material in which the principal axes do not rotate in an element of the material. For this load combination, the shearing stresses $\tau_{r\theta} = \tau_{\theta z} = \tau_{rz} = 0$ so that the axial, radial, and circumferential directions are principal directions regardless of the ratio of σ_z to σ_θ. The general form of the yield function, Equation (4.4), is applicable. It is then easy to show that

$$d\gamma_{\theta z} = d\gamma_{r\theta} = d\gamma_{rz} = 0 \tag{4.31}$$

by the flow rule, Equation (4.5), when the shearing stresses are all identically zero. In view of Equation (4.31) and of Equation (3.18) which defines the incremental translation of the yield surface, we have

$$d\alpha_{\theta z} = d\alpha_{r\theta} = d\alpha_{rz} = 0$$

and since the principal axes are fixed

$$\alpha_{\theta z} = \alpha_{r\theta} = \alpha_{rz} = 0. \tag{4.32}$$

Euqation (4.32) establishes the validity of Equation (4.30) but the latter indicates that the yield surface, Equation (4.29), moves out of the subspace.

Now, using the incompressibility condition and adding $c\epsilon_r$ to each of the normal stress terms (the yield condition is independent of the mean normal stress), Equation (4.30) becomes

$$q\left[\sigma_\theta - c(2\varepsilon_\theta + \varepsilon_z),\ \sigma_z - c(2\varepsilon_z + \varepsilon_\theta)\right] = k^2. \tag{4.33}$$

This lies in the same subspace as that of Equation (4.29) but normality of motion is not maintained. The following transformation, suggested by Shield and Ziegler,[9] namely

$$\begin{aligned} s_\xi &= \tfrac{1}{2}(\sigma_\theta + \sigma_z) & s_\eta &= \tfrac{\sqrt{3}}{2}(\sigma_\theta - \sigma_z) \\ e_\xi &= \varepsilon_\theta + \varepsilon_z & e_\eta &= \tfrac{1}{\sqrt{3}}(\varepsilon_\theta - \varepsilon_z) \end{aligned} \tag{4.34}$$

will be found useful at this point. Equations (4.34) convert Equations (4.29 and (4.33) to

$$h(s_\xi, s_\eta) = k^2 \tag{4.35}$$

for initial yielding and to

$$h\left(s_\xi - \tfrac{3}{2}c e_\xi,\ s_\eta - \tfrac{3}{2}c e_\eta\right) = k^2 \tag{4.36}$$

after yielding. Note that Equations (4.35) and (4.36) are valid for any yield criterion assuming initial isotropy and independence of mean stress.

Now consider specifically the von Mises criterion of yielding, which is given in terms of the non-zero stresses as

$$\sigma_z^2 - \sigma_\theta \sigma_z + \sigma_\theta^2 = \sigma_o^2 \quad . \tag{4.37}$$

However, using the transformation, Equation (4.34) we obtain

$$S_\xi^2 + S_\eta^2 = \sigma_0^2 \tag{4.38}$$

for the initial yield surface and

$$\left(S_\xi - \tfrac{3}{2} c e_\xi\right)^2 + \left(S_\eta - \tfrac{3}{2} c e_\eta\right)^2 = \sigma_0^2 \tag{4.39}$$

for the yield surface after strain-hardening. In this subspace, the Mises condition is represented by a circle whose center undergoes a translation during hardening. This coincides with Shield and Ziegler's result.

For the Tresca criterion of yielding in terms of σ_θ and σ_z we have, in the case of axial tension with internal pressure

$$\begin{aligned} &\sigma_z = \sigma_0 \quad \text{when } \sigma_z > \sigma_\theta \\ \text{and} \qquad &\sigma_\theta = \sigma_0 \quad \text{when } \sigma_\theta > \sigma_z . \end{aligned} \tag{4.40a}$$

If we have a combination of axial compression and internal pressure, then initial yielding by Tresca is

$$\sigma_\theta - \sigma_z = \sigma_0 . \tag{4.40b}$$

The transformation, Equation (4.34), when applied to Equation (4.40a) for the case of axial tension combined with internal pressure gives

$$\begin{aligned} &S_\xi - \frac{1}{\sqrt{3}} S_\eta = \sigma_0 \quad \text{when } \sigma_z > \sigma_\theta \\ \text{and} \qquad &S_\xi + \frac{1}{\sqrt{3}} S_\eta = \sigma_0 \quad \text{when } \sigma_\theta > \sigma_z \end{aligned} \tag{4.41a}$$

for initial yielding and gives

$$\left(S_\xi - \tfrac{3}{2} c e_\xi\right) - \frac{1}{\sqrt{3}}\left(S_\eta - \tfrac{3}{2} c e_\eta\right) = \sigma_0 \quad \text{when } \sigma_z > \sigma_\theta$$

and (4.42a)

$$\left(S_\xi - \tfrac{3}{2} c e_\xi\right) + \frac{1}{\sqrt{3}}\left(S_\eta - \tfrac{3}{2} c e_\eta\right) = \sigma_0 \quad \text{when } \sigma_\theta > \sigma_z$$

for yielding after strain hardening. Similarly, for the combination of axial compression and internal pressure, Equation (4.40b), we have now

$$\frac{2}{\sqrt{3}} S_\eta = \sigma_0 \tag{4.41b}$$

for initial yielding and

$$\frac{2}{\sqrt{3}}\left(S_\eta - \tfrac{3}{2} c e_\eta\right) = \sigma_0 \tag{4.42b}$$

for yielding after strain hardening. The above analysis for the Tresca yield criterion is suggested but not fully developed by Shield and Ziegler.

Figures 16 and 17 are plots of the Mises and Tresca yield surfaces in the S_ξ - S_η subspace. As before, these may be regarded as kinematic models, after Prager,[8] in which the yield curve is considered to be a rigid ring. In this subspace, the vector $d\epsilon_{ij}$ has only the components de_ξ and de_η.

Now let us turn our attention to the maximum reduced stress criterion of yielding and its appearance in the S_η - S_ξ subspace. For combinations of axial force and internal pressure, state points lie on sides GL, GH, or HI of this yield surface as seen in Figure 7. These three possibilities are stated in terms of σ_θ and σ_z as

$$\begin{aligned} 2\sigma_z - \sigma_\theta &= 2\sigma_0 \quad && \text{when } \sigma_z > 2\sigma_0 \\ \sigma_z + \sigma_\theta &= 2\sigma_0 \quad && \text{when } 2\sigma_\theta > \sigma_z > \frac{\sigma_\theta}{2} \end{aligned} \tag{4.43}$$

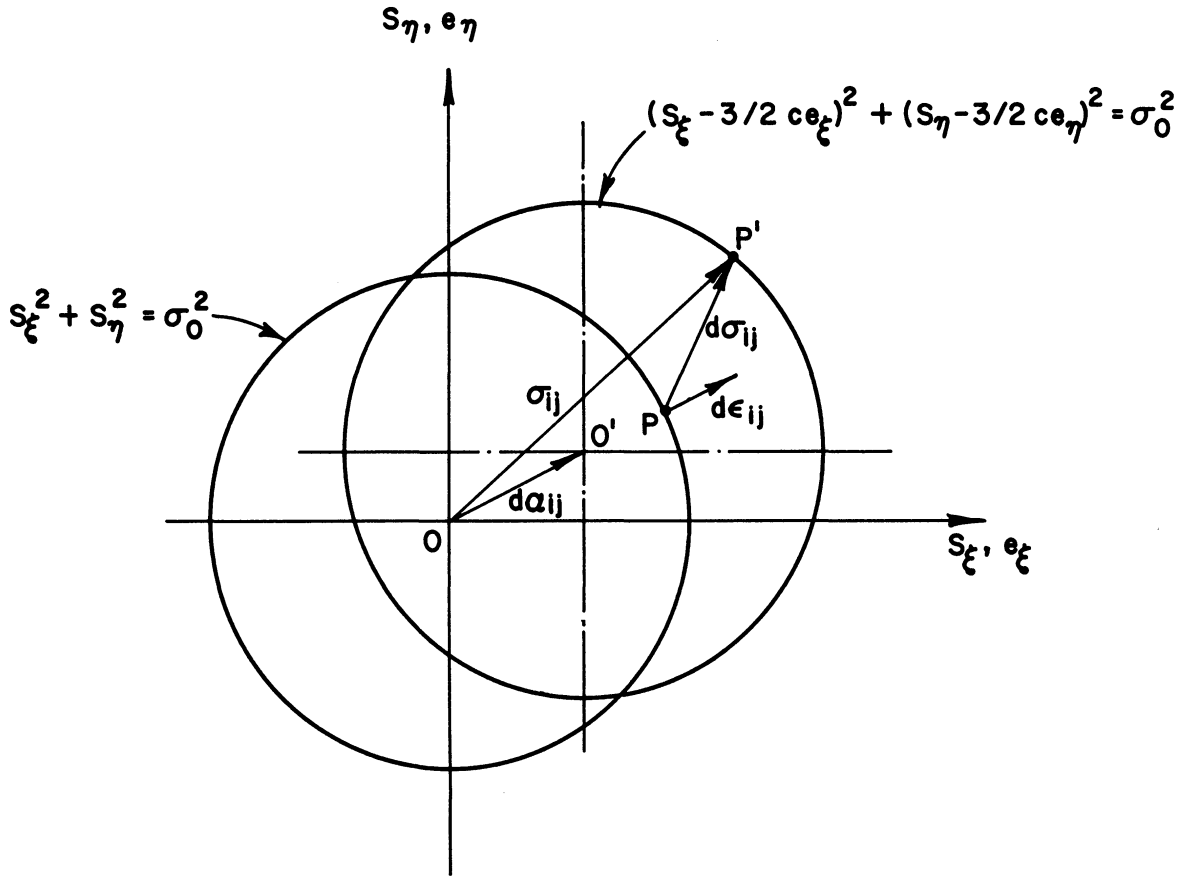

Figure 16. Kinematic hardening for the von Mises yield condition. Tension-internal pressure loading.

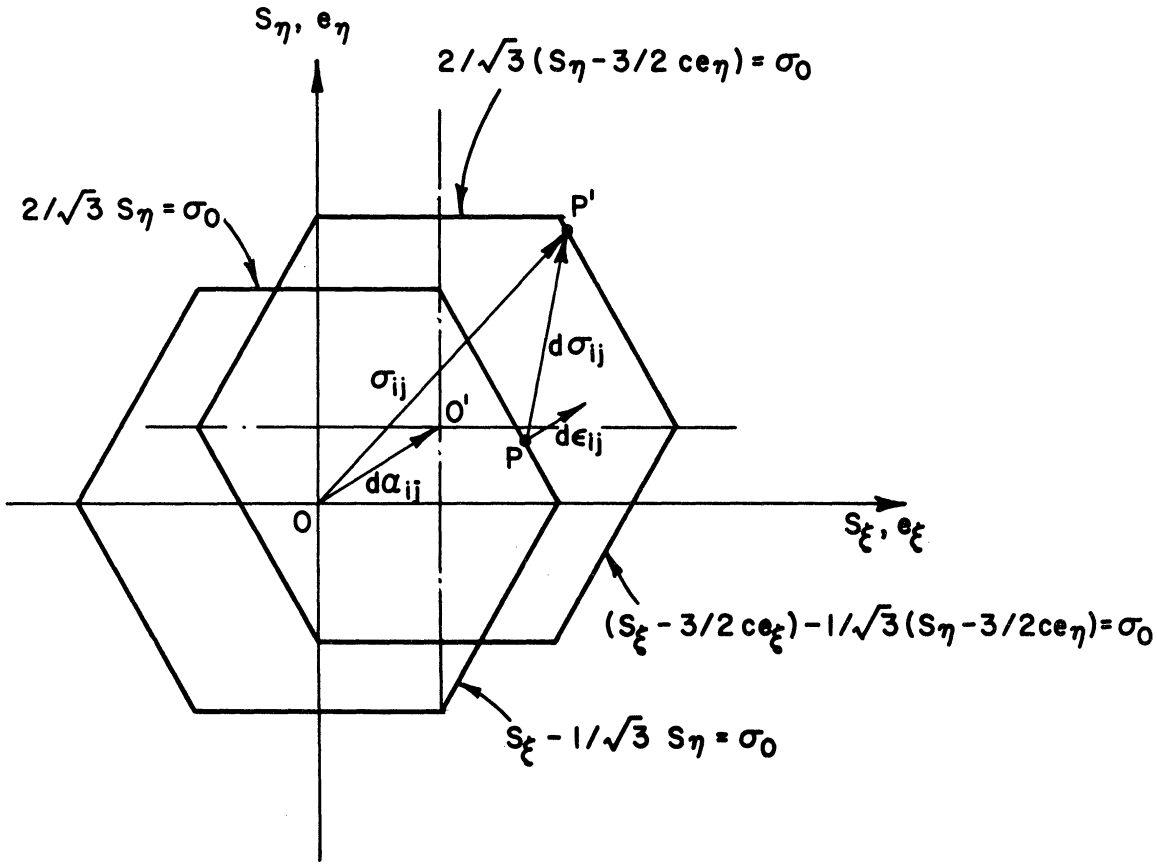

Figure 17. Kinematic hardening for the Tresca yield condition. Tension-internal pressure loading.

and $$2\sigma_\theta - \sigma_z = 2\sigma_0 \quad \text{when} \quad \frac{\sigma_\theta}{2} > \sigma_z \ .$$

Note, that the last case includes axial compression and internal pressure. The transformation, Equation (4.34), when substituted into Equation (4.43), gives the maximum reduced stress criterion in the S_ξ - S_η subspace as

$$\begin{aligned} S_\xi - \sqrt{3}\, S_\eta &= 2\sigma_0 \quad && \text{when } \sigma_z > 2\sigma_0 \\ S_\xi &= \sigma_0 && \text{when } 2\sigma_0 > \sigma_z > \tfrac{\sigma_\theta}{2} \\ \text{and} \quad S_\xi + \sqrt{3}\, S_\eta &= 2\sigma_0 && \text{when } \tfrac{\sigma_\theta}{2} > \sigma_z \end{aligned} \tag{4.44}$$

for initial yielding. In view of Equation (4.36), after strain hardening has occurred, these become

$$\begin{aligned} (S_\xi - \tfrac{3}{2} c e_\xi) - \sqrt{3}(S_\eta - \tfrac{3}{2} c e_\eta) &= 2\sigma_0 \quad && \text{when } \sigma_z > 2\sigma_0 \\ (S_\xi - \tfrac{3}{2} c e_\xi) &= \sigma_0 && \text{when } 2\sigma_0 > \sigma_z > \tfrac{\sigma_\theta}{2} \\ \text{and} \quad (S_\xi - \tfrac{3}{2} c e_\xi) + \sqrt{3}(S_\eta - \tfrac{3}{2} c e_\eta) &= 2\sigma_0 && \text{when } \tfrac{\sigma_\theta}{2} > \sigma_z . \end{aligned} \tag{4.45}$$

This analysis for the maximum reduced stress yield criterion is believed to be original. Figure 18 depicts the form of the criterion in the S_ξ - S_η subspace and shows the motion of the surface in the subspace for a typical $d\sigma_{ij}$.

One general comment on the extent of motion of the yield surface in any of these subspaces may be in order. For those cases for which the yield surface appears as a circle in the particular subspace, only incremental motions or rather incremental stress changes can be accom-

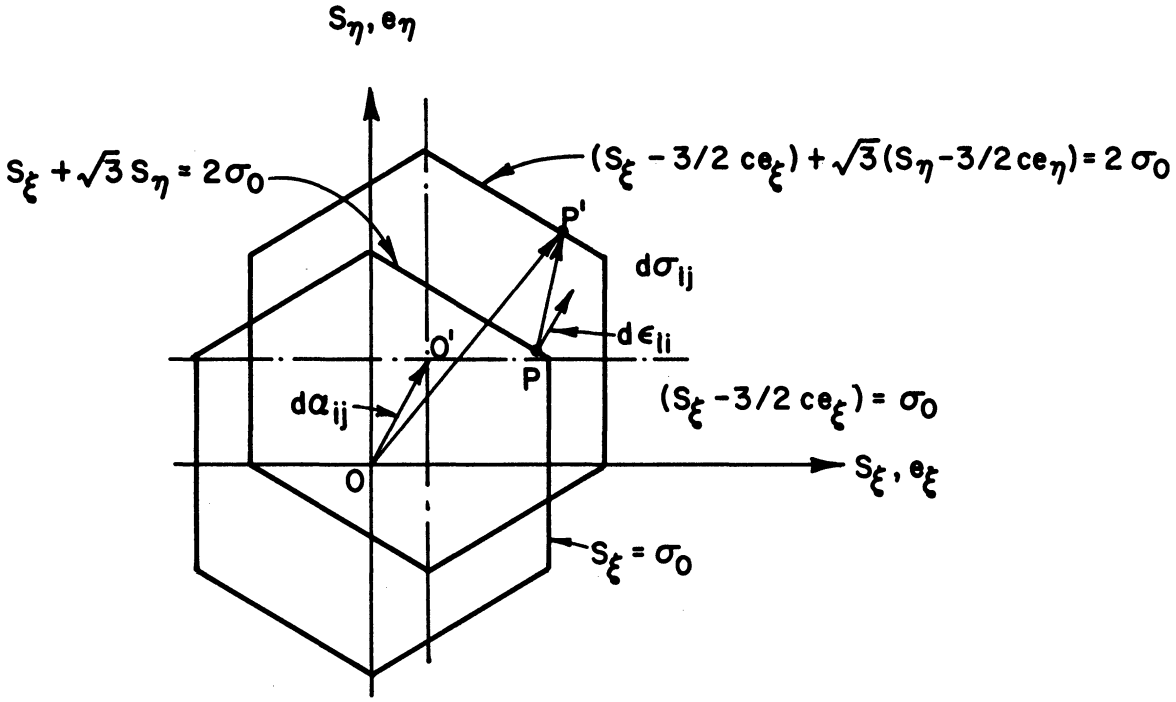

Figure 18. Kinematic hardening for the maximum reduced stress yield condition. Tension-internal pressure loading.

modated. This is true because the incremental stress-strain relationships, which have in general the form given in Equation (3.13) or Equation (3.20), can be integrated to obtain finite strains only under certain conditions. Handleman and Warner[17] show that integration is possible if

$$Q\frac{\partial F}{\partial \sigma_{ij}} = h_{ij}(F) \tag{4.46}$$

using the form of Equation (3.13). In Equation (4.46) the h_{ij} must be differentiable functions of the yield function $F(\sigma_{ij})$. If Equation (4.46) holds,

$$d\varepsilon_{ij} = h_{ij}(F)\cdot\frac{\partial F}{\partial \sigma_{kl}}\, d\sigma_{kl} \tag{4.47}$$

is integrable. However, the $h_{ij}(F)$, which depend on the direction of the normal, must not change along the stress path. Another way to state this is that $d\epsilon_{ij}$ must have a constant direction, as also noted by Hodge.[12] The latter is realized for radial loading or for a general loading if the stress state point remains on a plane side of the yield surface.

CHAPTER V

REVIEW OF PREVIOUS EXPERIMENTAL INVESTIGATIONS

In recent years, a large literature has accumulated which concerns experimental evaluation of the plastic response of materials. The author does not wish to imply that what follows is a comprehensive review of this literature. On the contrary, a selection has been made so that the papers discussed are germane to the subject of this dissertation. Investigations of strain-hardening and plastic stress-strain relations are emphasized. Initial yielding will be discussed briefly.

INITIAL YIELDING

Both the Tresca yield condition, Equation (3.7), and the von Mises yield condition, Equation (3.6), have been known for a long period of time. Both theories have the simplicity which is desirable from the theoretical viewpoint but they are, in essence, continuum mechanics theories and require verification for real materials. As early as 1900, Guest[18] performed combined tension-torsion tests on mild steel tubes and his results supported the Tresca or maximum shearing stress criterion. A somewhat more well known piece of research was conducted by W. Lode[19] in 1926. Lode's experiments involved thin tubes of steel, copper, and nickel subjected to combined axial tension and internal pressure. Apparently Lode felt that, in view of the von Mises criterion of yielding, the intermediate principal stress should have an influence on yielding and his experiments showed that this was true. Thus Lode confirmed the von

Mises criterion. Ros and Eichinger[20] conducted tests similar to Lode's on steel tubes under axial load and internal pressure. Their results, too, were similar to those of Lode, confirming the von Mises criterion.

Shortly thereafter, Taylor and Quinney[15] published the results of a comprehensive series of carefully conceived experiments that supported the von Mises criterion of yielding. They tested isotropic tubes of copper, mild steel, and aluminum under combined tension and torsion.

Still further confirmation of the von Mises criterion came with the work of Lessels and MacGregor.[21] Their results were obtained on medium alloy steel (approximately SAE 4340) thin-walled tubes subjected to axial force and internal pressure. Radial loading was used.

There follow a group of papers which deal with initial yielding and with various aspects of plastic stress-strain relationships and will thus be considered again later. Marin and Hu[22] in 1952 published the results of tests on 14S-T4 aluminum alloy tubes under axial force and internal pressure. Data from constant stress ratio tests were in good agreement with the von Mises criterion. However, in another series, the authors used a loading program that in one case followed the von Mises yield surface and in another case followed the Tresca yield surface. Appreciable plastic strain was observed in both cases and the authors conclude that, for variable stress ratios, neither criterion is rigorously correct, since the plastic strain should be zero for a "neutral" loading. This kind of test may not be conclusive, however, since it is very difficult to "follow" the yield surface without producing some plastic strain.

Marin and Hu[23] performed similar tests on 14S-T6 aluminum alloy tubes. Again a loading path which followed the von Mises yield surface did not result in zero plastic strain. Hu and Marin[24] extended their experiments on tubes under axial tension and internal pressure later to 24S-T aluminum alloy. As observed previously, a loading path which followed the Mises yield criterion gave measurable plastic strain. In the last set of experiments, a loading path which followed a criterion proposed by Prager[25] was also tried. (For plane principal stresses the Prager criterion gives a yield surface that looks like the Tresca criterion but with rounded corners.) The circuit of the Prager yield surface gave a very small final plastic strain. Extending their work still further, Marin and Hu,[26] in 1956, reported tests on SAE 1020 steel tubes under the same loading combination. In this case, constant stress ratio tests confirmed the von Mises criterion. However, when the load path followed the von Mises yield surface, large plastic strains were observed.

In order to determine whether the initial yield function depends only on the components of principal stress, Phillips and Kaechele[27] performed a "rotation" test. Here thin-tubes of 2S-0 aluminum were loaded in tension up to the initial yield surface. Then the principal stress magnitudes were kept constant while the directions were changed by suitably combining axial tension, torsion, and internal pressure. Very small plastic strains were observed indicating that the yield criterion is a function of the principal stress magnitudes. In other words, the material is isotropic.

The question of the dependence of the yielding process on the mean stress or hydrostatic component of stress has been investigated in particular by Bridgeman.[28,29] In the first reference, tests of solid cylindrical specimens under axial tension and external pressure are reported. For a range of mean stress from zero up to a value equal to the applied tensile stress, it was found that the flow stress for beginning of yielding and for small plastic strains was independent of mean stress in several steels. The second reference presents data from tests in simple compression in which the plastic volume change was measured. As has been demonstrated in Chapter III, the plastic volume change should be zero in a stable plastic material for which the yield is independent of mean stress. Tests results showed small plastic changes in volume for several plain-carbon steels, copper, brass, and duralumin. Ros and Eichinger[20] also showed that the yield strength of an annealed cast steel is independent of the mean stress for tests performed under axial compression and external pressure. Based on these results the assumption of independence of mean stress of the yield process appears to be justified at least as a first approximation.

STRAIN-HARDENING BY THE ISOTROPIC THEORY

A form of the isotropic theory of strain hardening which employs effective stress-effective-strain curves has been used by many investigators and, in fact, until about 1950 was the only theory available. Since this particular concept was widely used, it will be discussed

briefly before considering the experimental investigations. The discussion will follow that presented by Hill.[7]

Use of effective stress-effective strain plots is based on an isotropic strain-hardening hypothesis that

$$\bar{\sigma} = H\left(\int d\bar{\epsilon}\right) \tag{5.1}$$

where $\bar{\sigma}$ is an effective stress and $\overline{d\epsilon}$ is an effective plastic strain increment. Now if one assumes that the von Mises criterion of yielding is valid throughout strain-hardening, the effective stress may be defined as

$$\bar{\sigma} = \left(\frac{3}{2} s_{ij} s_{ij}\right)^{1/2} \tag{5.2}$$

where the s_{ij} are the components of the stress deviator tensor. For example, in a tube subjected to tension and torsion, Equation (5.2) becomes

$$\bar{\sigma} = \left(\sigma_z^2 + 3\tau_{\theta z}^2\right)^{1/2}. \tag{5.3}$$

The corresponding effective plastic strain increment is

$$d\bar{\epsilon} = \left(\frac{2}{3} d\epsilon_{ij} d\epsilon_{ij}\right)^{1/2}. \tag{5.4}$$

These increments can be integrated if the principal axes of strain do not rotate with respect to an element of the material. For this to be true the principal axes of stress must remain fixed in an element of an initially isotropic material. In this event, the principal axes of stress and strain are initially coincident and remain coincident. However, this condition requires proportional or radial loading in the case of combined

axial force and torsion of a tube. When integration is possible the effective total strain is

$$\int d\bar{\epsilon} = \bar{\epsilon} = \left(\frac{2}{3}\epsilon_{ij}\epsilon_{ij}\right)^{1/2} \tag{5.5}$$

where ϵ_{ij} are the components of the plastic strain tensor. For the tube under tension and torsion, Equation (5.5) becomes

$$\bar{\epsilon} = \left[\frac{4}{3}(\epsilon_\theta^2 + \epsilon_\theta\epsilon_z + \epsilon_z^2) + \frac{1}{3}\gamma_{\theta z}^2\right]^{1/2} . \tag{5.6}$$

Note that $\gamma_{\theta z}$ is the engineering shearing strain. The numerical factors are introduced so that the function $H(\bar{\epsilon})$ of Equation (5.1), with Equation (5.5), is the relation between stress and strain in the simple tension test. Equation (5.1) relates to plastic strains, strictly speaking. However, it may be applied to total strains if the elastic portion of the strain is negligible. An idea somewhat similar to the preceding would be to relate the maximum shearing stress and maximum shearing strain under the assumption that the Tresca criterion of yielding was valid.

Davis[30,31] has used these ideas to interpret the results from axial tension-internal pressure tests on tubes of annealed copper and of a medium carbon steel. In both cases he plots his results as octahedral shearing stress vs. octahedral shearing strain which are proportional to $\bar{\sigma}$ and $\bar{\epsilon}$ respectively. Fairly good correlation (points lying on a single curve) of the data points was observed. Correlation was not as good in plots of maximum shearing stress vs. maximum shearing strain. In later tests[32] on mild steel tubes under tension and torsion, Davis found excellent correlation of data on a plot of octahedral shearing stress vs.

octahedral shearing strain. The directions of principal strain were held constant in the latter experiments.

Cunningham, Thomsen, and Dorn[33] conducted tests on AZ61 magnesium alloy tubes under a combination of axial force and internal pressure and employed plots of $\bar{\sigma}$ vs. $\bar{\epsilon}$ to examine their data. A fairly good correlation of the points to a single curve was obtained for constant stress ratio tests. Variable stress ratio tests were also performed. The plastic strains observed in the tests were compared with strains predicted from

$$d\varepsilon_{ij} = \frac{d\bar{\varepsilon}}{\bar{\sigma}} s_{ij} \qquad (5.7)$$

where $d\bar{\epsilon}$ and $\bar{\sigma}$ were obtained from an experimentally determined $\bar{\sigma}$ vs. $\bar{\epsilon}$ curve. Remarkably good agreement was obtained. Equation (5.7) is, except for a constant, the stress-strain relationship given by Hill for isotropic hardening [see Equation (30) on page 39 of Reference 7].

Osgood's[34] experiments on tubes of 24S-T aluminum alloy subjected to axial load and internal pressure resulted in reasonably good correlation of data points when plotted as octahedral shearing stress vs. octahedral shearing strain or as maximum shearing stress vs. maximum shearing strain. Stresses were maintained in constant ratio during loading.

Tension-torsion tests on thin tubes under variable stress ratios were conducted by Morrison and Shepherd.[35] The materials involved were a nickel-steel and a silicon-aluminum alloy. Typical loading programs involved the application of tension up to a selected point followed by

loading in torsion with tension held constant. Torsion followed by tension was also used. Plastic strains were computed from an equation similar to (5.7), i.e., by assuming isotropic hardening. Good agreement of observed strains and computed strains was found in many cases.

Marin, Ulrich, and Hughes[36] developed a variant of the isotropic strain hardening hypothesis in which the stress-strain relationship becomes

$$d\varepsilon_{ij} = dB\,(3 s_{ij}) \tag{5.8}$$

where

$$dB = F(\bar{\sigma}) \cdot d\bar{\sigma} .$$

By a rather complex procedure dB is determined from experimental tensile stress-strain curves. This technique was then used to predict strains for tension-internal pressure tests on 75S-T6 aluminum alloy tubes, in which variable stress ratios were used. Measured strains agreed well with predicted strains. In addition strains predicted by a deformation theory of plasticity were also in agreement with the measured values. In a subsequent paper, Hu and Marin[37] propose the use of Equation (5.7), after Hill, but with the assumption of

$$\bar{\varepsilon} = k \bar{\sigma}^{n} \tag{5.9}$$

for the effective stress-strain curve. As noted by Hu and Marin, the latter assumption is valid only for large strains.

Marin and Hu[22] used these theories to predict plastic strains in tests on 14S-T4 aluminum alloy tubes under tension and internal pressure. Variable stress ratios were used in one portion of the experimental work.

In one case, the internal pressure was applied first and then held constant while tension was applied and vice versa. Multiple loading paths involved an initial loading in tension, unloading, and then application of internal pressure. This procedure was also reversed. In all cases, predicted plastic strains were in good agreement with measured plastic strains. In another portion of the experimental work, stress ratios were held constant and the data points correlated fairly well when plotted as effective stress vs. effective strain.

An investigation of 2S-0 aluminum tubes subjected to tension and torsion by Phillips and Kaechele[27] gave results that correlated poorly on a plot of octahedral shearing stress vs. octahedral shearing strain. However, stress ratios were not held constant.

Gill and Parker[38] employed another combination of loads that has some advantages experimentally. They loaded tubes of alpha brass in combined internal pressure and torsion, thus avoiding the alignment problems attendant to axial loading. Effective stress-strain plots were used to compare the results but rather poor correlation for various stress paths was obtained. Gill and Parker attribute this to anisotropy and better correlation of results is found when an anisotropy which is rotationally symmetric about the tube axes is postulated.

It appears that isotropic hardening gives useful predictions of behavior in those investigations for which the assumptions of the theory are satisfied. In nearly all cases, the stress path is one which continually moves the yield surface outward. For such a stress path, it may be difficult to distinguish between strain-hardening theories and

thus the correctness of isotropic theory predictions is not surprising.

STRAIN-HARDENING BY THE SLIP THEORY

Probably the first break from the concept of isotropic strain hardening was the slip theory proposed by Batdorf and Budiansky.[39] This theory is based on the ideas of slip in crystals and while somewhat difficult to apply does provide the useful prediction that corners form in a smooth yield surface when it is pierced by a stress state point.

Budiansky, Dow, Peters, and Shepherd[40] performed experiments on thin tubes of 14S-T4 aluminum alloy stressed in axial compression and torsion to check for the development of corners. In their tests, the specimen was loaded initially in compression to a point beyond the yield surface. Then compression and torsion were applied in various ratios so that various stress paths were followed from this point. In accordance with incremental theories of plasticity, the initial shear modulus for the combined loading is elastic. For stress paths in which $d\tau_{\theta z}/d\sigma_z$ is negative, yielding occurred at a smaller stress than would be predicted by isotropic hardening but at the approximate stress predicted by the slip theory. Note that the prediction of the slip theory for the strain-hardened yield surface is obtained by drawing a pair of lines through the compression loading point and tangent to the initial yield surface.

Marin and Hu[23] have presented data which appear to support the slip theory. As a part of the work on 14S-T6 aluminum tubes, under tension and internal pressure, loading was carried beyond the initial yield surface followed by unloading along the subsequent yield surface predicted

by slip theory. Very small plastic strains were observed. However, these results could be explained equally well by assuming that the Tresca condition of initial yielding is valid. Hu and Marin[24] also indicated that results of similar tests on 24S-T aluminum alloy tubes suggested the formation of a corner on the yield surface. It might be noted that in the paper just mentioned, Hu and Marin consider but reject the possibility that the yield surface might move as a unit.

The tests reported by Marin and Hu[26] for cold drawn, mild steel tubes in axial tension and internal pressure are particularly significant. For one specimen, stresses were increased (non-radially) to a point beyond the yield surface. The specimen was then unloaded in a stepwise fashion so that the subsequent yield surface was followed. It is obvious from examination of the results that isotropic hardening is not valid. Although Marin and Hu interpret the result as supporting the slip theory it is just as possible to say that the result supports the kinematic theory of hardening.

Naghdi and Rowley[41] tested tubes of 24S-T4 aluminum alloy in tension-torsion in a manner like that reported by Budiansky, Dow, Peters, and Shepherd.[40] Initial loading was in tension to a point beyond the initial yield surface. Combinations of tension and torsion were then applied so that various stress paths were followed. Only for those cases in which $d\tau_{\theta z}/d\sigma_z = -2$, was elastic behavior observed in the second part of the test. From this it is assumed that a corner develops or that the slip theory applies.

Naghdi, Rowley, and Beadle[42] extended the work reported above to a complex loading path in which radial loading proceeds to a point beyond the initial yield surface. At this point a zig-zag loading path is followed by alternating the tension and torsion loads. Data from this type of test seem to show that the directions of the stress increment vector and the strain increment vector coincide. This would not be expected if the yield surface is smooth and thus it is concluded that a corner forms on the yield surface.

The salient point from the work discussed in this section is that isotropic hardening often gives incorrect predictions. Postulating the appearance of corners on subsequent yield surfaces is one way to explain observed phenomena.

THE FORM OF SUBSEQUENT YIELD SURFACES

Experiments in which the forms of one or more subsequent yield surfaces are defined provide a more conclusive demonstration of the type of hardening theory which may be used.

For example, Gill[43] loaded thin tubes of alpha brass in torsion and internal pressure so that, after an initial torsion loading beyond the initial yield surface, the loading followed an expanded von Mises or Tresca yield surface. Isotropic hardening was assumed to apply. Small plastic strains were observed when following the expanded von Mises yield surface while larger plastic strains were observed when following the expanded Tresca yield surface. Normality of strain increment vectors was found. The author concludes that the actual subsequent yield surface

falls inside the surface followed in the test. One might suppose that kinematic hardening would provide such a yield surface.

Naghdi, Essenburg, and Koff[44] have published an even more thorough investigation of subsequent yield surfaces. The results were obtained from tests 24S-T4 aluminum alloy tubes loaded in combined tension and torsion. Non-radial loading was used. Unstrained specimens are used to define the initial yield surface. For the first subsequent yield surface, all specimens were initially stressed in torsion to a point beyond the initial yield surface, unloaded, and then reloaded along a non-radial path to yielding. For the second subsequent yield surface, the initial loading for all specimens is in pure torsion to a point beyond the first subsequent yield surface. The motion of the yield surface is studied on a plot of $\tau_{\theta z}$ vs. σ_z. It appears that the yield surface of von Mises deforms slightly during hardening by elongating in the positive $\tau_{\theta z}$ direction.

Somewhat similar results were obtained by Hu and Bratt[45] who ran tension-internal pressure tests on 2S-F aluminum alloy tubes. After an initial loading in tension to a point beyond the initial yield surface, the tubes were unloaded. Loading then proceeded under various combined loadings up to yielding. Results of the test program give a subsequent yield surface which is distorted so that it is elongated in the positive σ_z direction.

McComb,[46] too, noted an elongation of the yield surface in the direction of plastic straining. McComb performed tests on 2014-T61 alum-

inum alloy tubes in tension-torsion. For all tests, the initial loading was in tension to a point beyond the initial yield surface. The specimens were then unloaded and reloaded along various paths with the ratio of tension to torsion held constant. The distortion of the yield surface is noted when the results are plotted in $\tau_{\theta z}$-σ_z space.

An elaborate experimental program conducted by Talypov[47] demonstrated that the yield surface is displaced in the direction of preliminary plastic deformation and may be expanded in addition. This conclusion was based on experiments performed on steel tubes under axial force and internal pressure. Multiple loading paths were employed.

Finally, Ivey[48] has published the results of a series of tests very similar to those of Naghdi, Essenburg, and Koff[44] but for several aluminum alloys. The initial loading for all specimens was in torsion to a point beyond the initial or preceding yield surface. Results are presented in $\tau_{\theta z}$-σ_z space. Ivey shows that the yield surface translates in the direction of prestrain and that it also distorts. The distortion in this case involves a shortening of the minor axis (parallel to $\tau_{\theta z}$) of the elliptical yield surface, but not like that observed by Naghdi, et al.

Although distortion of subsequent yield surfaces is reported by several investigators, it should be recalled that the analysis presented in Chapter IV indicates that distortion of the yield surface can be expected in the $\tau_{\theta z}$-σ_z subspace or the σ_θ-σ_z subspace. Although isotropic hardening is not in agreement with experiments, kinematic or piecewise-linear theories are not eliminated by the investigations just discussed.

CHAPTER VI

COMPARISON OF EXPERIMENTAL RESULTS AND THEORETICAL PREDICTIONS

In this chapter, the body of experimental data obtained on Zamak-3 tubes under the loading conditions described in Chapters I and II is used to test the theoretical predictions outlined in Chapters III and IV. It might be well to reiterate that the objectives of the research concern first the initial yield behavior of this brittle material and second, its response in the strain-hardening range of plastic behavior. The experiments have been planned in such a way that basic assumptions of the theory can be checked and that predictions of the theory can be expected to hold.

ISOTROPY

In the last section of Chapter III, it is shown that an isotropic tube under the action of pure tension along the z-direction should exhibit a ratio of circumferential plastic strain to axial plastic strain of -0.5. Total plastic strains can be considered rather than plastic strain increments because the stress path is a radial one. The above ratio does not depend on the form of the yield condition but is predicted by the flow rule in conjunction with any yield condition which, in addition to isotropy, assumes the yield of the material is independent of mean stress. Plastic incompressibility follows from the latter.

Perhaps more important it is shown in Chapter III that a material having anisotropy which is rotationally symmetric about the r-direction

would have a ratio of circumferential plastic strain to axial plastic strain different from -0.5. See Equation (3.53). Anisotropy which is rotationally symmetric about the z-direction would not be detected by a measurement of this ratio of strains.

Figure 19 presents a plot of axial plastic strain, ϵ_z^p, against circumferential plastic strain, $-\epsilon_\theta^p$, for two tension tests. The test data marked OP-12 were obtained at 78°F and the test data marked OP-14 were obtained at 32°F. These strains were measured with foil strain gages attached with Eastman 910 cement. For OP-12, the ratio of circumferential plastic strain to axial plastic strain is -0.53 while for OP-14 the ratio is -0.54. In order to estimate the degree of anisotropy indicated by these observations, refer again to Chapter III. If Equations (3.48) and (3.50) are substituted into Equation (3.53) it becomes

$$-\frac{d\epsilon_\theta^p}{d\epsilon_z^p} = \frac{F}{F+H} = 1 - \frac{1}{2}\left(\frac{\sigma_\theta^*}{\sigma_r^*}\right)^2 \qquad (3.53a)$$

Now the ratio $\sigma_\theta^*/\sigma_r^*$ can be found for known values of the ratio $d\epsilon_\theta^p/d\epsilon_z^p$. When $d\epsilon_\theta^p/d\epsilon_z^p = -0.54$, $\sigma_\theta^*/\sigma_r^* = 0.959$ and when $d\epsilon_\theta^p/d\epsilon_z^p = -0.53$, $\sigma_\theta^*/\sigma_r^* = 0.970$. The above would imply that the yield strength in the circumferential direction, σ_θ^*, and the yield strength in the radial direction, σ_r^*, differ at most by about 4 percent. This indicates a very slight, if any, anisotropy of the postulated type.

A measurement of plastic volume change in the internal cavity of the specimen, somewhat like the experiments of Taylor and Quinney,[15] was also performed at a testing temperature of 32°F. Figure 20 is a sketch of a

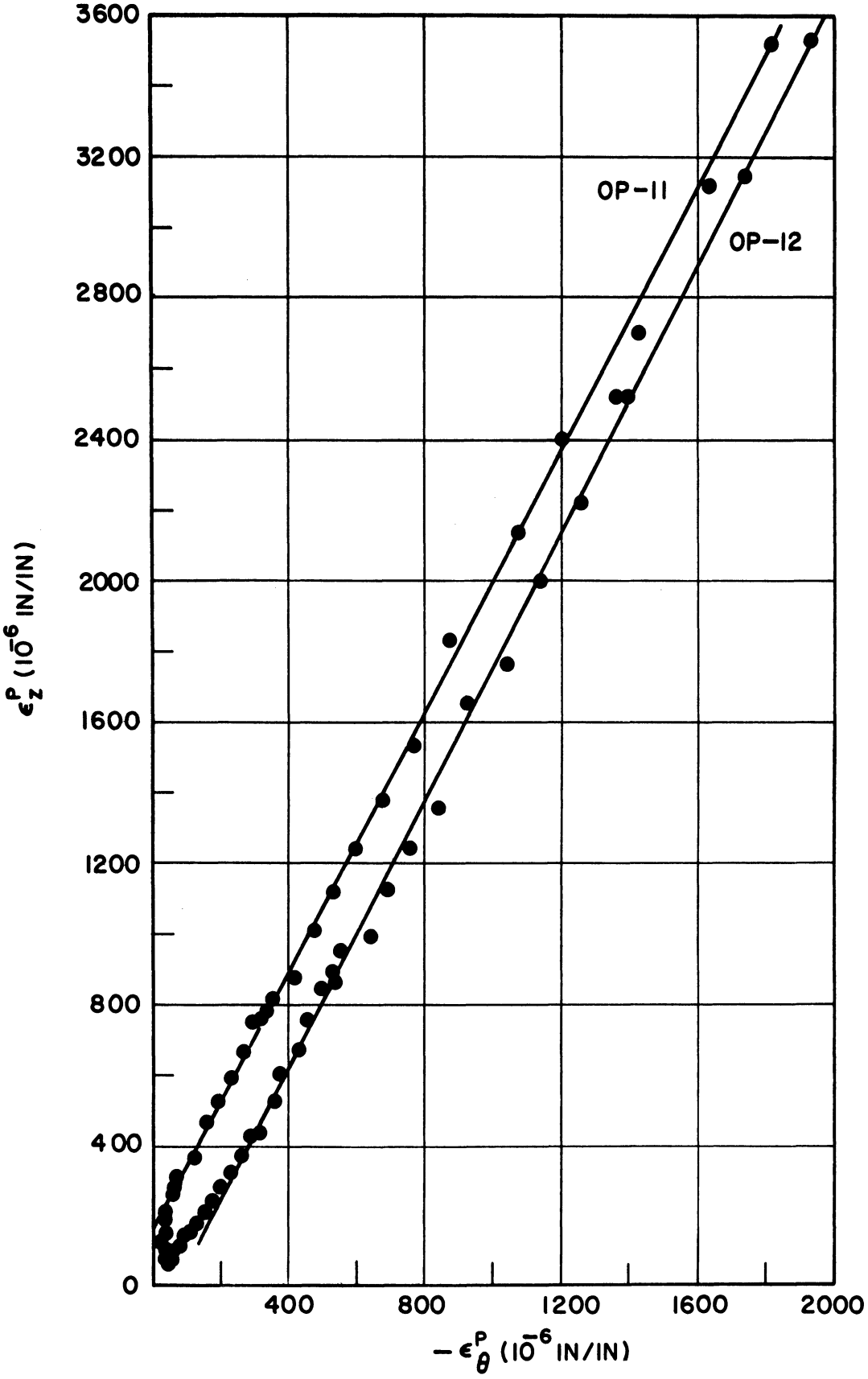

Figure 19. Axial and circumferential plastic strains in pure tension.

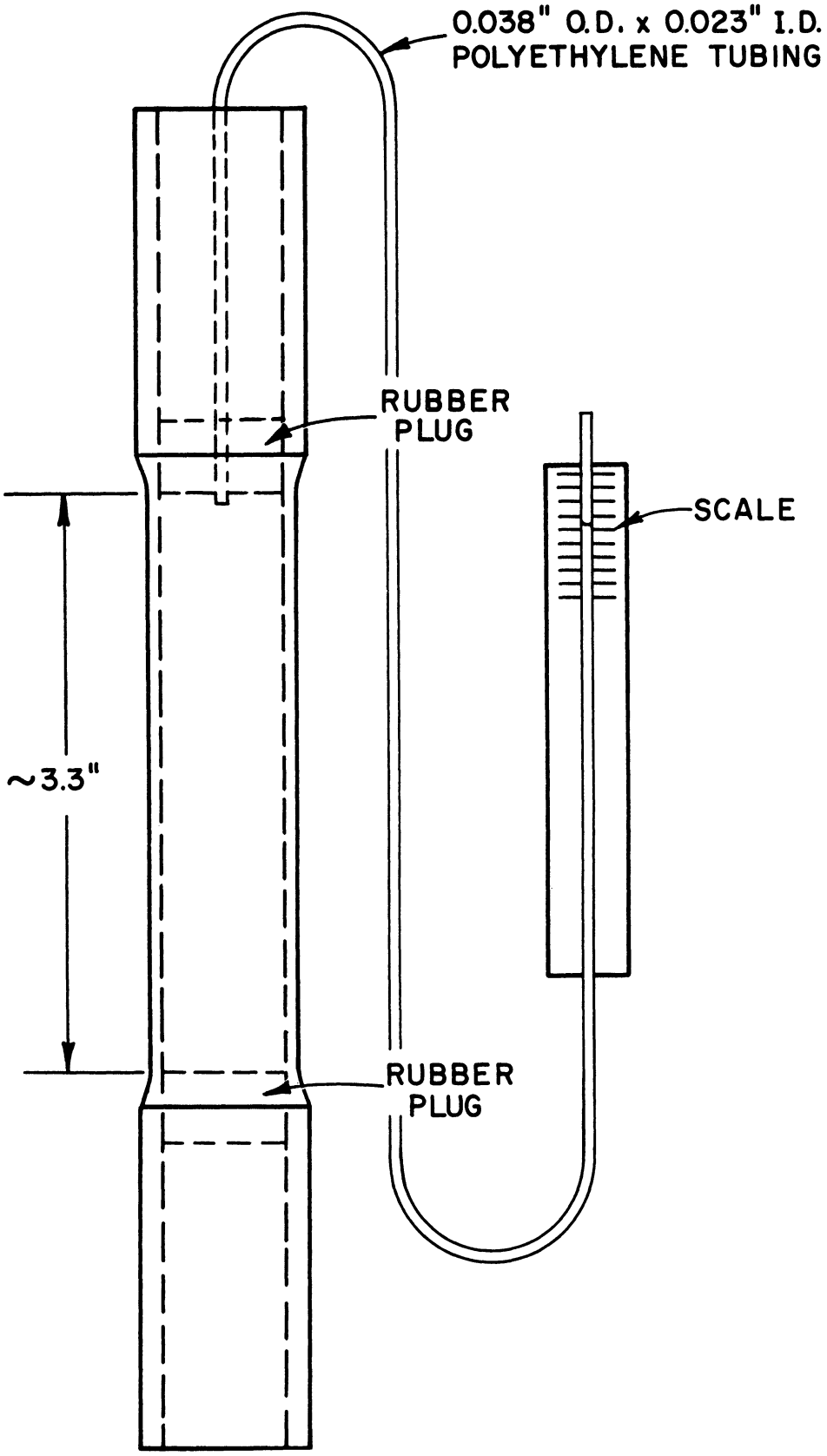

Figure 20. Specimen adapted for measurement of internal volume change.

specimen with rubber plugs and plastic tubing in place. The region lying between the rubber plugs (i.e., in the region of the reduced section of the specimen) and the tubing was filled with water. Any change in volume of the internal cavity lying between the rubber plugs would be indicated by a change in water level in the plastic tubing. During loading of the specimen in pure tension, the change in water level was measured on a scale at roughly the same height as the specimen itself.

Of course this apparatus measures both elastic and plastic volume change. To determine the portion of the total change of volume which is plastic, a plot has been made in Figure 21 of the actual or measured volume change against a computed elastic volume change. In a tension test, the elastic volume change in the internal cavity is given by

$$\Delta V = \pi r^2 \ell \frac{(1-2\nu)}{E} \sigma_z \qquad (6.1)$$

where

r = 0.344-inch

ℓ = 3.3 inches

ν = 0.25

and E = 11.4 x 10^6 psi.

Figure 21 indicates that the measured volume change in the internal cavity of the tube is almost entirely a result of elastic deformation in the tube.

At the higher stresses, i.e., the upper part of the graph of Figure 21, the elastic volume change is greater than the observed volume change

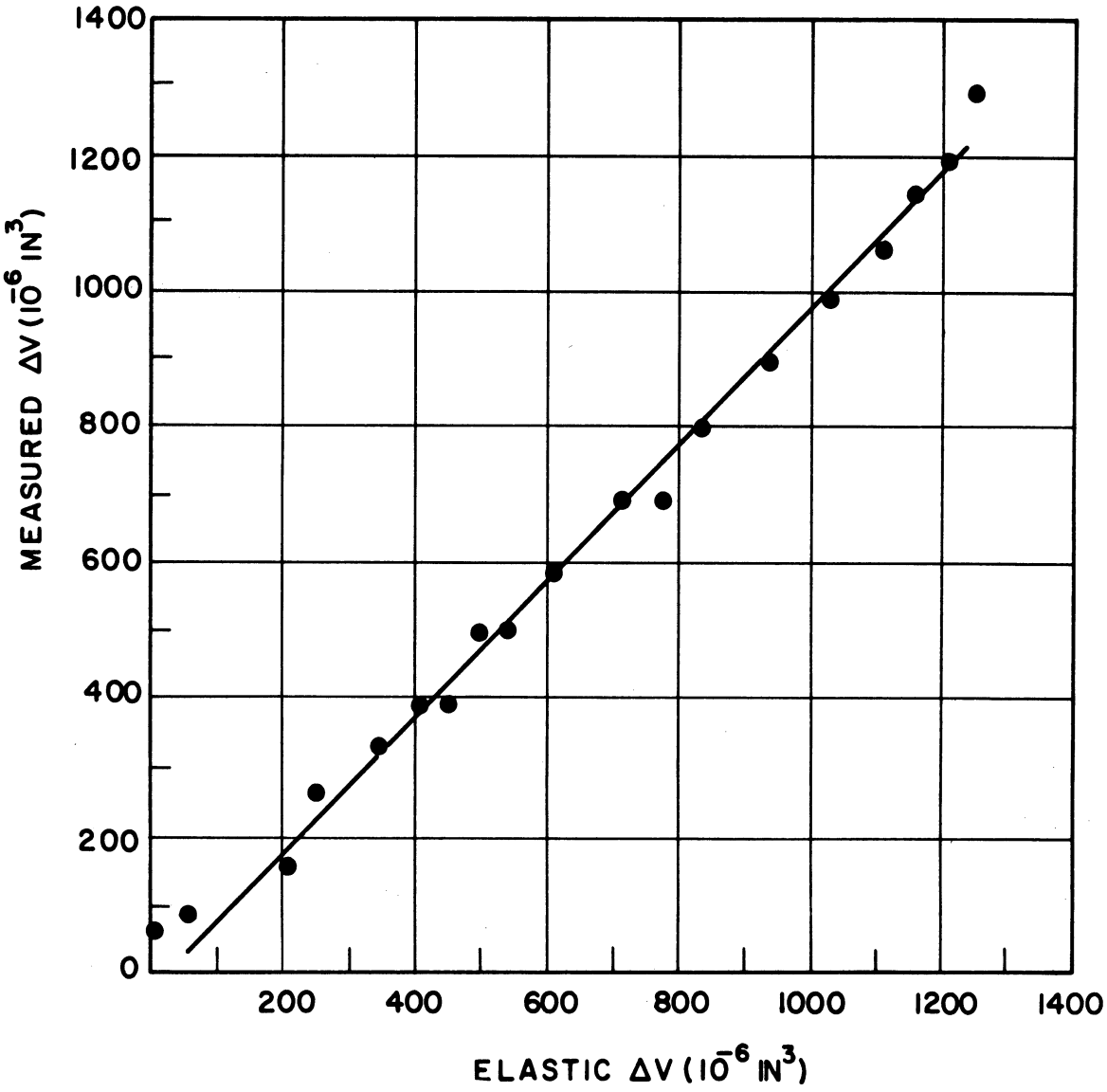

Figure 21. Volume change in internal cavity of tube.

which means that the plastic volume change is negative. This is in accord with the axial and circumferential strain measurements since Equation (3.55) will yield a negative ΔV for $d\epsilon_\theta/d\epsilon_z = -0.53$ or -0.54.

Since the results in this test complement the results of the strain measurements, further evidence is obtained that the Zamak-3 tubes are isotropic for practical purposes.

MATERIAL RESPONSE TO SIMPLE STATES OF STRESS

Since Zamak-3 zinc-alloy is a material whose mechanical properties are not widely-known, stress-strain curves in simple axial loading and simple torsion are presented.

Figure 22 presents results of tensile tests at both 78°F and 32°F. The data shown include the entire range of loading up to the point of fracture, the strains at fracture ranging from about 0.006 to about 0.009. It is to be noted that the range of elastic behavior (stress proportional to strain) is limited and ceases at a stress of about 6000 psi. Further, in the plastic range of behavior, the curves are not coincident. This latter observation is characteristic of the material itself, rather than the specimen, since a similar behavior was seen in the results for 1/4-inch diameter solid cylindrical specimens.

Reducing the testing temperature from 78°F to 32°F seems to have a relatively small effect on the tensile stress-strain curve although the data in the plastic range for the higher temperature do lie slightly below the data taken at 32°F.

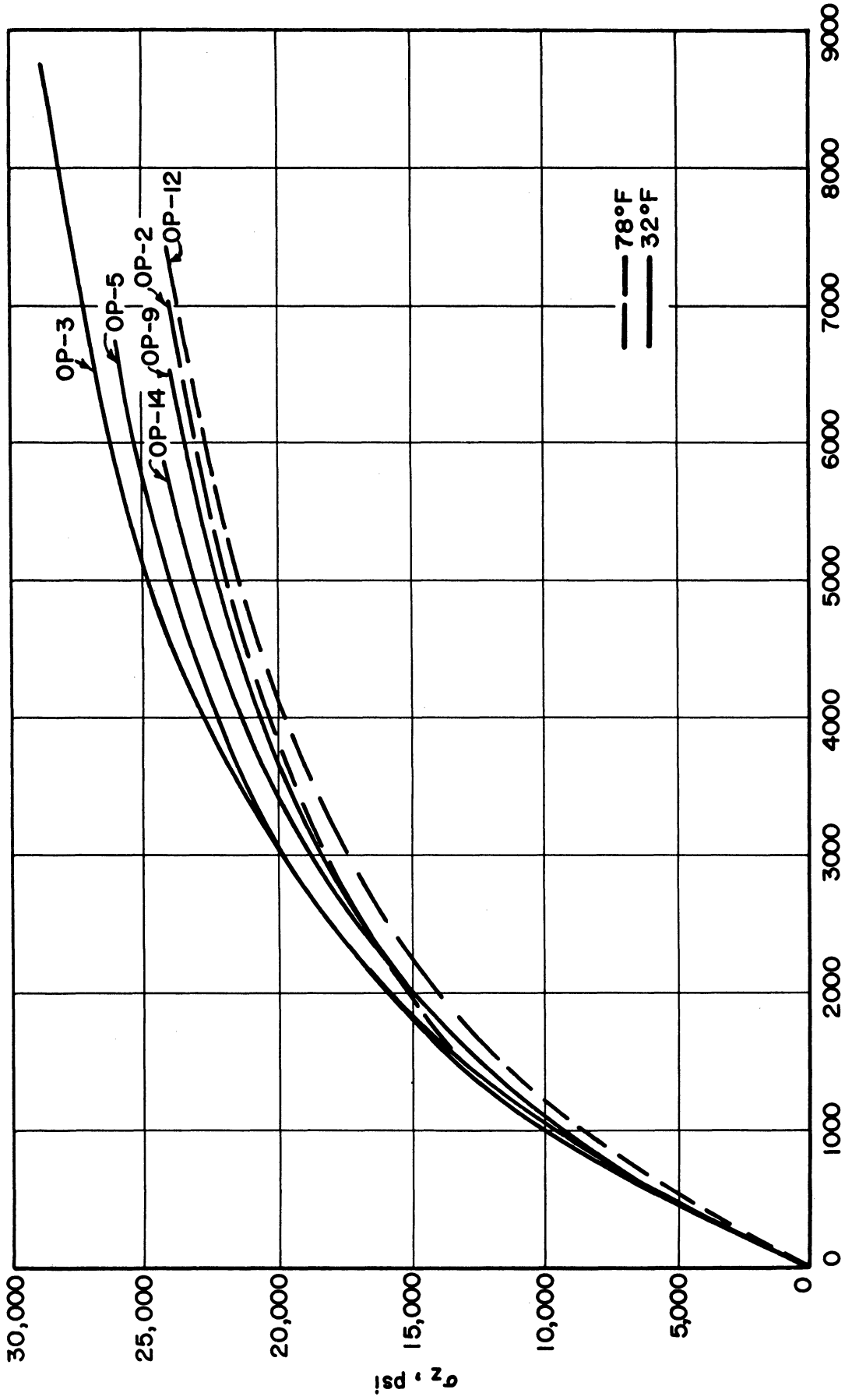

Figure 22. Tensile stress-strain curves, 78°F, 32°F.

To afford a comparison of behavior in simple tension and simple compression, Figure 23 is included. It is seen that essentially identical tensile and compressive stress strain curves are obtained, thus justifying this assumption in the theoretical development. The test for which data are shown was not carried to fracture.

Stress-strain curves obtained in torsion at both 78°F and 32°F are shown in Figure 24. Here it is observed again that the response of the material in torsion is approximately the same at both test temperatures. In both of these torsion tests, measurements were terminated before rupture occurred.

INITIAL YIELDING UNDER COMPLEX STATES OF STRESS

In the ensuing discussion, the yield stress is defined as the proportional limit stress since, for practical purposes, the proportional limit stress and the elastic limit stress coincide. This point was verified during one test run by a program of loading and unloading, each subsequent loading stopping at a higher stress. The appearance of a plastic strain at zero stress on unloading showed the previous stress for which plastic deformation began. In this case the proportional limit stress appeared to coincide with the elastic limit stress.

For the combined load tests, the yield stress was determined in the following manner. Measured values of σ_z and σ_θ or σ_z and $\tau_{\theta z}$ were plotted against the largest measured normal strain. The smallest stress value was noted at which the plot deviated from linearity, e.g., if the σ_θ plot deviated first the "proportional limit" value was noted. The other stress

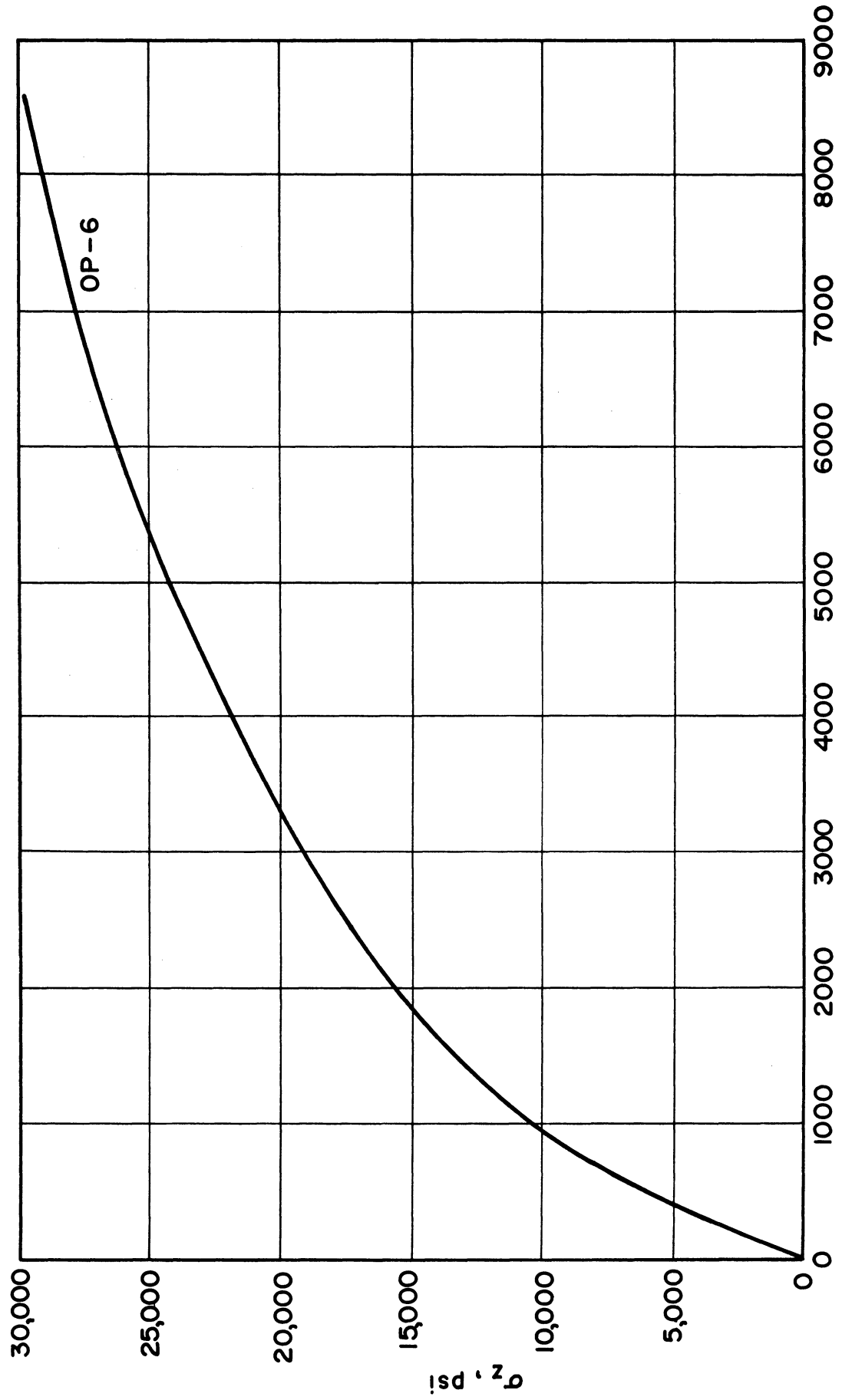

Figure 23. Compressive stress-strain curve, 32°F.

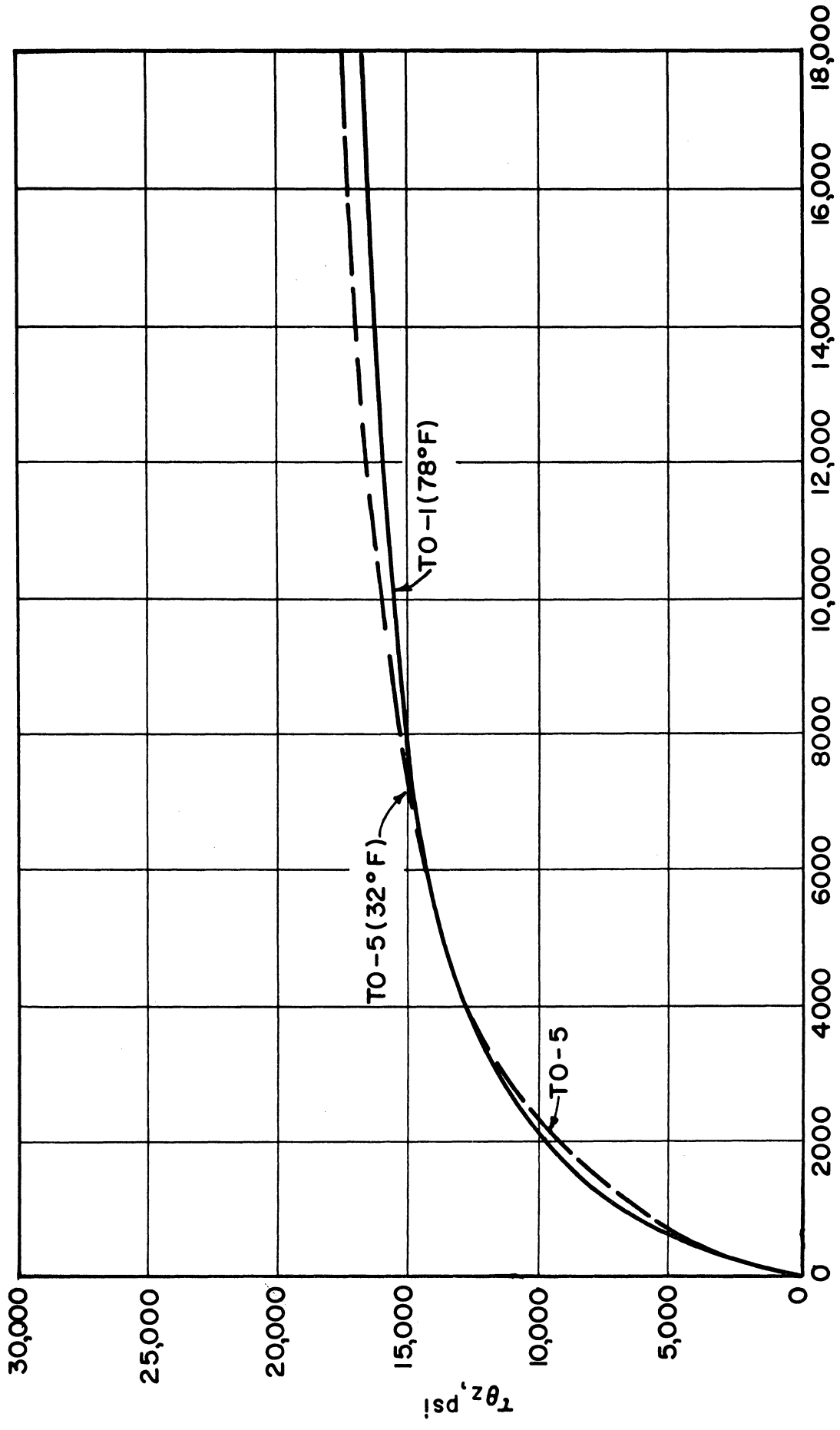

Figure 24. Torsion stress-strain curves, 78°F, 32°F.

component that was observed concurrently with the smallest value was also noted. Thus the pair of stress components representing yielding were in all cases a pair of values that had been observed at a given time.

The process just outlined may be clarified by referring to Figure 25, a set of stress-strain diagrams for a typical tension-internal pressure test. Considering the plots of σ_z vs. ϵ_z and σ_θ vs. ϵ_z, it is observed that the latter deviates from linearity first. The σ_θ at the "proportional limit" is 4360 psi. On referring to the recorded data it is found that a value of σ_z of 7400 psi was observed at the same time as the noted value of σ_θ. This pair of stresses constitutes the yield value. Incidentally, the data shown in Figure 25 comprise only the initial portion of the test results. As a matter of general interest, the left hand portion of Figure 25, showing σ_θ as a function of ϵ_θ, is included. Although plotted to the left of the origin, the ϵ_θ's are positive.

Since selection of the point of deviation from linearity in the stress-strain plot is difficult to do with precision, other definitions of yielding are sometimes used. The most common of these is to define the point of yielding by means of an "offset" yield strength, i.e., to define yielding as the stress at which a selected plastic strain occurs. However, for combined stresses, a consistent measure of this sort would require plotting of an "effective" stress—"effective" strain curve. As discussed previously, this in effect requires an assumption to be made for the yield condition and in the author's opinion has no place in a program to test yield conditions.

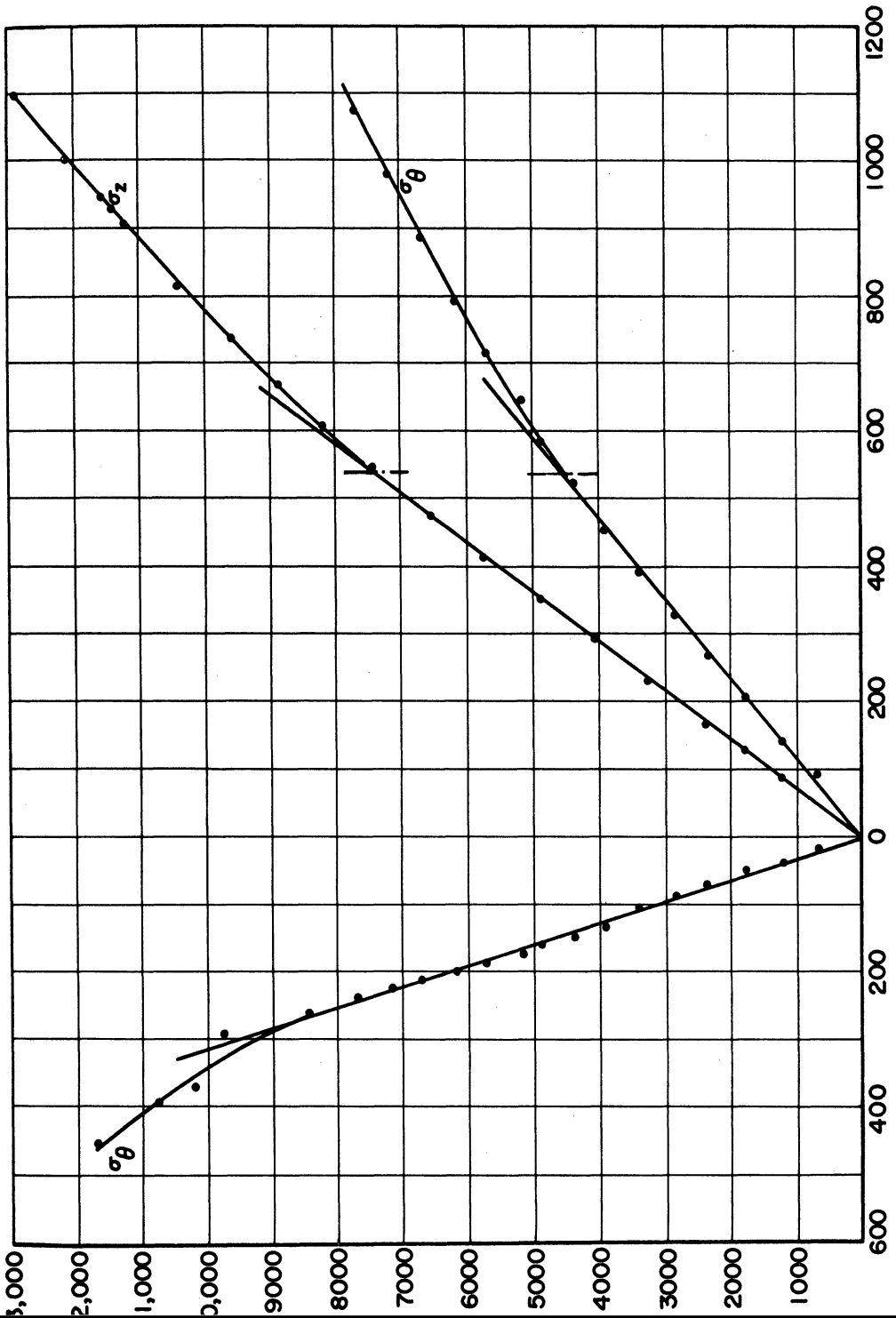

Figure 25. Stress-strain diagrams for test PP-4, combined axial tension and internal pressure.

Figure 26 is a plot in the octahedral plane of initial yield data for all tests performed at 78°F. The x-y coordinate system shown can be used to locate points in the octahedral plane. These x-y coordinates are related to the principal stresses σ_1 and σ_2 ($\sigma_3 = \sigma_r = 0$) as follows:

$$x = \frac{1}{\sqrt{2}}(-\sigma_1 + \sigma_2)$$
$$y = -\frac{1}{\sqrt{6}}(\sigma_1 + \sigma_2) \quad . \tag{6.2}$$

For tests in combined axial force and internal pressure, $\sigma_1 = \sigma_z$ and $\sigma_2 = \sigma_\theta$ while the definition of σ_1 and σ_2 for combined axial force and torque tests is

$$\sigma_{1,2} = \frac{\sigma_z}{2} \pm \sqrt{\left(\frac{\sigma_z}{2}\right)^2 + \tau_{\theta z}^2}$$

The various numbers adjacent to data points identify the specific test and type of loading. The key to the test designations is given in Table 1.

TABLE 1

TEST DESIGNATIONS

Symbol	Type of Loading
TO	Torsion only
TP	Axial force and torsion
OP	Axial force only
PP or X	Axial force and internal pressure
PO	Internal pressure only

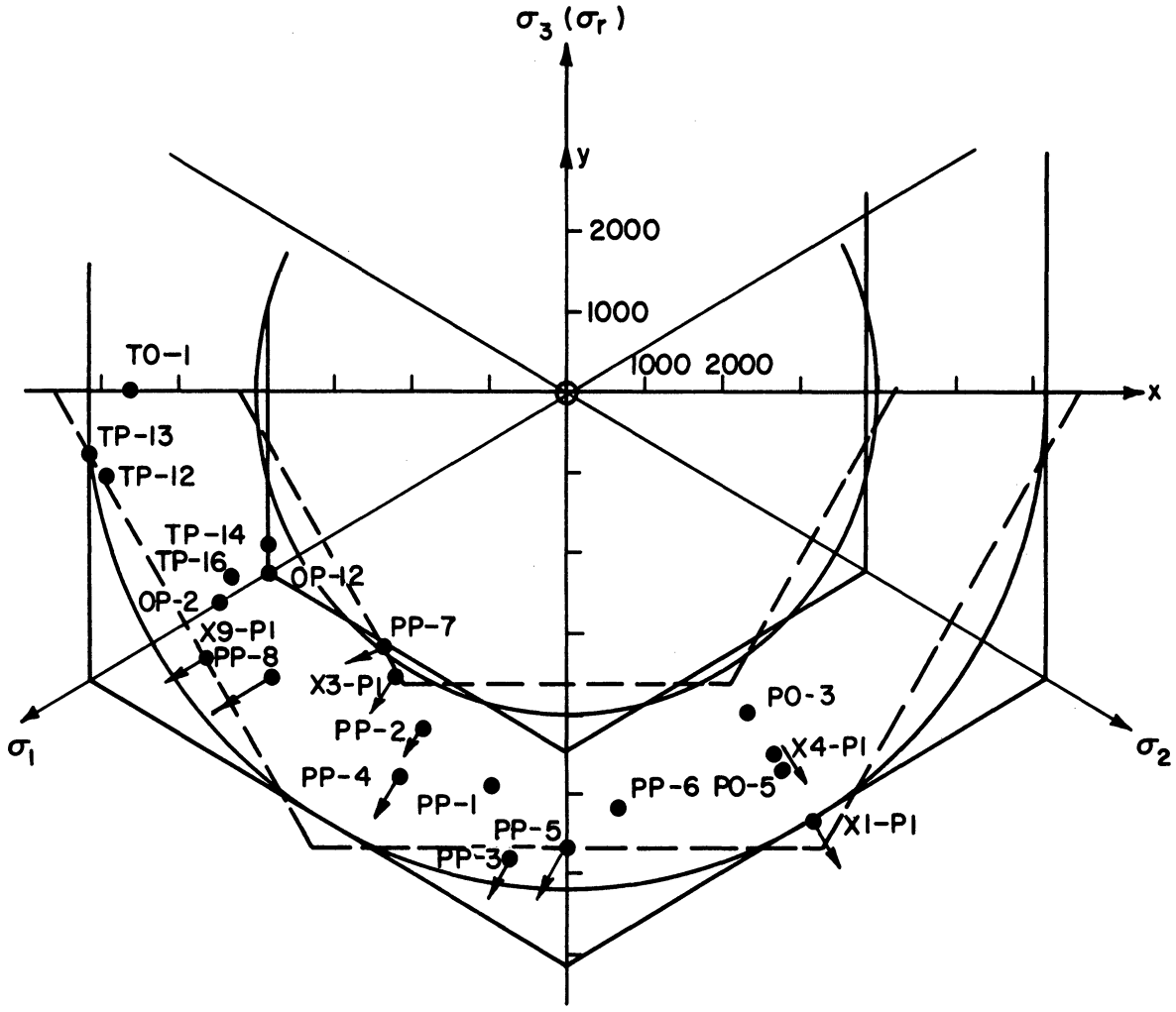

Figure 26. Initial yield data at 78°F.

It might be noted that the X designation refers to multiple load path tests to be described later. The points under this designation in Figure 26 represent yielding on initial loading.

As discussed in Chapter III, the von Mises criterion of yielding, Equation (3.6), is represented as a circle in the octahedral plane. Since there is considerable scatter in the data points, yield surfaces which pass through the innermost points and the outermost points are drawn. The circles shown in Figure 26 are such a pair of von Mises yield surfaces. To afford a measure of scatter and to facilitate comparison between conditions, values of σ_o, the yield value appearing in Equation (3.6), for inner and outer surfaces are listed in Table 2 for the various yield criteria.

TABLE 2

YIELD VALUES AT 78°F

Yield Criterion	σ_o, Inner Surface	σ_o, Outer Surface
von Mises	4950 psi	7550 psi
Tresca	5450 psi	8700 psi
Maximum Reduced Stress	4450 psi	6970 psi

The Tresca yield criterion, Equation (3.7), plots as a hexagon in the octahedral plane and the bounding hexagons for these data are shown in solid lines. Finally the dashed hexagons correspond to the maximum reduced stress criterion of yielding, Equation (3.8), and again bounding figures are shown.

The degree of scatter in the data of Figure 26 obviate the selection of a particular yield criterion. However, the yield surfaces having plane sides appear to fit the data as well as the von Mises criterion, and, consequently, their use appears justified in the later analyses of strain hardening. Further, the data points seem to scatter evenly between the bounding figures. Since the mean stress increases systematically from the pure torsion points to the points for which $\sigma_z = \sigma_\theta$, it is suggested that the data support the contention that initial yielding is independent of mean stress at this temperature.

For a few typical points, the plastic strain increment vector at initial yielding is shown. Increments in the octahedral plane are determined from the plastic strain increments as follows:

$$dx = \frac{1}{\sqrt{2}}(-d\varepsilon_1 + d\varepsilon_2)$$
$$dy = -\frac{3}{\sqrt{6}}(d\varepsilon_1 + d\varepsilon_2). \qquad (6.3)$$

When the loading is a combination of axial force and internal pressure, we set $d\epsilon_1 = d\epsilon_z$ and $d\epsilon_2 = d\epsilon_\theta$. In general, the strain increment vectors are normal to the ill-defined yield surface. Again there is enough scatter so that no particular yield surace is indicated.

The initial yield data for all tests at 32°F are shown on an octahedral plane plot in Figure 27. All of the test symbols have been defined in Table 1. As before, the circles in Figure 27 represent the bounding von Mises yield surface, the bounding Tresca yield surfaces are the solid hexagons, and the maximum reduced stress criterion is represented

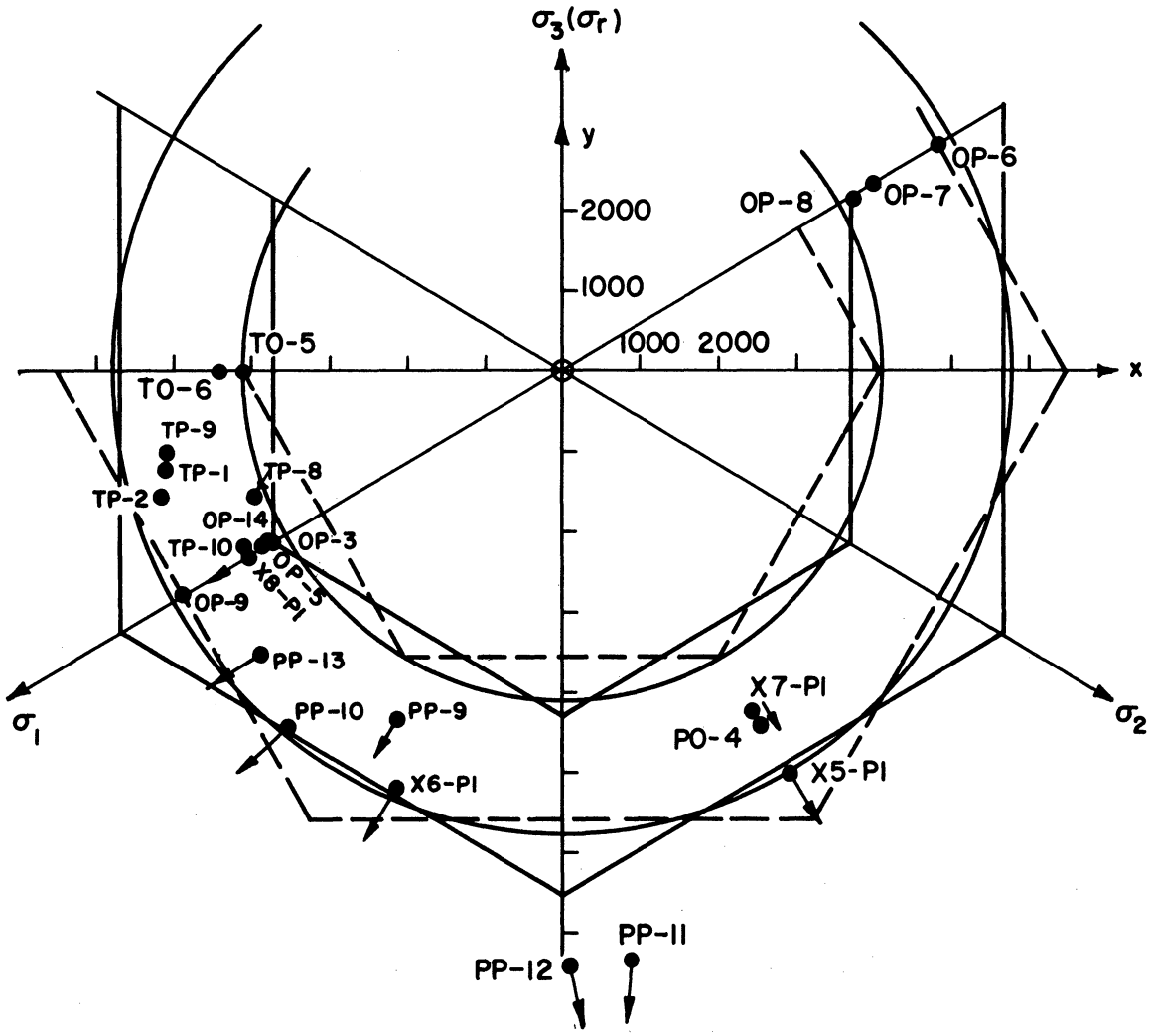

Figure 27. Initial yield data at 32°F.

sented by the dashed hexagons. Yield values, σ_o, are listed in Table 3.

TABLE 3

YIELD VALUES AT 32°F

Yield Criterion	σ_o, Inner Surface	σ_o, Outer Surface
von Mises	5030 psi	7060 psi
Tresca	5230 psi	8050 psi
Maximum Reduced Stress	4380 psi	6920 psi

The limiting σ_o values for a particular yield criterion are nearly the same for the two testing temperatures.

Bounding yield surfaces in Figure 27 are drawn, however, without considering points PP-11 and PP-12. Both of these points lie outside even the largest of the Tresca yield surfaces that bound the other points. Two plausible explanations of this behavior are offered. First, it could be interpreted as the appearance of anisotropy but measurements discussed earlier indicate that the material is isotropic. Second, it could represent an effect of mean stress on the yield process. To explore this possibility, Figure 28 has been prepared. In this figure, a representative stress for each criterion of yielding is plotted against $I_1 = \sigma_{ii}$, the first invariant of the stress tensor. The representative stress in the upper graph is the yield stress in simple tension corresponding to the data points of Figure 27 assuming that the von Mises criterion applies. This stress is, in fact, the σ_o which would be computed from Equation (3.6) if the various principal stress combinations at yielding were introduced.

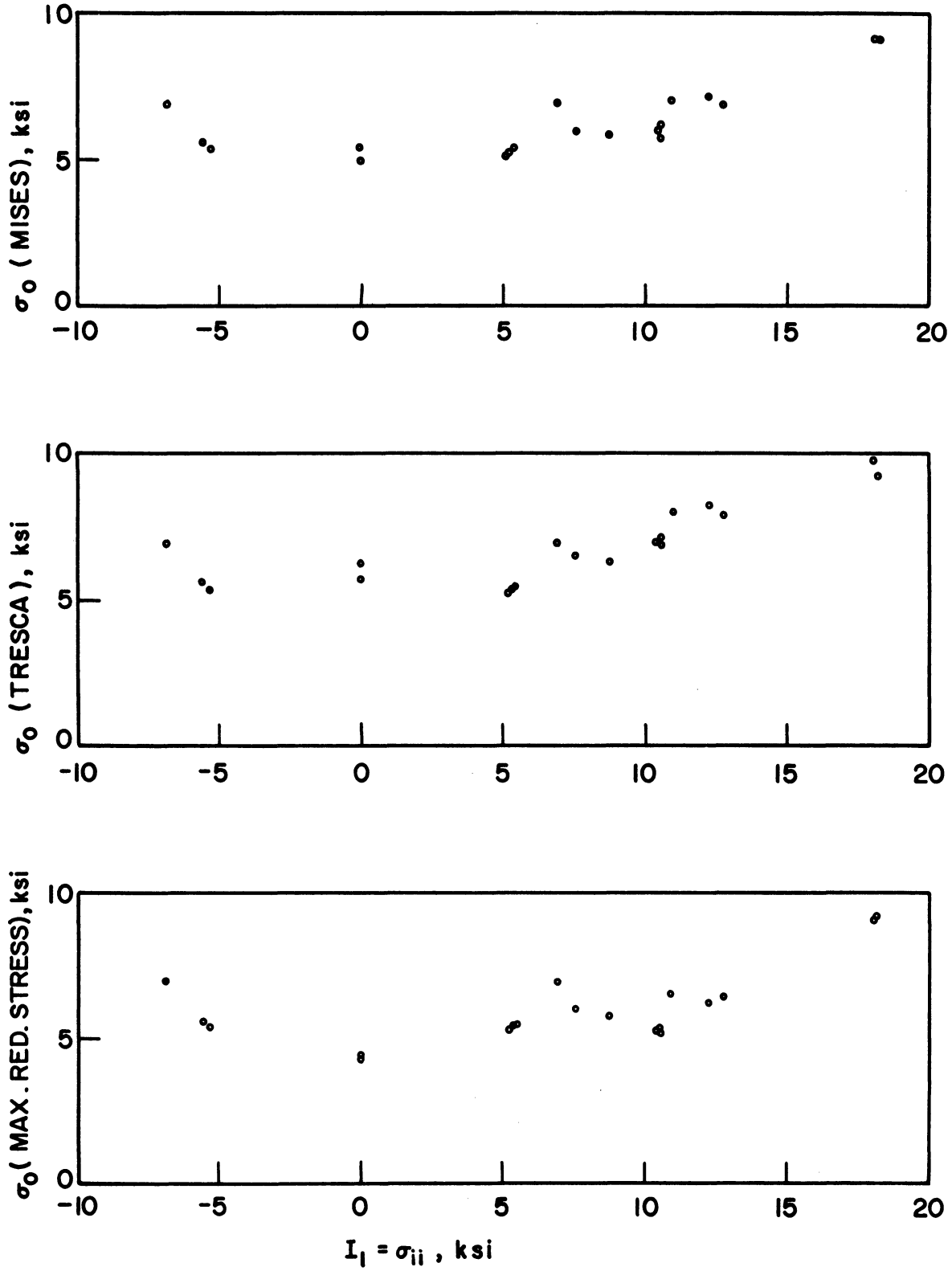

Figure 28. Representative stress vs. I_1 for data at 32°F.

The middle graph is a similar set of points based on the Tresca criterion, Equation (3.7) and the lower graph is also similar but is based on the maximum reduced stress criterion, Equation (3.8). The abscissas, σ_{ii}, are equal to three times the mean stress. Thus a yield process which is independent of mean stress would give points which plot along a horizontal line in Figure 28. This is in general realized for these data regardless of the yield condition except for two points at the largest values of σ_{ii}. These two points are for tests PP-11 and PP-12. Thus an effect of mean stress on initial yielding is suggested by the experimental observations. If, in fact, the effect exists, it must be described as an increase of σ_o with increasing mean stress. Interpreting this geometrically, the yield surface in principal stress space is a cone-like figure which expands in the direction of positive mean stress, a rather surprising result to say the least.

Figure 27 also shows data for tension tests (OP-3,5,9,14) and compression tests (OP-6,7,8). The observations reported for these tests tend to justify the assumption that yield stresses in tension and compression are equal.

As before, the plastic strain increments for some of the yield stress points are superposed on Figure 27. A rough indication of normality of the strain increment vectors is given for these data at 32°F. Since the degree of scatter in both stress points and directions of strain increment vector is comparable to that in Figure 26, it cannot be said that

the data support a particular criterion of initial yielding.

STRAIN HARDENING UNDER COMPLEX STATES OF STRESS

A series of multiple loading path tests were performed to afford a check of the various strain hardening theories. The general procedure in these tests was to load first along a given path (radial in all cases) to a point well beyond the initial yield surface, then to completely unload the specimen and to load along a second radial loading path to fracture. All of the data were obtained by using combinations of axial force and internal pressure so that rotation of the principal axes of stress would not occur during the loading program.

In the analyses, the Tresca yield criterion and the maximum reduced stress yield criterion are used because of their relative simplicity in connection with the strain-hardening theories. As has been noted previously, the plastic strain increment and consequently the motion of the yield surface is partially independent of the stress path when the yield surface has plane sides. It has also been seen that under these conditions the plastic strain increments are integrable and thus large motions of the yield surface can be accommodated.

Figure 29 gives the results for test X-1 which was performed at 78°F. Initial loading in this case was internal pressure alone. The point designated X1-P1 represents initial yielding while X1-P1MAX denotes the largest stress combination reached on the first path. Hexagon ABCDEFA represents the initial Tresca yield surface and hexagon GHIJKLG represents the initial maximum reduced stress yield surface. These are

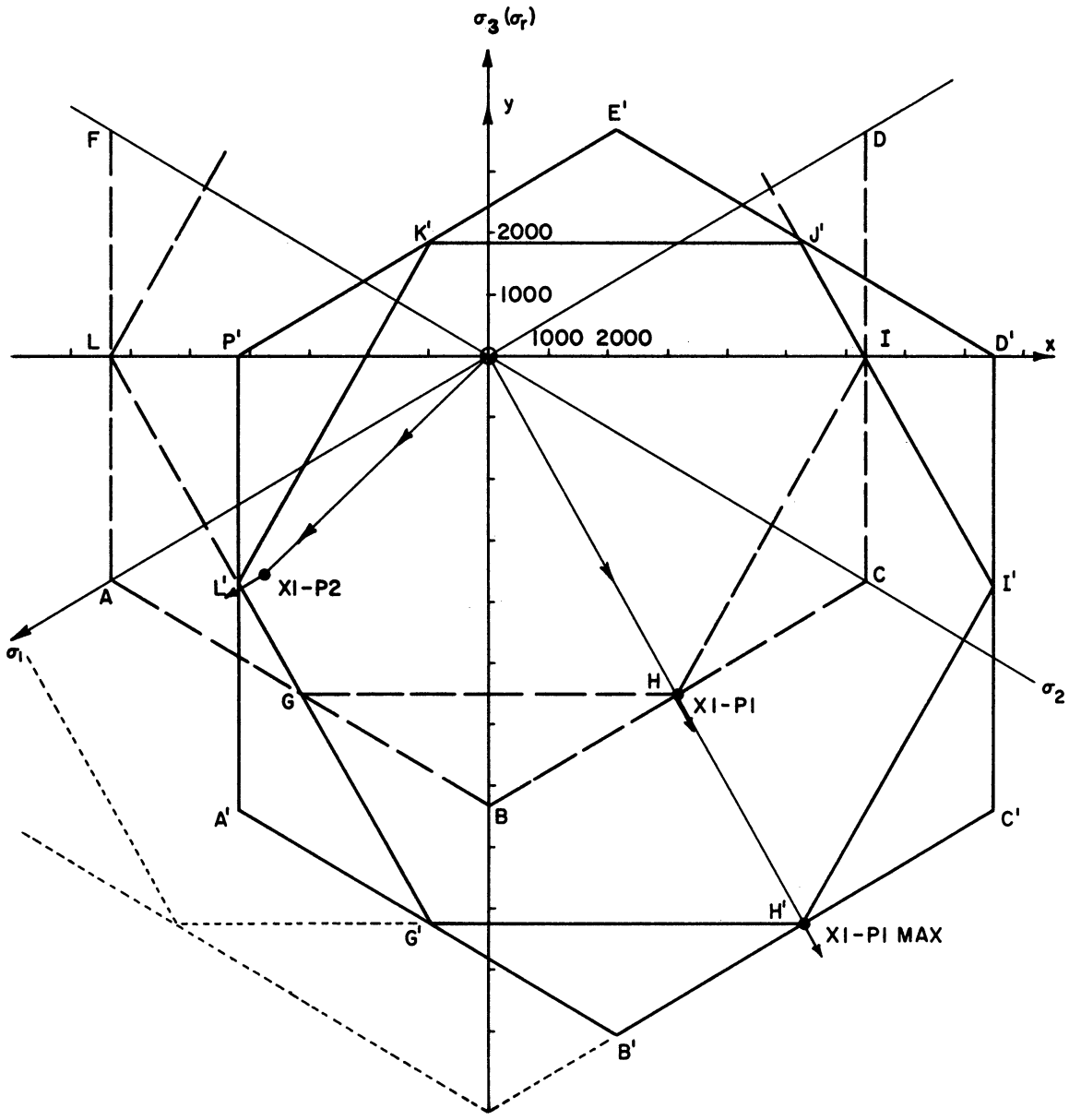

Figure 29. Strain-hardening behavior, test X-1, 78°F.

outlined in dashed lines. Note that X1-P1MAX lies on a subsequent yield surface denoted by the solid hexagons A'B'C'D'E'F'A' and G'H'I'J'K'L'G' if the kinematic hardening hypothesis applies. The appropriate figures for isotropic hardening are shown by dotted lines.

The second loading was a combination of tension and internal pressure and point X1-P2 represents yielding during second loading. It is apparent that yielding on second loading did occur at approximately the point predicted by the kinematic hardening theory. Isotropic hardening would predict a combination of stresses at yielding that is much too large in comparison with the observed yield data on second loading.

Strain increment vectors shown in Figure 29 appear to be in accord with the theoretical requirement of normality for a conservative material.

Figures 30 and 31 present other multiple loading path results for 78°F. In test X-3, Figure 30, the initial loading was a combination of tension and internal pressure although as indicated the path is not radial. Second loading for test X-3 was internal pressure alone. In test X-4, Figure 31, the loading program is essentially the same as that for test X-1, Figure 29. The results of Figure 30 appear to agree very well with the predictions of the theory of kinematic hardening both in regard to the position of point X3-P2, representing yielding on second loading, and in regard to directions of the strain increment vectors. In Figure 31, the point X4-P2 for yielding on second loading indicates that the translated maximum reduced stress yield surface, G'H'I'J'K'L', predicts a yield stress-combination which is much too small. The translated Tresca yield surface, A'B'C'D'E'F', gives better but imperfect agree-

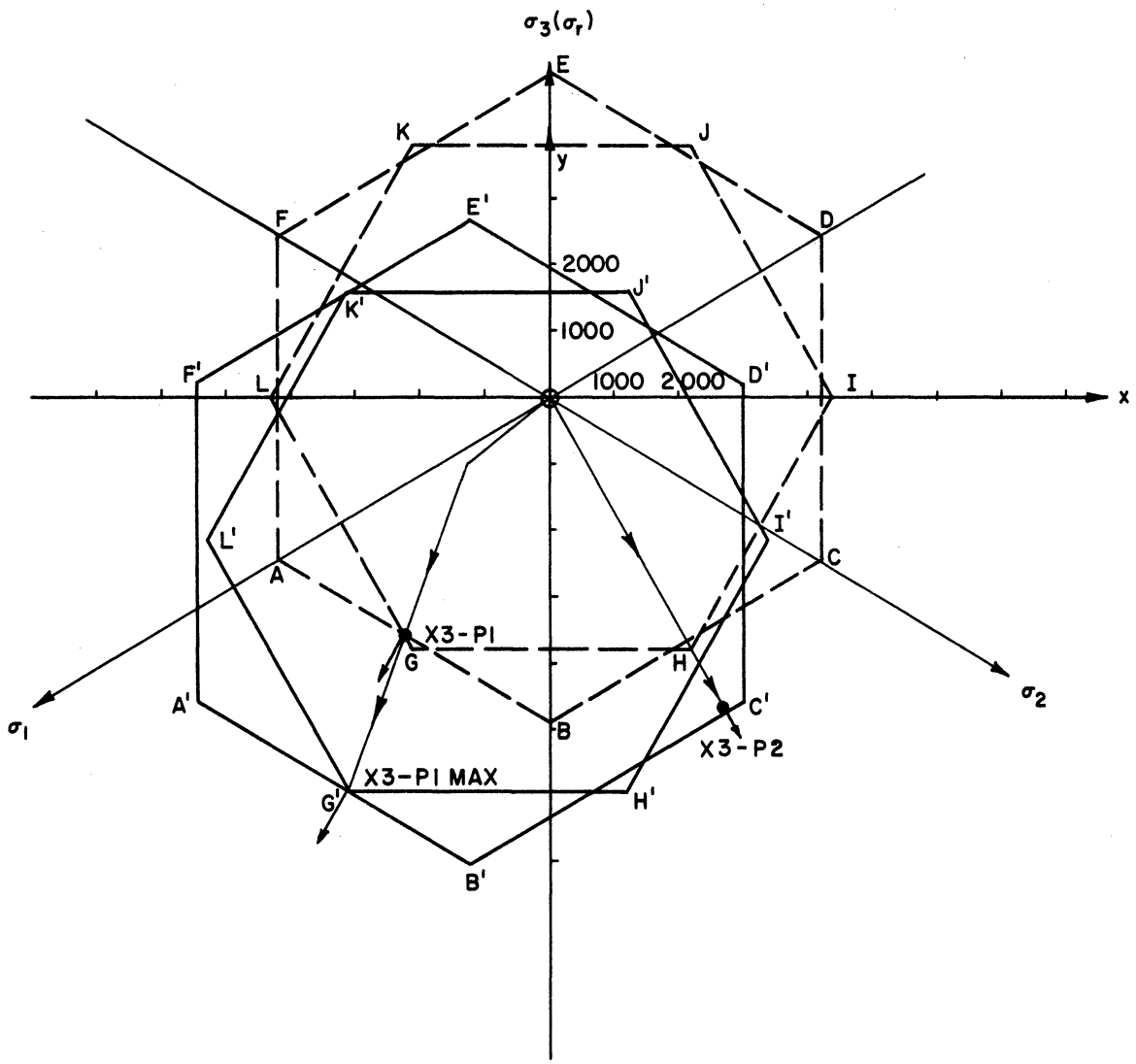

Figure 30. Strain-hardening behavior, test X-3, 78°F.

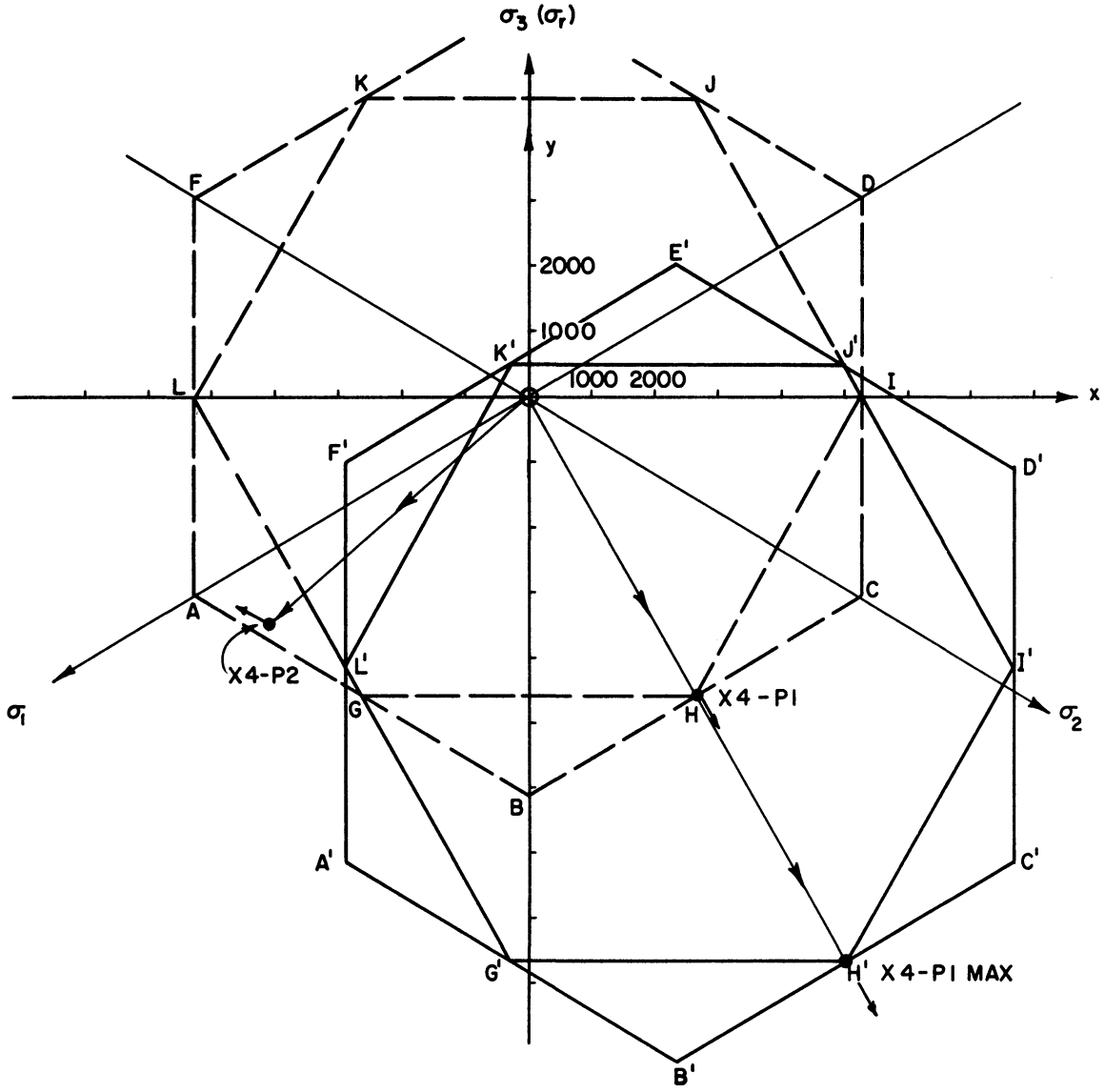

Figure 31. Strain-hardening behavior, test X-4, 78°F.

ment with the observed data. The direction of the plastic strain increment vector at point X4-P2 suggests that the point is in contact with a side of orientation K'L'. Thus one might conjecture that the initial yield surface is somewhat too small, a possibility suggested by comparing Figures 29 and 31, or that the yield surface expands while translating. The latter would be in accord with piecewise linear hardening.

Surfaces corresponding to isotropic hardening are not included in Figures 30 and 31. However, if it is noted that both initial surfaces must expand symmetrically so that they pass through points X3-P1MAX or X4-P1MAX for this theory, it is apparent that isotropic hardening would predict a yield stress-combination which was much too large.

Figure 32 contains further data on strain hardening at 78°F. In obtaining the data shown the initial combination of loads was tension with small internal pressure while the second loading was in compression. This loading program permits the probing of opposite sides of the yield surface during strain hardening. Point X9-P2, which represents the yield point during second loading, is in good agreement with the point predicted by kinematic hardening for this stress path. Obviously isotropic hardening would give a grossly inaccurate prediction in this case.

Figures 33, 34, 35, and 36 present the results of multiple load path tests at 32°F. Again it is observed that for various initial loading paths, the translated yield surfaces which move in accord with kinematic hardening do predict a point of yielding in agreement with experimental observations. It might be noted that in Figure 34 the point of yielding

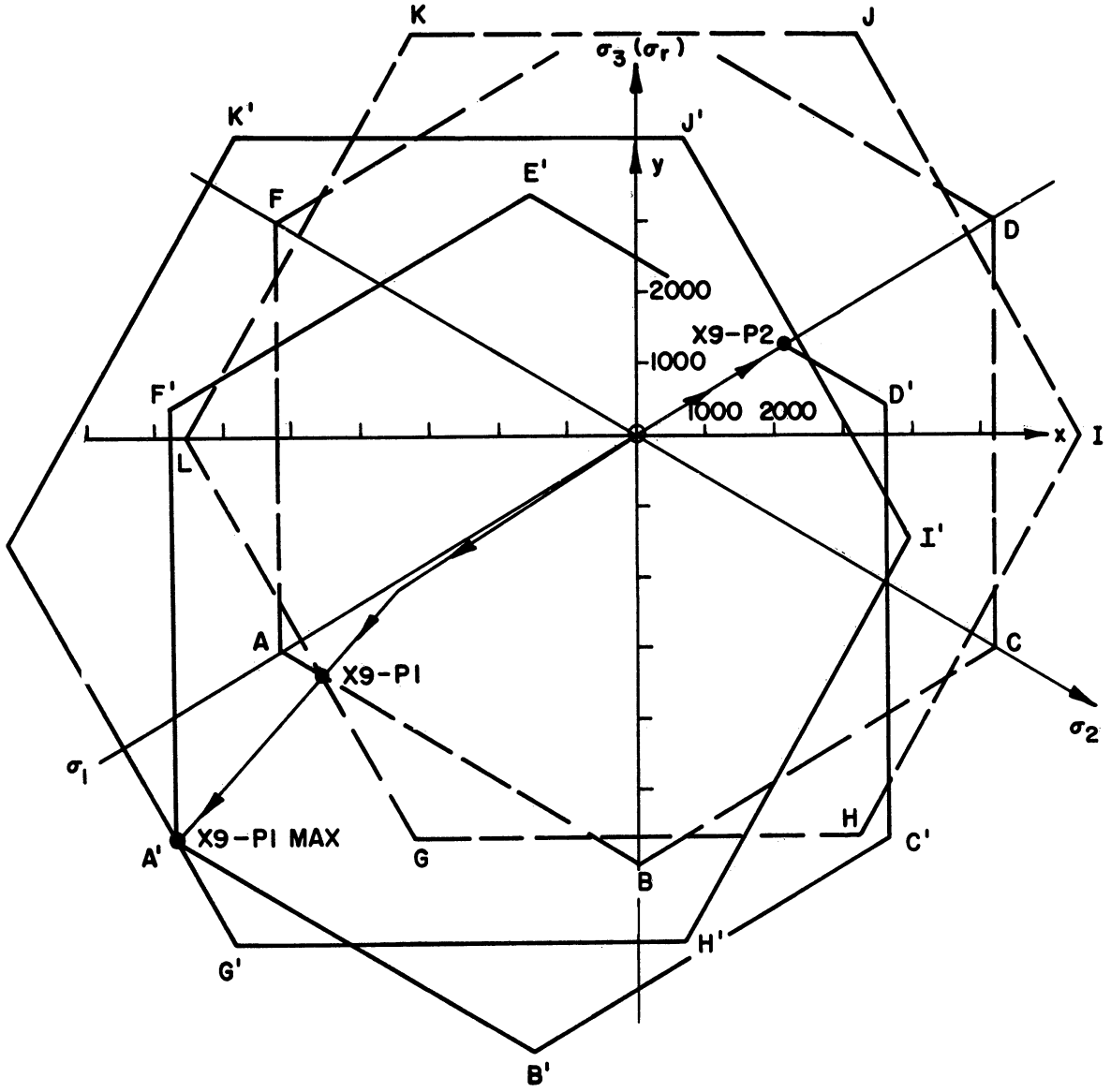

Figure 32. Strain-hardening behavior, test X-9, 78°F.

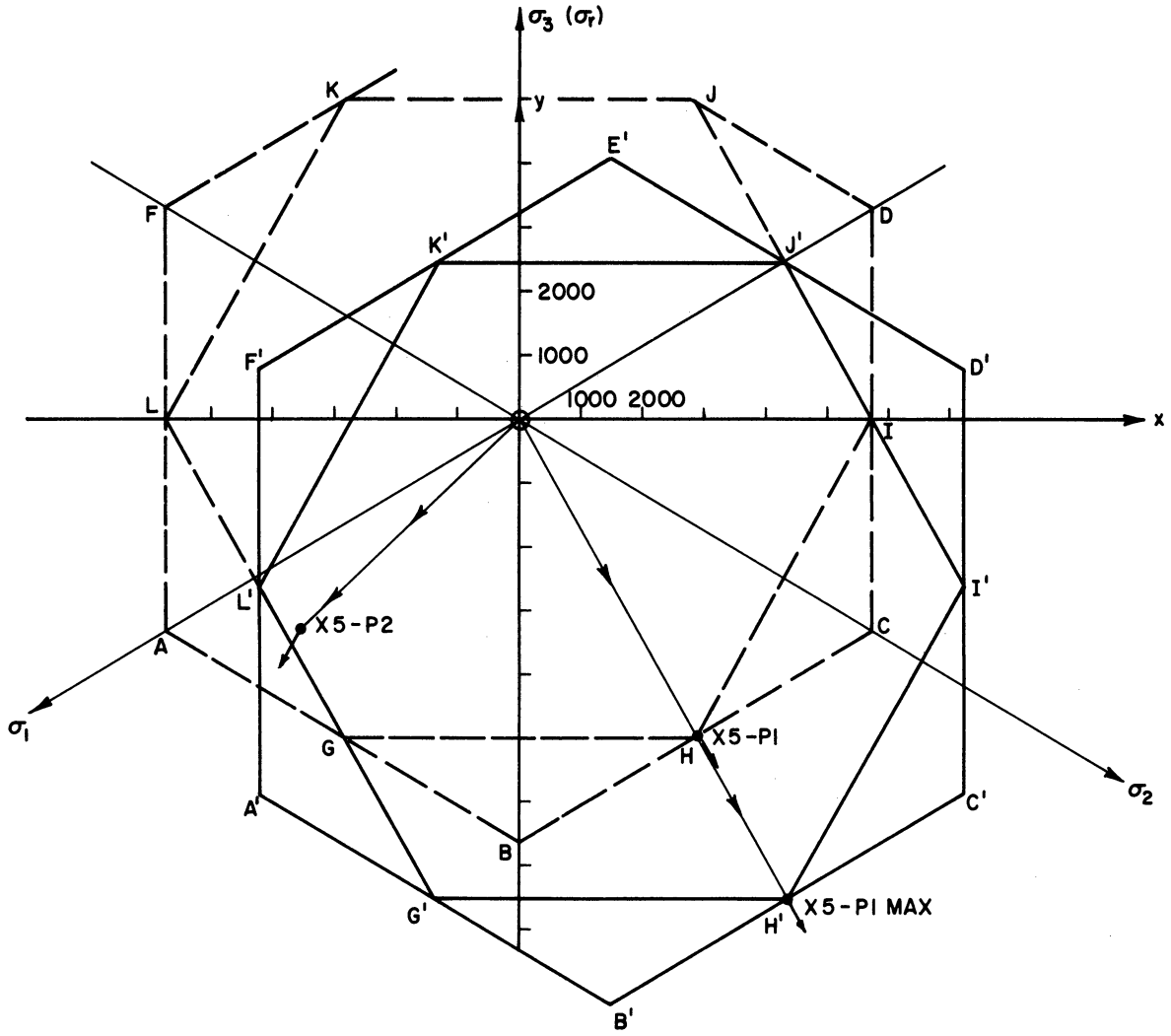

Figure 33. Strain-hardening behavior, test X-5, 32°F.

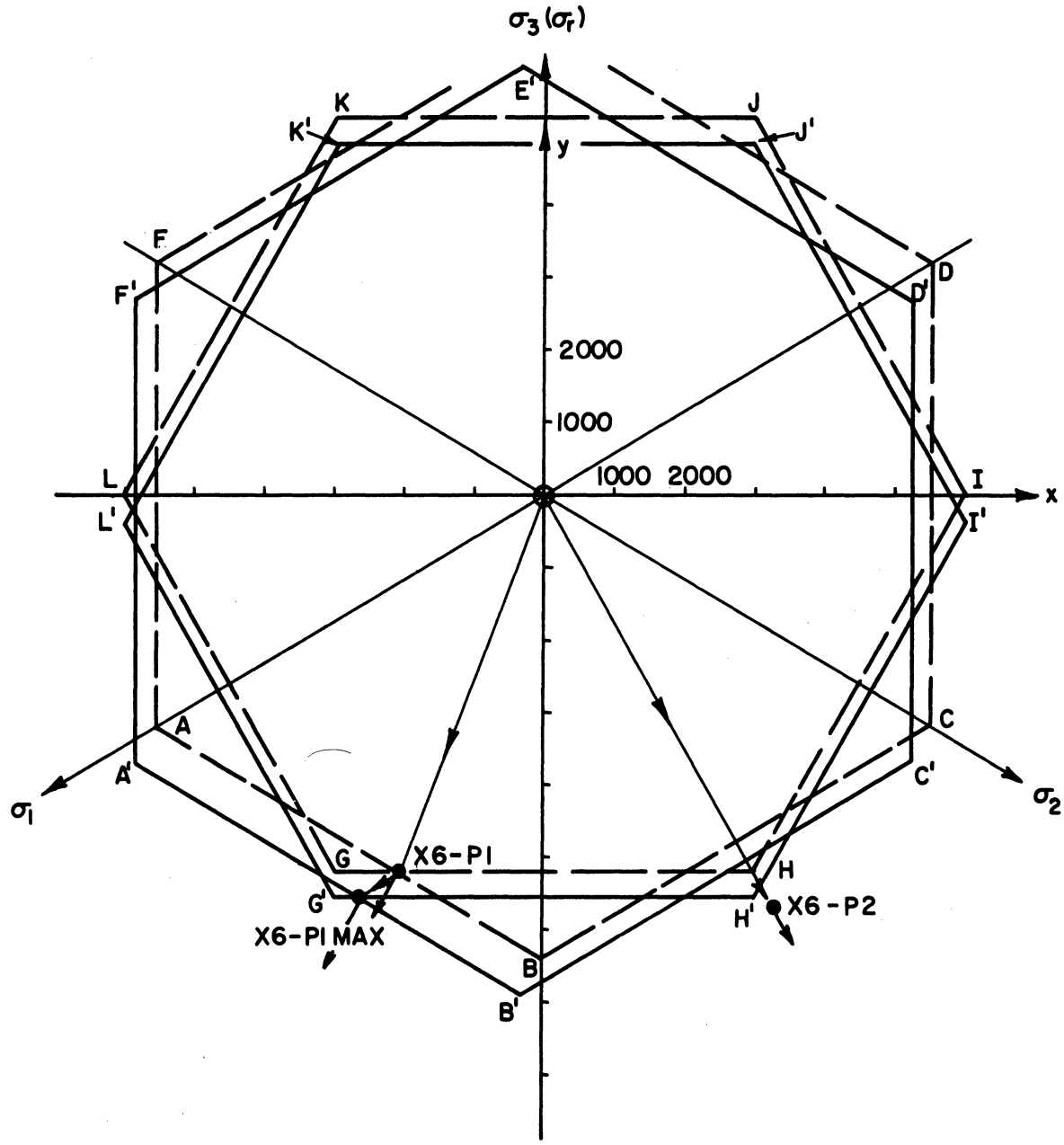

Figure 34. Strain-hardening behavior, test X-6, 32°F.

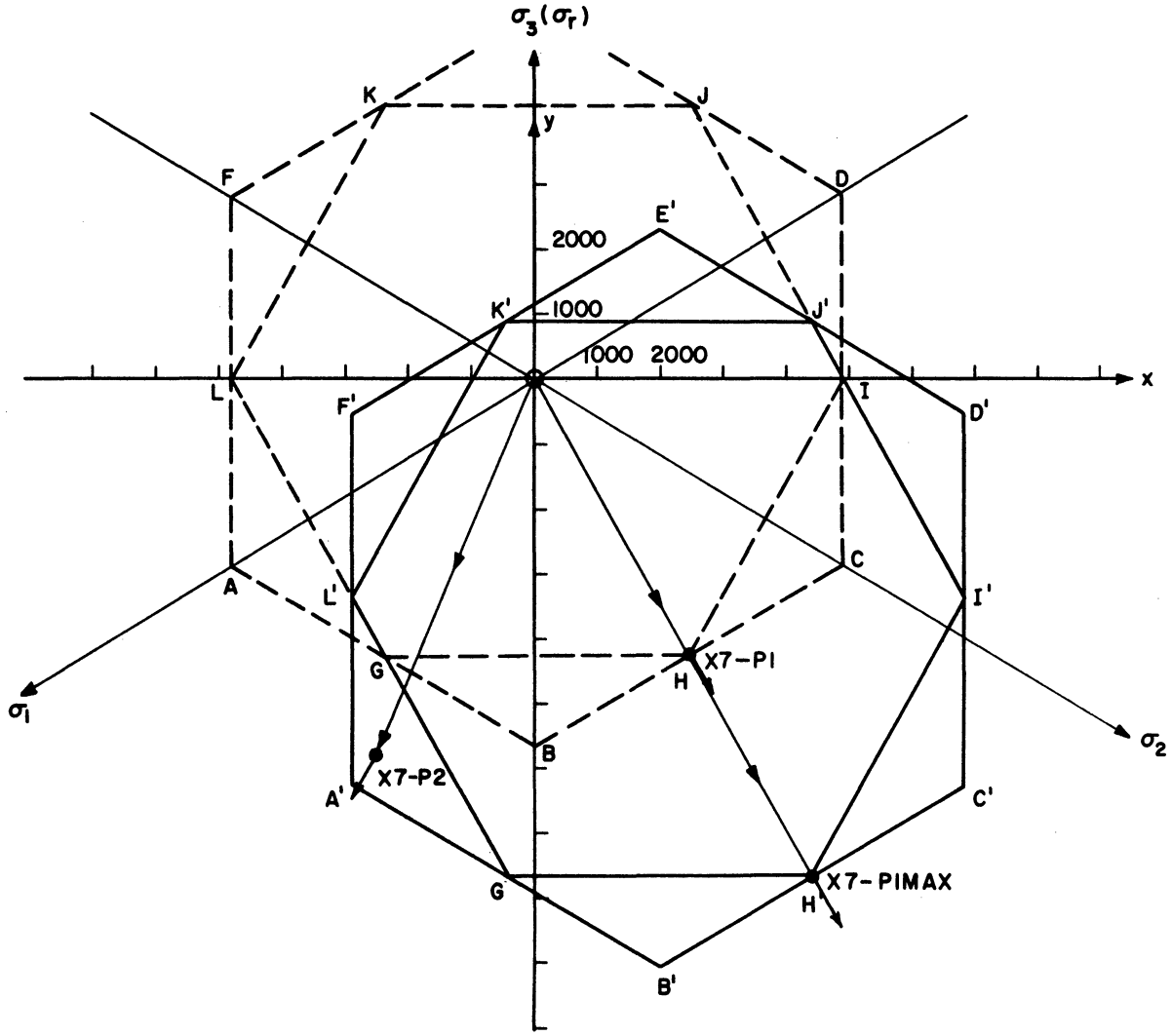

Figure 35. Strain-hardening behavior, test X-7, 32°F.

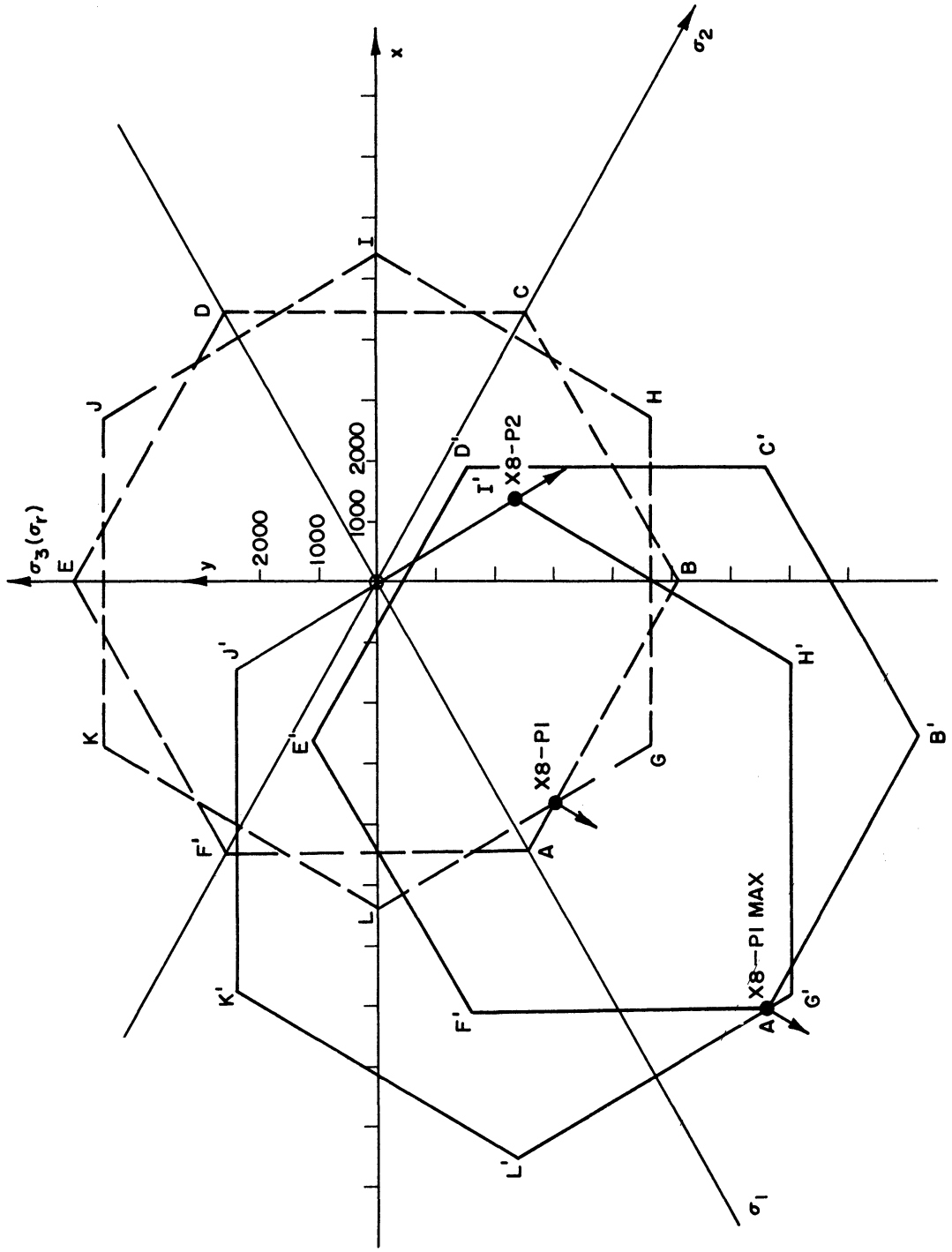

Figure 36. Strain-hardening behavior, test X-8, 32°F.

would be predicted equally well by the isotropic strain hardening theory. In Figure 36, test X8, yielding immediately on second loading would be expected if the Tresca yield criterion is considered. Thus the observed yield data indicate that the maximum reduced stress criterion gives more correct predictions in this particular case. The observed plastic strain increment vectors appear to be in accord with the requirement of normality.

Obviously the experiments discussed here were not planned to permit a detailed investigation of the form of the translated yield surface. However, the test data do indicate that the kinematic hardening theory in conjunction with either Tresca or maximum reduced stress yield criteria gives good predictions of the state of stress at yielding on second loading. This appears to be true even for fairly large translations of the yield surface.

No treatment of these experimental data in the subspaces described in Chapter IV is presented here. The subspaces appropriate for combined axial force and internal pressure are, in fact,identical to the octahedral plane except perhaps for a constant factor. Combined tension-torsion loading was not included in the strain-hardening investigation since it was desired that the principal axes of stress remain fixed in an element of the material during both initial and second loading.

CHAPTER VII

CONCLUSIONS OF THE RESEARCH

The data and analysis presented in the preceding appear to justify the following conclusions for a material exhibiting brittle rupture characteristics:

1. Thin tubes of the material respond to plastic straining as if isotropic or at most exhibit anisotropy which is rotationally symmetric about the axis of the tube.
2. Although there is scatter in the test results, it appears that initial yield criteria which assume isotropy and independence of mean stress are applicable for 78°F. At 32°F, an effect of mean stress on yielding may be indicated by data from two tests conducted at the highest mean stress.
3. Strain hardening behavior can be successfully predicted by a kinematic hardening theory in conjunction with either the Tresca or maximum reduced stress yield criterion.

REFERENCES

1. D. C. Drucker, "A More Fundamental Approach to Plastic Stress-Strain Relations," Proceedings of the First U.S. National Congress of Applied Mechanics (1951), ASME, 1952, pp. 487-491.

2. D. C. Drucker, "A Definition of Stable Inelastic Material," Journal of Applied Mechanics, Transactions of the American Society of Mechanical Engineers, Vol. 81, 1959, pp. 101-106.

3. R. von Mises, "Mechanik der plastischen Formänderung von Kristallen," Zeitschrift für Angew. Math. und Mech., Vol. 8, 1928, pp. 161-185.

4. R. von Mises, "Mechanik der festen Körper im plastisch deformablen Zustand," Göttinger Nachrichten Math-phys, Klasse, 1913, pp. 582-592.

5. H. Tresca, "Memoire sur l'ecoulement des corps solides" Mem. prés. par div. Savants, Vol. 18, 1868, pp. 733-799.

6. R. M. Haythornthwaite, "Range of Yield Condition in Ideal Plasticity," Journal of the Engineering Mechanics Division, No. E. M. 6, Proceedings of the American Society of Civil Engineers, Vol. 87, 1951.

7. R. Hill, "The Mathematical Theory of Plasticity," Oxford University Press, 1950, pp. 23-49.

8. W. Prager, "The Theory of Plasticity: A Survey of Recent Achievements," Proceedings of the Institution of Mechanical Engineers, Vol. 169, 1955, pp. 41-57.

9. R. T. Shield and H. Ziegler, "On Prager's Hardening Rule," Zeitschrift für Angewandte Mathematik und Physik, Vol. 9a, 1958, pp. 260-276.

10. W. T. Koiter, "Stress-Strain Relations, Uniqueness, and Variational Theorems for Elastic-Plastic Materials With a Singular Yield Surface," Quarterly of Applied Mathematics, Vol. 11, 1953, pp. 350-354.

11. P. G. Hodge, Jr., "A General Theory of Piecewise Linear Plasticity Based on Maximum Shear," Journal of the Mechanics and Physics of Solids, Vol. 5, 1957, pp. 242-260.

12. P. G. Hodge, Jr., "The Theory of Piecewise Linear Isotropic Plasticity," Deformation and Flow of Solids, International Union of Theoretical and Applied Mechanics (Colloquium, Madrid, September, 1955), 1956, p. 147.

13. J. L. Sanders, Jr., "Plastic Stress-Strain Relations Based on Linear Loading Functions," Proceeding of the 2nd. U.S. National Congress of Applied Mechanics (1954), ASME, 1955, pp. 455-460.

14. Hill, loc. cit., p. 318.

15. G.I. Taylor and H. Quinney, "Plastic Distortion of Metals," Philosophical Transactions of the Royal Society, London, A, Vol. 230, 1931, p. 323.

16. H.L.D. Pugh, "A Note on the Test of the Plastic Isotropy of Metals," Journal of the Mechanics and Physics of Solids, Vol. 1, 1953, pp. 284-286.

17. G. H. Handleman and W. H. Warner, "Loading Paths and the Incremental Strain Law," Journal of Mathematics and Physics, Vol. 33, 1954, pp. 157-164.

18. J. J. Guest, "On the Strength of Ductile Materials Under Combined Stress," Philosophical Magazine, Vol. 50, 1900, p. 69.

19. W. Lode, "Versuche uber den Einfluss der Mittleren Hauptspannung aug das Flussen der Metalle Eisen, Kupfer, und Nickel," Zeitschrift für Physik, Vol. 36, 1926, p. 913.

20. M. Ros and A. Eichinger, "Versuche zur Klaerung der Frage der Bruchgefahr, III. Metalle," Eidgenoss. Material prüf. u. Versuchsanstalt Ind. Bauw. ü. Gewerbe, Zürich, Diskussionsbericht, No. 34, 1929.

21. J. M. Lessels and C. W. MacGregor, "Combined Stress Experiments on a Nickel-Chrome-Molybdenum Steel," Journal of the Franklin Institute, Vol. 230, 1940, pp. 163-181.

22. J. Marin and L. W. Hu, "Plastic Stress-Strain Relations for Biaxial Tension and Variable Stress Ratios," Proceedings of the American Society for Testing Materials, Vol. 52, 1952, pp. 1098-1125.

23. J. Marin and L. W. Hu, "On the Validity of Assumptions Made in Theories of Plastic Flow for Metals," Transactions of the American Society of Mechanical Engineers, Vol. 75, 1953, pp. 1181-1190.

24. L. W. Hu and J. Marin, "Anisotropic Loading Functions for Combined Stress in the Plastic Range," Journal of Applied Mechanics Transactions of the American Society of Mechanical Engineers, Vol. 77, 1955, pp. 77-85.

25. W. Prager, "Strain Hardening Under Combined Stress," Journal of Applied Physics, Vol. 16, 1945, pp. 837-840.

26. J. Marin and L. W. Hu, "Biaxial Plastic Stress-Strain Relations of a Mild Steel for Various Stress Ratios," Transactions of the American Society of Mechanical Engineers, Vol. 78, 1956, pp. 499-509.

27. A. Phillips and L. Kaechele, "Combined Stress Tests in Plasticity," Journal of Applied Mechanics, Transactions of the American Society of Mechanical Engineers, Vol. 78, 1956, pp. 43-48.

28. P. W. Bridgeman, "Effects of High Hydrostatic Pressure on the Plastic Properties of Metals," Reviews of Modern Physics, Vol. 17, 1945, p. 3.

29. P. W. Bridgeman, "Volume Change in the Plastic Stages of Simple Compression," Journal of Applied Physics, Vol. 20, 1949, pp. 1241-1251.

30. E. A. Davis, "Increase of Stress With Permanent Strain and Stress-Strain Relations in the Plastic State for Copper Under Combined Stress," Journal of Applied Mechanics, Transactions of the American Society of Mechanical Engineers, Vol. 65, 1943, pp. A-187-196.

31. E. A. Davis, "Yielding and Fracture of Medium Carbon Steel Under Combined Stress," Journal of Applied Mechanics, Transactions of the American Society of Mechanical Engineers, Vol. 67, 1945, pp. A-13-24.

32. E. A. Davis, "Combined Tension-Torsion Tests With Fixed Principal Directions," Journal of Applied Mechanics, Transactions of the American Society of Mechanical Engineers, Vol. 77, 1955, pp. 411-415

33. D. M. Cunningham, E. G. Thomsen, and J. E. Dorn, "Plastic Flow of Magnesium Alloy Under Biaxial Stresses," Proceedings of the American Society for Testing Materials, Vol. 47, 1947, pp. 546-553.

34. W. R. Osgood, "Combined Stress Tests on 24S-T Aluminum Alloy Tubes," Journal of Applied Mechanics, Transactions of the American Society of Mechanical Engineers, Vol. 69, 1947, p. A-147.

35. J.L.M. Morrison and W M. Shepherd, "An Experimental Investigation of Plastic Stress Strain Relations," Proceedings, Institution of Mechanical Engineers, Vol. 163, 1950, pp. 1-9.

36. J. Marin, B. H. Ulrich, and W. P. Hughes, "Plastic Stress-Strain Relations for 75S-T6 Aluminum Alloy Subjected to Biaxial Tensile Stress," National Advisory Committee for Aeronautics, Technical Note 2425, August, 1951.

37. L. W. Hu and J. Marin, "Determination of Theoretical Plastic Stress-Strain Relations for Variable Combined Stress Ratios," Journal of Applied Mechanics, Transactions of the American Society of Mechanical Engineers, Vol. 74, 1952, p. 485.

38. S. S. Gill and J. Parker, "Plastic Stress-Strain Relationships—Some Experiments on the Effect of Loading Path and Loading History," Journal of Applied Mechanics, Transactions of the American Society of Mechanical Engineers, Vol. 81, 1959, pp. 77-87.

39. S. B. Batdorf and B. Budiansky, "A Mathematical Theory of Plasticity Based on the Concept of Slip," National Advisory Committee for Aeronautics, Technical Note 1871, April, 1949.

40. B. Budiansky, N. F. Dow, R. W. Peters, and R. P. Shepherd, "Experimental Studies of Polyaxial Stress-Strain Laws of Plasticity," Proceedings of the First U.S. National Congress of Applied Mechanics (1951), ASME, 1952, pp. 503-512.

41. P. M. Naghdi and J. C. Rowley, "An Experimental Study of Biaxial Stress-Strain Relations in Plasticity," Journal of the Mechanics and Physics of Solids, Vol. 3, 1954, pp. 63-80.

42. P. M. Naghdi, J. C. Rowley, and C. W. Beadle, "Experiments Concerning the Yield Surface and the Assumption of Linearity in the Plastic Stress-Strain Relations," Journal of Applied Mechanics, Transactions of the American Society of Mechanical Engineers, Vol. 77, 1955. pp. 416-420.

43. S. S. Gill, "Three 'Neutral' Loading Tests," Journal of Applied Mechanics, Transactions of the American Society of Mechanical Engineers, Vol. 78, 1956, pp. 497-502.

44. P. M. Naghdi, F. Essenburg, and W. Koff, "An Experimental Study of Initial and Subsequent Yield Surfaces in Plasticity," Journal of Applied Mechanics, Transactions of the American Society of Mechanical Engineers, Vol. 80, 1958, pp. 201-209.

45. L. W. Hu and J. F. Bratt, "Effect of Plastic Deformation on the Yield Condition," Journal of Applied Mechanics, Transactions of the American Society of Mechanical Engineers, Vol. 80, 1958, p. 411 (Brief Note).

46. H. G. McComb, Jr., "Some Experiments Concerning Subsequent Yield Surfaces in Plasticity," National Aeronautics and Space Administration, Technical Note D-396, June, 1960.

47. G. B. Talypov, "Flow Limit and Rupture of Low Carbon Steels in the Cases of Simple and Complex Loading. The Influence of Aging," Izvestiia, Akademii Nauk SSSR, Otdelenie Tekhnicheskikh Nauk (Mekhanika i Mashinostroenie), No. 6, 1961, pp. 125-130.

48. H. J. Ivey, "Plastic Stress-Strain Relations and Yield Surfaces for Aluminum Alloys," Journal of Mechanical Engineering Science, Vol. 3, 1961, pp. 15-31.